

EXPERIMENTAL STUDIES ON INTERFACE BOND
STRENGTH OF ULTRA-THIN WHITETOPPING
PAVEMENTS UNDER STATIC AND DYNAMIC
LOADING CONDITIONS

Thesis

Submitted in partial fulfillment of the requirement for degree of
Doctor of Philosophy

by

JAYAKESH K



DEPARTMENT OF CIVIL ENGINEERING
NATIONAL INSTITUTE OF TECHNOLOGY KARNATAKA
SURATHKAL, MANGALURU-575 025

July, 2018

D E C L A R A T I O N

by the Ph.D. Research Scholar

I hereby *declare* that the Research Thesis/~~Synopsis~~ entitled **Experimental Studies on Interface Bond Strength of Ultra-Thin Whitetopping Pavements Under Static and Dynamic Loading Conditions**, which is being submitted to the **National Institute of Technology Karnataka, Surathkal** in partial fulfillment of the requirements for the award of the Degree of **Doctor of Philosophy** in Civil Engineering is a *bonafide report of the research work carried out by me*. The material contained in this Research Thesis/~~Synopsis~~ has not been submitted to any University or Institution for the award of any degree.

135058CV13F01, JAYAKESH K.,
(Register Number, Name & Signature of the Research Scholar)
Department of Civil Engineering

Place: NITK-Surathkal

Date: 02-07-2018

C E R T I F I C A T E

This is to *certify* that the Research Thesis/~~Synopsis~~ entitled **Experimental Studies on Interface Bond Strength of Ultra-Thin Whitetopping Pavements Under Static and Dynamic Loading Conditions**, submitted by JAYAKESH K., (Register Number: 135058CV13F01) as the record of the research work carried out by him/~~her~~, is *accepted as the Research Thesis/~~Synopsis~~ submission* in partial fulfillment of the requirements for the award of degree of **Doctor of Philosophy**.

(Dr. Suresha S N)
Research Guide
(Name and Signature with Date and Seal)

Chairman - DRPC
(Signature with Date and Seal)

*DEDICATED TO MY
PARENTS*

ACKNOWLEDGEMENTS

I would like to express my sincere gratitude to my research supervisor, Dr. Suresha S N, for his guidance, help, and co-operation rendered during various stages of the research, the facilities provided and the support.

Thanks and sincere appreciations to Dr. Ravishankar, Dept. of Metallurgical and Materials Engineering and Dr. Sitaram Nayak, Dept. of Civil Engineering, Members, RPAC, for their comments, suggestions, and the encouragement provided at various stages of this work.

I would like to express my gratitude to former Heads, Department of Civil Engineering, Prof. Katta Venkataramana, Prof. K N Lokesh, Prof. D Venkat Reddy and Prof. Varghese George, Chairman, DRPC and Head, Department of Civil Engineering, for extending the facilities of the Department for this work. I sincerely express thanks to the Director of the Institute (NITK), for the financial support provided and for extending the facilities for the research.

I appreciate the co-operation and help rendered by the staff of laboratories and the office of the Civil Engineering Department. My heartfelt thanks to Mr. Purushotham B and Mr. Shashikanth, who helped me to complete my laboratory studies safely and smoothly.

Thanks to all my research colleagues and former M.Tech students (2014-2017) who made me to realize the gist of silence over speech that made me to concentrate on my research. Finally, I thank all, who directly or indirectly helped for smooth conduct of the research.

Date: 02-07-2018
NITK, Surathkal

JAYAKESH K

ABSTRACT

The concrete overlays on existing asphalt pavements are classified into three categories namely whitetopping, thin-whitetopping and ultra-thin whitetopping (UTW). The interface bond strength between the existing hot mix asphalt (HMA) pavement and the UTW overlay is the key factor towards the success of UTW overlays.

The aim of the present work is to study the interface bond strength of UTW overlays subjected to different interface treatment techniques. Because loss of bond and layer delamination affects the composite behavior of UTW overlay. This will leads to premature failure and reduction in design service life of UTW overlays. Therefore, a good surface preparation method is required to improve the interface bond strength and to meet the design service life of UTW overlays. In order to achieve the objective of the present work experimental studies were conducted under laboratory conditions. An optimized cementitious fiber reinforced concrete (FRC) mix proportion for UTW was arrived using Taguchi method. The HMA mixture specimens of cylindrical and prism were casted using superpave gyrator and compression loading machine, respectively. Later, HMA-UTW composite specimens such as cylindrical and prism were casted with different interface treatment techniques. The different interface treatment techniques adopted for cylindrical specimens are single groove (SG), double groove (DG), piercing and piercing with different percentage of bonding. The HMA-UTW prism composite specimens with different percentage of bonding at the interface were adopted. To enumerate the interface bond strength for different interface treatment techniques two test methods were adopted namely direct shear test and flexural test. Both the tests were conducted under (i) static and (ii) dynamic loading conditions

From direct shear test the effect of different interface treatment techniques on interface shear bond strength, k-modulus and number of cycles at failure were obtained. Similarly, in the flexural test, the flexural bond strength and number of cycles at failure were determined for different percentage of bonding. Based on the laboratory test results two interface treatment techniques such as groove interface technique with an inclination of 45 degrees and piercing interface treatment has been proposed. From flexural bond strength test results 75 mm HMA thickness had obtained highest flexural bond strength of 1.71 MPa and 1.4 million number of fatigue cycles. An HMA failure was noticed in 75 mm HMA thick composites subjected to dynamic loading condition.

A Finite Element Analysis (FEA) using a contact friction model successfully simulated the interface behavior of HMA-UTW composites. An error of 4 to 14 % were obtained between laboratory test and the simulated model for piercing interface treatment and different HMA thickness subjected to different percentage of bonding.

Keywords: Ultra-thin whitetopping; Taguchi method; Box test; Direct shear test; Flexural fatigue test; Interface shear bond strength; k-modulus; Groove interface treatment; Piercing; Different percentage of bonding; Interface shear bond fatigue; HMA thickness; Flexural bond strength; Finite element analysis and Contact friction model.

TABLE OF CONTENTS

	Page
LIST OF FIGURES	v
LIST OF TABLES	viii
1 INTRODUCTION	
1.1 BACKGROUND AND MOTIVATION	1
1.2 RESEARCH OBJECTIVES AND SCOPE	5
1.3 THESIS ORGANIZATION	6
2 EVALUATION OF CEMENTITIOUS FRC MIXTURES FOR UTW OVERLAY	
2.1 BACKGROUND	8
2.2 EXPERIMENTAL STUDY	13
2.2.1 Materials and Research Methodology	13
2.2.2 Mixture Design and Sample Preparation	15
2.2.2.1 Taguchi method	16
2.2.2.2 Sample preparation and test methods	19
2.3 FRESH PROPERTY	21
2.3.1 Slump Cone	21
2.3.2 Surface Voids Ranking	22
2.4 HARDENED PROPERTY	27
2.4.1 Compressive Strength	27
2.4.2 Flexural Strength	29
2.4.3 Split Tensile	29
2.4.4 Tangent Modulus	30
2.4.5 Data Analysis of the S/N Ratios for Optimum Mix	31
2.4.6 Test Results for Optimum Mixture	32
2.5 FLEXURAL FATIGUE LIFE	32

2.5.1	Analysis of Fatigue-Life Distribution Using Statistical Method	32
2.5.2	Analysis of Fatigue-Life Distribution Using Weibull Distribution Parameters	35
2.5.3	Failure Probability and Stress Ratio-Number of Cycles (S-N) Relationship	38
2.6	SUMMARY	39

3 QUANTIFYING THE INTERFACE SHEAR BOND STRENGTH OF HMA-UTW COMPOSITES SUBJECTED TO DIRECT SHEAR TEST

3.1	BACKGROUND	40
3.2	PREVIOUS STUDIES ON INTERFACE BOND STRENGTH	41
3.2.1	Asphalt-Asphalt Interface Bond Verification Test	41
3.2.2	PCC-Asphalt Interface Bond Verification Test	45
3.2.3	PCC-PCC Interface Bond Verification Test	47
3.3	INTERFACE SHEAR BOND STRENGTH TEST	58
3.3.1	Test Apparatus	58
3.3.2	Interface Treatment	59
3.3.3	Materials	60
3.3.4	Specimen Preparation	61
3.3.5	Test Procedure	62
3.3.6	Evaluation of ISBS and k-modulus Under Static Loading	64
3.4	RESULTS AND DISCUSSION	65
3.4.1	Effect of Rate of displacement on ISBS	65
3.4.2	Effect of Groove Interface Treatment on ISBS and k-modulus	67
3.4.3	Effect of Piercing Interface Treatment with Different Percentage of Bonding on ISBS	70

3.4.4	Effect of Piercing Interface Treatment with Different Percentage of Bonding on k-modulus	73
3.5	INTERFACE SHEAR BOND FATIGUE	75
3.6	SUMMARY OF FINDINGS	77
4	QUANTIFYING THE EFFECT OF HMA THICKNESS ON FLEXURAL BOND STRENGTH OF HMA-UTW COMPOSITES UNDER FLEXURAL LOADING	
4.1	BACKGROUND	79
4.2	SAMPLE PREPARATION	80
4.3	TEST PROCEDURE	81
4.4	RESULTS AND DISCUSSION	82
4.4.1	Effect of HMA Thickness and Percentage of Bonding on Flexural Bond Strength	82
4.4.2	Effect of HMA Thickness and Percentage of Bonding on Flexural Fatigue Life	83
4.4.3	Analysis of Fatigue-Life Distribution Using Weibull Distribution Parameters	84
4.4.4	Failure Probability and S-N Relationship	87
4.5	SUMMARY OF FINDINGS	89
5	SIMULATING HMA-UTW INTERFACE FRACTURE BY SUPERIMPOSING CONTACT FRICTION MODEL USING DIRECT SHEAR AND FLEXURAL LOADING TEST DATA	
5.1	BACKGROUND	90
5.2	RESULTS AND DISCUSSION	95
5.3	SUMMARY OF FINDINGS	97
6	CONCLUSION AND FUTURE WORK	98

APPENDIX A – E	101-109
REFERENCES	110
BIO-DATA	125

LIST OF FIGURES

Figure No.	Description	Page No.
1.1	Represents the structural capacity loss over time and with traffic	2
1.2	The effect of the composite action on UTW overlays	3
1.3	Flow chart for assessing the influence of various interface surface treatment techniques on interface bond strength of UTW overlays	6
2.1	Combined gradation curve	14
2.2	Research methodology	15
2.3	Illustrates the surface voids ranking apparatus (a) Box test apparatus and needle vibrator (b) & (c) are surface voids of T17 mix	20
2.4	Slump cone results for control mixes, (a) group A and (b) group B mixtures	22
2.5	(a), (b) and (c) represents overall surface void ranking for eighteen mixes	26
2.6	Compressive strength test results for control, (a) group A and (b) group B mixtures	28
2.7	Flexural strength test results for control, group A and group B mixtures	29
2.8	Split tensile strength test results for control, group A and group B mixtures	30
2.9	Tangent modulus for control, group A and group B mixtures	31
2.10	<i>S/N</i> ratios of 28 days flexural strengths	32
2.11	Fatigue life distribution of optimized FRC mixture	33
2.12	Graphical analysis of fatigue life data for FRC (a) stress ratio = 0.85 (b) stress ratio = 0.75 (c) stress ratio = 0.65	37
2.13	P_f - <i>S-N</i> diagram for FRC mixture	39
3.1	Possible modes of pavement interface failure during service life	41
3.2	Direct shear test apparatus	58

3.3	Different HMA-UTW interface treatments (a) DG (b) Piercing with different debonding (unbonded) region	59
3.4	Illustrates (a) DG interface treatment (b) piercing interface treatment and (c) HMA-UTW composite specimens	62
3.5	Schematic diagram of groove interface treated samples subjected to different loading direction	63
3.6	Interface shear bond test procedure using direct shear test apparatus	63
3.7	Typical specimen interface response under the influence of shear load	64
3.8	Effect of different rate of displacement and interface treatment on (a) ISBS and (b) k-modulus	66
3.9	Effect of groove interface treatment on ISBS	68
3.10	Interface failure surfaces of the UTW shear strength specimens (a) groove interface treatment subject to parallel loading and (b) piercing interface treatment	69
3.11	Effect of groove interface on k-modulus at (a) 7 days and (b) 28 days	70
3.12	ISBS for piercing and different percentage of bonding at (a) 7 days and (b) 28 days	72
3.13	Reduction in ISBS at 7 and 28 days	73
3.14	Effect of percentage of bonding on k-modulus	74
3.15	Schematic representation of determining displacement and number of cycles at failure under the influence of shear bond fatigue	75
3.16	Represents one of the HMA failed specimens with 100 % bonding interface	76
3.17	Relationship between shear bond fatigue life and applied stress for piercing technique and different percentage of bonding	77
4.1	Represents the prism mould and HMA specimens with 50 % interface treatment	81
4.2	Represents the repeated load test for HMA-UTW composite prism specimens and 50 % interface bonding failure specimen	82

4.3	Flexural bond strength of HMA-UTW prism composites at 7 and 28 days for 50 and 100 percent bonding	83
4.4	Relationship between stress ratio and fatigue life of 75 mm HMA thickness HMA-UTW prism composites	84
4.5	Graphical analysis of fatigue life data for (a) 100% and (b) 50% bonding HMA-UTW prism composites	87
4.6	Pf-S-N diagram for (a) 100% and (b) 50% bonding HMA-UTW prism composites	88
5.1	The stress variation at the interface for 97 % bonding specimen subjected to direct shear loading	94
5.2	Stress variation at the interface for 75 mm HMA thick with 100% bonded interface subjected to flexural loading	95
5.3	Comparison of experimental and model ISBS of piercing interface treatment and piercing with different percentage of bonding	96
5.4	Regression coefficient values for simulated model and experimental result for ISBS	96
5.5	Comparison of experimental and simulated model for the samples subjected to interface flexural bond strength	97
C.1	Load verses displacement curve for groove interface treatment specimens subjected to 6.0 mm/min rate of loading	105
D.1	Graphical analysis of fatigue life data for 100% bonding at different stress ratios (a) 0.75 (b) 0.65 (c) 0.55	108
D.2	Graphical analysis of fatigue life data for 50% bonding at different stress ratios (a) 0.75 (b) 0.65 (c) 0.55	109

LIST OF TABLES

Table No.	Description	Page No.
2.1	Typical UTW mix proportions	9
2.2	Properties of cement, GGBS, and SF	13
2.3	Physical properties of Fiber	13
2.4	Taguchi method of orthogonal arrays [L18 (4*3)] of the experimental design	17
2.5	Introduced levels for each factor in Taguchi experimental design	17
2.6	Details of UTW mix proportions used for control mixtures and Taguchi optimization	18
2.7	Box test ranking for different surface voids	20
2.8	Response table mean signal-to-noise (<i>S/N</i>) ratio for flexural strength factor and significant interaction	31
2.9	Static flexural failure load of individual samples	32
2.10	Summary of flexural fatigue test results	34
2.11	Weibull parameters for fatigue of FRC mixtures	36
2.12	Calculated fatigue lives of FRC mixtures for different probabilities of failure	38
3.1	Summary of literature review	49
3.2	Physical Properties of Asphalt Binder (VG-30)	60
3.3	Aggregate Gradation for HMA Mixtures	60
3.4	Test Results of Interface Angle Groove	68
3.5	ISBS Test Results of Different Percentage of Bonding	70
3.6	Interface k-modulus Test Results of Different Percentage of Bonding	74
3.7	Interface Shear Bond Fatigue Test Results for 100% Bonding (Piercing)	76
4.1	Aggregate composition for HMA mixture	80
4.2	Summary of flexural fatigue life of HMA-UTW prism composites	85

4.3	Weibull parameters for fatigue lives of HMA-UTW composites with 50 and 100% bonding interface	87
5.1	Summary of literature for simulation of interface bond strength in FEM	92
5.2	Interface properties from direct shear test	94
C.1	ISBS test results of NT specimens	105
D.1	Interface Shear Bond Fatigue Test Results for 97% Bonding (Piercing+25)	106
D.2	Interface Shear Bond Fatigue Test Results for 88% Bonding (Piercing+50)	106
D.3	Interface Shear Bond Fatigue Test Results for 75% Bonding (Piercing+75)	107
D.4	Interface Shear Bond Fatigue Test Results for 55% Bonding (Piercing+100)	107

CHAPTER 1

INTRODUCTION

1.1 BACKGROUND AND MOTIVATION

Overlay is the general method used to repair and strengthen the existing pavements. Primary purpose of the overlay is to extend the service life of the existing pavement by 10 to 15 years or structural capacity (SC) with respect to time and traffic as shown in Fig.1.1 (Torres et al. 2012; Bissonnette et al. 2013). Historically the HMA concrete surfaces are the most common rehabilitation method used for existing pavement structures. It is having an advantage of rapid placement and ability to open for traffic shortly after placement. But, HMA pavements exhibit various structural and material failures. Finally increases the maintenance cost of HMA overlays. In order to overcome the drawbacks in HMA overlays, in India and abroad several projects have experimented by constructing portland cement concrete (PCC) overlays (NCHRP 338 2004; IRC SP: 76 2008). PCC overlays are classified into bonded and unbonded concrete overlays. Bonded concrete overlays are classified into two categories, namely thin whitetopping and UTW and having a PCC slab thickness of 100-200 mm and 50-100 mm respectively. The unbonded overlays are classified into conventional whitetopping with PCC slab thickness more than 200 mm. UTW is a relatively new technique emerged from Europe and the United States in the year 1980 (Risser et al. 1993; NCHRP 338 2004).

The applications of UTW overlays could be found in low volume roads like urban streets and village roads, ramps, bus stops, intersections, general aviation runways and taxiways, parking lots etc., (Vandenbossche and Rettner 1998; Tia et al. 2002; Chunhua 2005; Roesler et al. 2008).

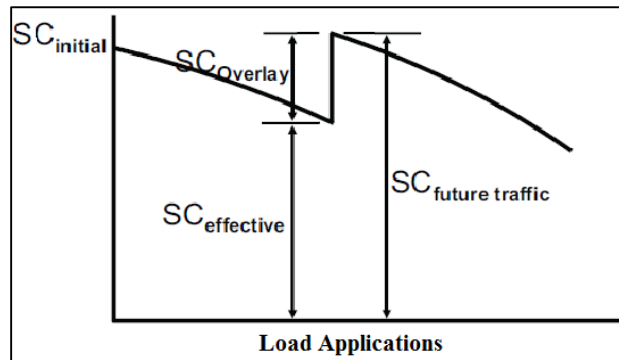


Fig. 1.1 Represents the structural capacity loss over time and with traffic (Torres et al. 2012)

The design service life of UTW depends on several factors such as interface bond strength, interface surface preparation method, material strength, slab thickness, underlying material condition and slab size.

Interface bond strength: The bond between existing HMA layer and freshly overlaid PCC pavement is mandatory in UTW overlays (IRC SP: 76 2008). Therefore the performance of UTW overlays depends upon the degree of bond between the HMA layer and UTW overlay. A sound bond at the interfaces makes the behavior of heterogeneous structure into composite action by shifting the neutral axis from the middle of the UTW slab to the bottom of UTW slab (Vandenbossche and Rettner 1998; IRC SP: 76 2008; Vandenbossche and Barman 2010). This increases the load carrying capacity of the heterogeneous structure by reducing the tensile stress in the UTW overlays. Also, reduces the lifting of the concrete panels at the edges and corners due to wheel load and warping stresses and uncontrolled cracks develop in debonded zones (NCHRP: 338 2004; Wu et al. 2007; Mu and Vandenbossche 2011).

Following are the advantages of interface bonded overlays

- i) Reduces the common occurrence of abrasion and erosion of individual pieces of aggregate under traffic and demand on noise in presence of cracking.
- ii) Resistance towards the percolation of water through the joints (Vandenbossche and Barman 2010; Chunhua 2005).

- iii) Minimize the reflection of cracks to the top surface and propagation of cracks through the adjacent panels (Tschegg et al. 2007; Wu et al. 2007).
- iv) A good load transfer efficiency between the adjacent slabs can be achieved. The critical stress at the interface can be reduced by maintaining a strong bond (Barman et al. 2017).

The effect of the composite action on the behavior of UTW overlays under flexural loading for bonded and unbonded condition is shown in Fig. 1.2.

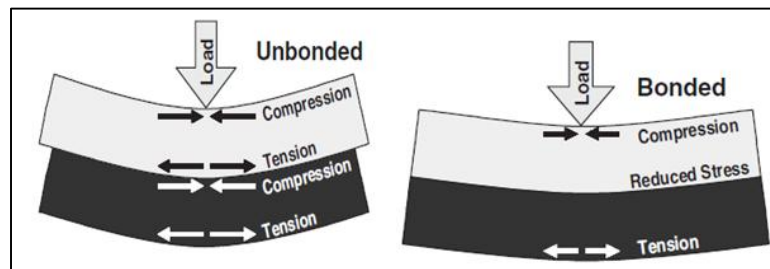


Fig.1.2 The effect of the composite action on UTW overlays (NCHRP: 338 2004)

Interface surface preparation: A fully bonded UTW overlay increases the effective stiffness of the heterogeneous structure by reducing the tensile stresses (Mu 2014). If UTW overlays are not well bonded to the HMA layer a premature pavement deterioration may occur such as loss of bond strength and layer delamination. The loss of bond strength may be due to repeated application of traffic and environmental loading. Generally, the loss of bond either takes place at the HMA-UTW interface or between the HMA lifts (Vandenbossche and Fagerness 2002; Nishiyama et al. 2005). Due to inadequate surface preparation of the existing HMA layer i.e. a very thin asphalt course left after milling method causes layer delamination in the HMA layer (Vandenbossche and Fagerness 2002; Mu 2014). Therefore, authors (Nishiyama et al. 2005; Mu 2014) suggested that good surface preparation methods on the existing HMA pavement reduce the premature failure.

Slab thickness: The thickness UTW overlay not only drive the performance but also cost. Thus, while selecting the slab thickness it has to balance the number factors such as traffic loading, the stiffness of the HMA layer, properties of UTW layer and the load transfer efficiency (NCHRP 338 2004).

Material strength: In the presence of debonded interface, UTW overlays will undergo large crack spacing and crack widths (Carlsward 2006). Hence adopting a better material property in the UTW overlay mixture can reduce the crack spacing and crack widths. Therefore, the long-term performance of UTW overlays depends on the material strength of the UTW overlays

Underlying material condition: The existing HMA pavement condition should be free from wide cracks, heavy rutting and sub-grade related problems. Also it has to provide sufficient uniformity and stable support for the UTW overlays. A minimum HMA thickness of 75mm should be available even after milling for placing UTW overlays (NCHRP: 338 2004; Cho and Koo 2006; IRC SP: 76 2008). To avoid debonding of interface in HMA-UTW overlays the stripping characteristics of the asphalt binder from the HMA layer has to be assessed.

Slab size: Depending on the UTW thickness the slab size will vary in the range of 0.6 m to 1.8 m. Due to smaller slab size and bond at the interface minimizes the slab bending, shrinkage cracking, slab curling and warping (Tia et al. 2002; Burnham 2005; Wu et al. 2007). Therefore bond between the HMA and UTW layer is the key factor towards the performance of UTW overlays.

In India, the UTW overlays are designed as per the guidelines published by Indian road congress (IRC SP: 76 2008). The guideline IRC SP: 76 2008 assumes fully bonded interface while designing the UTW slab thickness. This will leads to the unreliable design of UTW overlays. However, in reality, it is difficult to achieve 100 percent bonding at the interface. Also, IRC SP: 76 2008 do not mention the test methods to evaluate the interface bond strength of UTW overlays. Therefore, a study is required to understand the HMA-UTW composite behavior under different interface bonding conditions. Additionally a test method is required to evaluate the interface bond strength of UTW overlays.

1.2 RESEARCH OBJECTIVES AND SCOPE

The primary objective of the present research is to evaluate interface bond strength of HMA-UTW composites and to develop laboratory performance model. The specific research objectives are listed below:

- (i) To study the effect of various types of interface treatment techniques on the interface bond strength on HMA-UTW composites using direct shear test.
- (ii) To study the effect of degree of bonding on HMA-UTW interface under static and dynamic loading conditions subjected to direct shear and flexural test.
- (iii) To study the effect of HMA thickness on flexural bond strength and fatigue lives of HMA-UTW composites.
- (iv) To develop models to predict the performance of HMA-UTW composites under repeated direct shear and flexural loading conditions.
- (v) Simulation of laboratory test results using finite element method.

An optimized cementitious FRC mix proportion for UTW was arrived using Taguchi method. Cylindrical HMA mixture specimens were casted using Superpave gyrator. Further, these specimens were subjected to various interface treatment techniques such as no treatment (NT), single groove (SG), double groove (DG), piercing and piercing with different percentage of bonding. A freshly prepared FRC mix were poured on the top of the interface treated HMA layer and allowed to cure for 24 hours. A direct shear test was conducted on all the interface treated specimens under static and dynamic loading conditions.

Using strain controlled compression testing machine HMA prism specimens with varying thickness of 50 and 75 mm were casted. Later, these specimens were subjected to different interface treatments. A freshly prepared FRC mix was poured on the top of the HMA prism specimens until a total thickness of 125 and 150 mm was achieved. Later, HMA-UTW prism composite specimens were subjected to the flexural test under static and dynamic loading conditions. A Finite Element (FE) model was performed to simulate the performance of UTW and HMA composites when subjected to direct shear and flexural loading conditions.

To assess the influence of various interface treatment techniques on the interface bond strength, laboratory studies were carried out and is shown in Fig. 1.3.

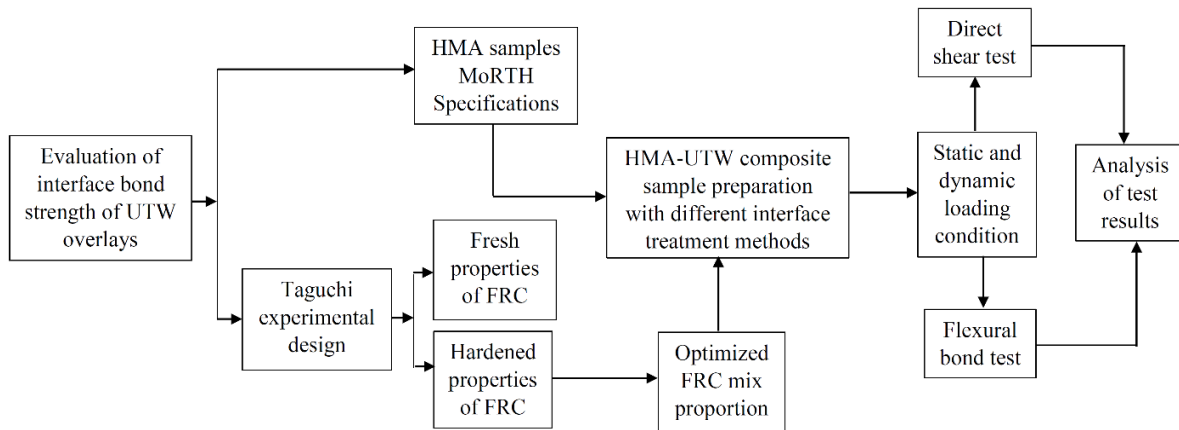


Fig.1.3 Flow chart for assessing the influence of various interface surface treatment techniques on interface bond strength of UTW overlays

1.3 THESIS ORGANIZATION

From the literature it can be seen that the existing concrete mix design for UTW overlays are predominantly perspective based, which would lead to the use of a higher amount of cement than needed. Subsequently increases the cost of construction and reduce the durability. Therefore an optimized supplementary cementitious FRC mix proportion is developed for UTW overlays and presented in Chapter 2.

Chapter 3 presents the effect of different interface treatment techniques on interface shear bond strength using direct shear test apparatus. The direct shear test was carried out under two different loading conditions namely, static at 7 and 28 days and repeated loading at 28 days. Displacement, interface shear bond strength, and k-modulus from static loading and number of cycles at failure with respect to displacement from repeated loading test were measured. The test results were analyzed to know the mode of failure i.e. either failure occurred in the HMA-UTW interface or the underlying HMA were discussed. A statistical regression model was performed to know the reduction in interface shear bond strength versus percentage of bonding in HMA-UTW composites.

In Chapter 4 the effect of HMA thickness on the flexural bond strength of UTW overlays when subjected to flexural loading are discussed. The HMA-UTW prism composite specimens with different percentage of bonding namely 50 and 100 % were subjected to flexural test and flexural fatigue test. Flexural bond strength and number of cycles to failure were calculated. The test results were analyzed to quantify the effective HMA thickness for placing UTW overlays. A two parameter Weibull distribution was performed to enumerate the probability of fatigue lives for HMA-UTW composites.

Chapter 5 describes the FE simulations using contact friction model in ANSYS software. The test results from Chapter 3 and 4 on the interface bond strength were used to perform the simulation.

Chapter 6 describes the conclusions, limitations applications and scope for future research.

CHAPTER 2

EVALUATION OF CEMENTITIOUS FRC MIXTURES FOR UTW OVERLAY

2.1 BACKGROUND

UTW is a relatively new technique emerged from Europe and the United States in the year 1980 (Risser et al. 1993; NCHRP 338 2004). In this technique, a very thin FRC of 50 to 100 mm is placed over existing HMA pavement. This reduction in thickness can be justified by using high quality and high strength concrete (Wu and Sheehan 2002). Several UTW are constructed over an existing asphalt layer using plain concrete as well as FRC and all these pavements have shown the reasonable effect on performance. While some of the authors and agencies have suggested typical concrete mix proportions for UTW overlays and are shown in Table 2.1. The mix proportions incorporated or suggested in the construction of UTW overlays represents prescriptive-based concrete mix proportions. Which can utilize higher amount of cement than needed and increases the cost of construction and reduce the durability of the mixture (Yurdakul et al. 2012). Therefore, an optimal mixture proportioning is needed that has to fulfill the desired concrete properties and to ensure the efficient use of cementitious materials, will be beneficial in improving the sustainability of UTW pavements.

Ground granulated blast furnace slag (GGBS) are by-products of metallurgical furnaces producing pig iron, steel, copper, nickel, and lead. GGBS, when mixed with cement, it undergoes pozzolanic reaction in the presence of lime and water medium, such as calcium hydroxide Ca(OH)_2 compound. At the end of the reaction of the GGBS and Ca(OH)_2 , the secondary cementitious phase will form such as C–S–H gel which gradually enhances the strength (Chen et al 2012). Several researchers have shown that the favorable effect of using GGBS in the concrete mixture. Hogen and Meusel (1981) studied the replacement of cement with 40%, 50%, and 60% GGBS and found that 7 days strength almost equal to the control mix and higher strength can be achieved thereafter.

Table 2.1 Typical UTW mix proportions

Ingredients	Speakman and Scott III (1996)	Indian Road Congress (IRC)-SP 76 2008	Roesler et al. (2008)	Mu and Vandebossche (2011)	Lin and Wang (2005)	Cho and Koo (2006)	Kumara et al (2005)	Rajan and Olek (2002)
Cement content (kg/m ³)	322	440	306-448	267-386	600	453.5	230	375
Coarse aggregate (kg/m ³)	696	947	1011-1161	NA	1007	946.9	816	995
Fine aggregate (kg/m ³)	617	596	594-724	704-764	666	747.5	597	745
Fiber (kg/m ³)	1.362	0.9	1.77-2.38	1.8-14.8	NA	NA	NA	10
W/C ratio	0.35	0.28-0.30	0.40-0.42	0.37-0.43	0.27	NA	0.28	0.36
Water (kg/m ³)	127	170	96-174	NA	152	165.1	60	160
Fly ash (kg/m ³)	NA	88	83	59-71	NA	NA	NA	70
GGBS	NA	Up to 70 %	NA	NA	NA	NA	NA	NA
Silica fume	NA	3 – 10%	NA	NA	NA	NA	NA	NA
Chemical admixture	5%	Up to 2%	NA	NA	1.8%	NA	1189 (mL)	3.9 liters/m ³
Slump (mm)	NA	25-50	NA	55-65	25	NA	87	63

Note: NA- Not Available

Using Bolomey and Feret strength equations (Oner and Akyuz 2007) studied the optimum usage of GGBS in the concrete. The compressive strength of the concrete increased for 50 to 55% replacement of cement with GGBS in concrete. The efficiency coefficient (k_e) of GGBS is more sensitive to the replacement rate and its efficiency is better than that of the cement at a later age (Abdelkader 2010).

However, the addition of GGBS not only enhances strength it can also increase the workability of concrete by replacing cement with 55% and 85% by its weight (Wainwright and Rey 2000). At lower water to binder ratio and replacing cement with GGBS in the range 30 to 60 % authors found that higher durability can be achieved (Cheng et al. 2005 and Hadjsadok et al. 2012).

In the early 1980s, North America and Europe started using silica fume (SF) systematically as a pozzolonic material in concrete (Galeota and Giammatteo 1989). Various authors have shown that SF has a positive effect on the mechanical properties of cementitious composites. Bentur and Goldman (1989) reported that concrete having SF content will show lesser shrinkage this is because of smaller weight loss on drying. By replacing cement with 15% to 20% of SF, the elastic modulus and toughness can be increased significantly (Khedr and Zeid 1994). Toutanji and El-Korchi (1995) studied the influence of SF on the compressive strength of mortar by partial replacement of cement by 16% and 25%. They concluded that the addition of SF greatly contributes to the increase in strength of mortar by improving the bond between cement and aggregate matrix. Authors (Poon et al. 1999; Barbhuiya et al. 2009; Erdogdu et al. 2011 and Bagheri et al. 2013) studied the properties of fly ash concrete with SF and reported that early age compressive strength and improved sorptivity can be achieved. Khorami and Ganjian (2013) observed that the samples with SF content having a lesser rate of losing load-bearing capacity compared to that of the control samples. Limbachiya et al. (2016) concluded that concrete with GGBS and SF had shown higher split strength than that of the control mix. However, the researchers have also indicated that the addition of SF to concrete reduces the ductility behavior (Xie et al. 1995 and Zhang et al. 2011). Therefore short fibers have been known and used for centuries to improve the ductility of concrete.

The fibers can be made from a natural material (asbestos, sisal, and cellulose) or are a manufactured product such as steel, glass, carbon, nylon, and polymer. The addition of fiber in concrete improves the toughness by transmitting the stress across the cracked section (Bentur 1989). The polypropylene fibers significantly delay the crack formation and limiting their extent (Haddad and Smadi 2004). Rasmussen and Rozycki (2004) suggested that adopting fibers in thin overlays minimizes the crack widths, reduce surface spalling, and increase wear resistance. The required concrete slab thickness can be reduced by the addition of macro-fibers (Altoubat et al. 2008; Roesler et al. 2008b). Cervantes and Roesler (2009) reported that fibers are expected to be beneficial as joint reinforcement in thin overlays and reduces deflections at joints and increase load transfer efficiencies. (Ozer et al. 2011) studied the toughness performance of the FFC mixture for UTW pavements. They concluded that high fiber and cement content in the FFC mixture will improve the design service life of UTW overlays. Zhang and Li (2013) studied the effect of polypropylene fiber on the durability of fly ash concrete with SF and concluded that fibers have more resistance to drying shrinkage and excellent durability on exposure to freeze-thaw cycling. Steel fiber improves the ductility, splitting tensile strength, flexural strength, and impact of the concrete (Nili and Afroghsabet 2010).

Fatigue refers to the phenomenon of rupture of a material when subjected to repeated loadings at a stress significantly less than the ultimate static strength. Consequently, concrete materials exhibit fatigue failure when stressed by bending, direct tension or compression, tension, or combinations of these (Mccal 1958). Flexural fatigue life of concrete is a major parameter in the design of concrete pavements for roads and airfields. After construction of these concrete pavements, it should carry million number of cycles of repeated loads from different vehicle configuration throughout its design life. Hence, highway engineers, have been aware of the need to understand the fatigue of concrete materials when subjected to repeated loads (Nordby 1958). Further, a number of studies have been carried out to evaluate the fatigue characteristics of plain concrete and FRC. Hilsdorf and Kesler (1966) studied the fatigue behavior of plain concrete subjected to repeated loads of varying magnitude. They found that fatigue life decreases with increasing magnitude of the higher stress

level. The flexural fatigue life distribution for plain concrete will vary with applied stress Oh (1991). Based on acoustic emission activity Jun and Stang (1998) studied the fatigue life distribution for different fiber types. They concluded that steel fiber concrete can accumulate more damage than the plain concrete and polypropylene FRC will improve fatigue strength marginally than that of the steel fiber. A probabilistic analysis was carried out by Singh and Kaushik (2001) and Singh et al. (2005) to predict the flexural fatigue strength for the different volume fraction of steel fibers incorporated in the concrete. Authors reported that addition of 1% fiber dosage in concrete increase the flexural fatigue performance. Goel et al. (2012) conducted four point flexural fatigue test to evaluate the fatigue life distribution of plain and self-consolidating FRC. The fatigue life corresponding to a 10% probability of failure, self-consolidating FRC had shown excellent fatigue performance at higher traffic load.

The mix proportions adopted for UTW overlays in the literature are prescriptive-based concrete mix proportions (refer Table 2.1). However, most of the work related to cementitious concrete available in the literature are based on the combination of cement, fly ash and SF. Research works on experimental studies of cement, GGBS, SF and polyester fiber under static and fatigue loading for UTW overlays are scarce in the literature. Therefore, a laboratory experimental work was carried out to determine the optimum mix proportion for sustainable UTW pavements. A simplified concrete mix design approach and Taguchi method were adopted to determine the optimum mix proportion. In addition, a simple and qualitative tool called box test were carried out to determine the impact of different FRC mixture variables for slip formed pavement mixtures. In order to achieve the optimum mix proportion for UTW overlays two control and eighteen FRC mixtures were prepared and the mechanical properties were evaluated. Based on the analysis of test results an optimum concrete mixture proportion was selected, and then flexural fatigue test was conducted. A statistical method and two-parameter Weibull distribution have been incorporated to evaluate the fatigue life distribution.

2.2 EXPERIMENTAL STUDY

2.2.1 Materials and Research Methodology

The concrete mixtures were prepared using Ordinary Portland Cement (OPC-43 Grade) conforming to Indian Standard (IS) 8112-1989, GGBS of IS 12089-1987, and SF of IS 15388-2003. A synthetic Recron 3s polyester fibers were used. The chemical composition and physical properties of cement, GGBS, and SF are shown in Table 2.2. The physical properties of Recron 3s polyester fibers are shown in Table 2.3.

Table 2.2 Properties of cement, GGBS, and SF (source: M/s. Concrete Solutions, Mangaluru)

	Cement	GGBS	SF
Chemical composition (%)			
CaO	63	41	-
SiO ₂	20	35	88.2
Al ₂ O ₃	6	11	-
Fe ₂ O ₃	3	1	-
Physical properties			
Loss of ignition	-	0.04%	2.8%
Specific gravity	3.14	2.8	2.2
Insoluble residue	0.5	0.3	-
Bulk density (kg/m ³)	1400	1200	601
Specific surface area (m ² /kg)	340	370	22000

Table 2.3 Physical properties of fiber (source: source: M/s. Concrete Solutions, Mangaluru)

Properties	Results
Cross section	Triangular
Form	Monofilament(Micro)
Length (mm)	12
Aspect ratio(l/d)	320 and 480
Specific gravity	1.36
Tensile strength (MPa)	578
Modulus of elasticity (MPa)	17240
Melting point	>250 (°C)

The locally available natural river sand as fine aggregate and crushed granite as coarse aggregate were used. UTW overlay have a thickness less than or equal to 100 mm, a nominal maximum size of 20 mm was preferred. The water absorption and saturated surface dry specific gravity of fine aggregate and coarse aggregate values are 1.1% and

2.53 and 1.0% and 2.68 respectively. From the literature (Yurdakul et al. 2012 and Talor et al. 2015) the fine aggregate-to-total aggregate ratio was selected as 0.39. The selected fine aggregate ratio of 0.39 and 0.61 coarse aggregates was checked by plotting the data in an IS 383-1970 and shown in Fig. 2.1. This combination could be the best aggregate blend that can be achieved with the materials available. Therefore 0.39 of fine aggregate and 0.61 of coarse aggregate in the total aggregate system were considered in the present study.

The volume of voids (V_v) refer to the space between the compacted combined aggregates. The bulk density and V_v were determined as per ASTM C29 (2003). The bulk density of the combined aggregate was 2031 kg/m^3 and the percentage of volume voids for combined aggregate was $V_v = 21.9\%$. Further, paste system was selected not only to fill the voids between the aggregate particles but also to cover the aggregates and separate them to reduce the interparticle friction between aggregates, when the mixture in fresh state. Here paste volume includes the volume of water and cementitious material (V_p). The calculated V_v (%) and V_p (%) for different mixtures are tabulated in Table 2.6.

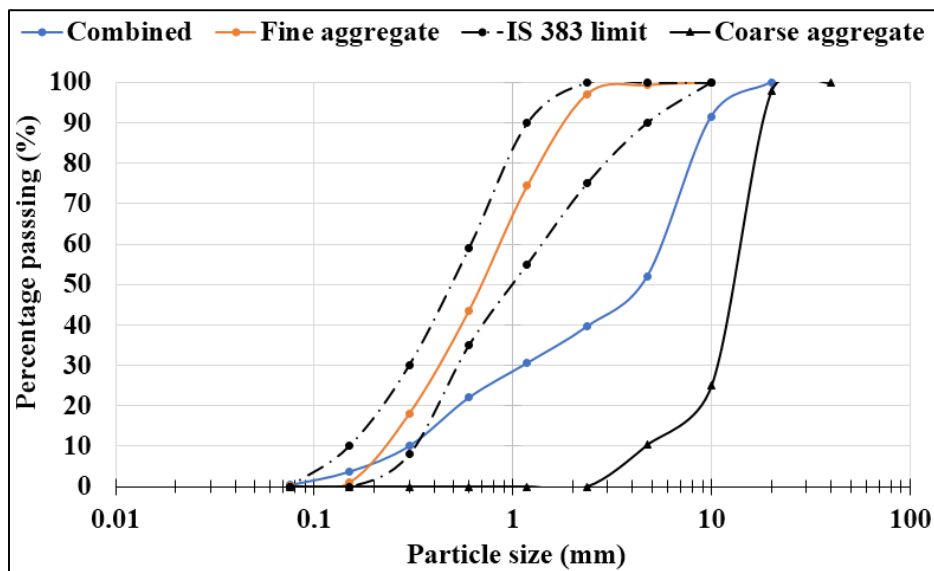


Fig. 2.1 Combined gradation curve

Chloride free Naphthalen Sulfonate (Conplast SP430) has been added to improve the workability of the mixture, without affecting the other concrete parameters such as segregation, ultimate strength and concrete permeability. Superplasticizer

Conplast SP430 is a 40% solid based super-plasticizer conforming to IS: 9103-1999. In order to achieve desired slump of 25 to 50 mm the amount of Conplast SP430 was varied up to 1.8% by weight of binder.

Initially fresh and hardened properties were carried out to obtain an optimum mix proportions for UTW overlays. Later, the optimized mix proportion was subjected to repeated load test. The research methodology is shown in Fig. 2.2.

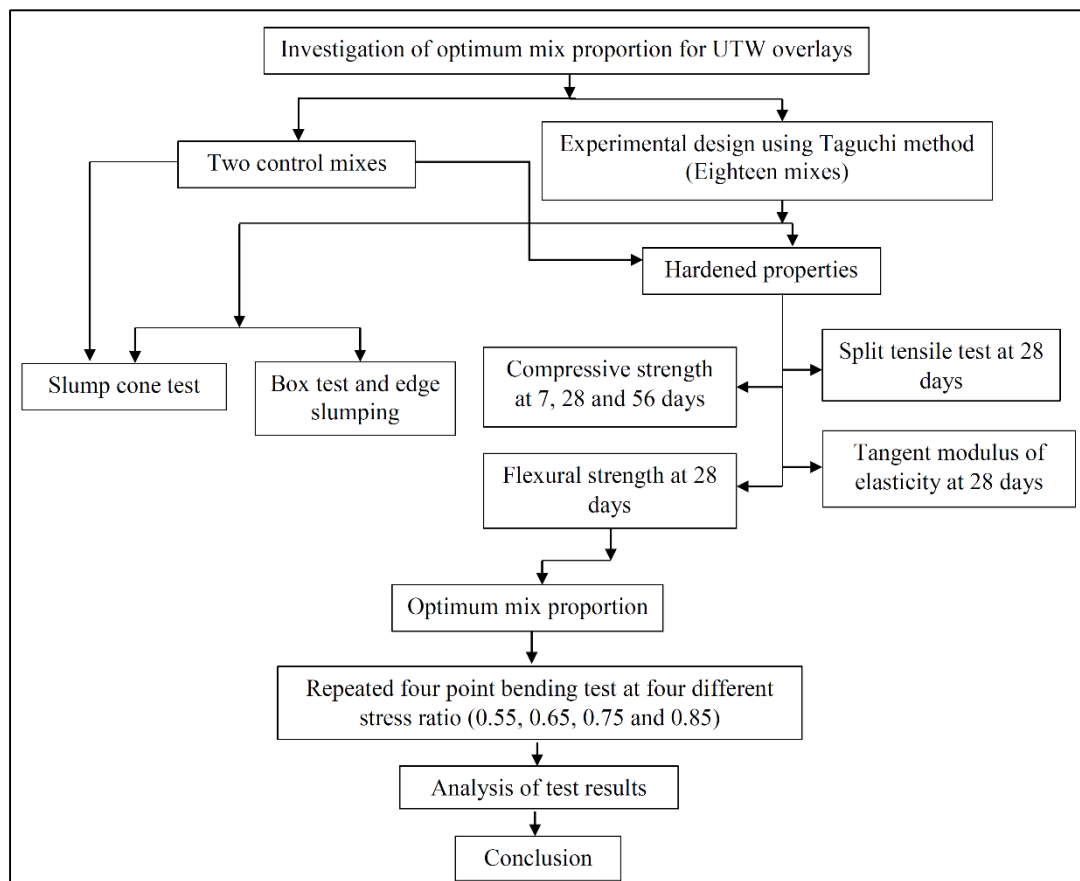


Fig. 2.2 Research methodology

2.2.2 Mixture Design and Sample Preparation

According to IRC SP: 76 2008 for UTW mixture the cement content and water/binder (w/b) ratio could be varied from 350 kg/m³ to 430 kg/m³ and 0.28 to 0.32, respectively. The present study includes two series of cement content of 350 and 430 kg/m³ with w/b of 0.32. The cement content was replaced with GGBS and SF in 20%, 40% and 60% and 4%, 8% and 12% by weight of cement. The fibers were added in 0.25%, 0.35% and 0.45% respectively. Hence two control and eighteen FRC mixture design were carried

out as per IS 10262-2009. The concrete mix design for FRC are described in Appendix A.

2.2.2.1 Taguchi method

Present research work includes Taguchi method of experimental design for the optimization of mix proportions to achieve better performance quality and keeping the experimental cost at the minimum level. The advantages of this method are (i) it minimizes the variability around the target (ii) the optimum levels determined from the laboratory can also be reproduced in full-scale production (Shi et al. 2015). Taguchi designed standard orthogonal arrays to know the real-time and independent effect of two or more parameters on the response variable using a minimum number of tests (Taguchi 1990). Further, a loss function is defined to calculate the deviations between the experimental value and the desired value. These loss functions are transferred into a signal-to-noise (S/N) ratio. There is several (S/N) ratio available depending upon the type of characteristics. For each type of characteristic S/N ratios can be calculated as shown in Eq. (2.1) to Eq. (2.3) (Taguchi 1990). Based on the process characteristic authors have adopted signal-to-noise (S/N) ratio function to evaluate the optimum value (Hascalik and Caydas 2008; Ozbay et al. 2009 and Kelestemur et al. 2014). Therefore, present study includes Eq. (2.2) for flexural strength at the age of 28 days.

1. Lower is the better characteristics

$$S/N = -10 * \log_{10} \left(\frac{1}{n} \sum_{i=1}^n Y_i^2 \right) \quad (2.1)$$

2. Higher is the better characteristics

$$S/N = -10 * \log_{10} \left(\frac{1}{n} \sum_{i=1}^n \frac{1}{Y_i^2} \right) \quad (2.2)$$

3. Nominal is the better characteristics

$$S/N = -10 * \log_{10} \left(\frac{1}{n} \sum_{i=1}^n (Y_i - Y_0)^2 \right) \quad (2.3)$$

However, in full factorial experiment method, four parameters at three levels would require 81 runs, whereas in Taguchi method reduced the number of tests to 18 runs ($L_{18} (4*3)$). The L_{18} orthogonal array is shown in Table 2.4. The control factors, levels and mixture design of all group are presented in Table 2.5 and Table 2.6.

Table 2.4 Taguchi method of orthogonal arrays [L18 (4*3)] of the experimental design

Group	Mix ID	Cementitious content	GGBS	SF	Fiber
Group A	T1	1	1	1	1
	T2	1	1	2	2
	T3	1	1	3	3
	T4	1	2	1	1
	T5	1	2	2	2
	T6	1	2	3	3
	T7	1	3	1	2
	T8	1	3	2	3
	T9	1	3	3	1
Group B	T10	2	1	1	3
	T11	2	1	2	1
	T12	2	1	3	2
	T13	2	2	1	2
	T14	2	2	2	3
	T15	2	2	3	1
	T16	2	3	1	3
	T17	2	3	2	1
	T18	2	3	3	2

Table 2.5 Introduced levels for each factor in Taguchi experimental design

Factors	Unit	Level 1	Level 2	Level 3
Cementitious content	kg/m ³	350	430	350/430
GGBS	wt. %	20	40	60
SF	wt. %	4	8	12
Fiber	wt. %	0.25	0.35	0.45

Table 2.6 Details of UTW mix proportions used for control mixtures and Taguchi optimization

Group	Mix ID	Cement (kg/m ³)	GGBS (kg/m ³)	SF (kg/m ³)	Fiber (kg/m ³)	Water (kg)	FA (kg/m ³)	CA (kg/m ³)	volume of voids (Vv) %	volume of paste (Vp) %	Vp/Vv
Control mix	C1	350	0	0	0	112	746	1236	21.9	18.90	86.32
	C2	430	0	0	0	138	696	1153	21.9	23.50	107.31
Group A	T1	266	70	14	0.665	112	746	1236	21.9	18.90	86.32
	T2	252	70	28	0.882	112	746	1236	21.9	18.90	86.32
	T3	238	70	42	1.071	112	746	1236	21.9	18.90	86.32
	T4	196	140	14	0.490	112	746	1236	21.9	18.90	86.32
	T5	182	140	28	0.637	112	746	1236	21.9	18.90	86.32
	T6	168	140	42	0.756	112	746	1236	21.9	18.90	86.32
	T7	126	210	14	0.441	112	746	1236	21.9	18.90	86.32
	T8	112	210	28	0.504	112	746	1236	21.9	18.90	86.32
	T9	98	210	42	0.245	112	746	1236	21.9	18.90	86.32
Group B	T10	327	86	17	0.817	138	696	1153	21.9	23.50	107.31
	T11	310	86	34	0.774	138	696	1153	21.9	23.50	107.31
	T12	292	86	52	1.023	138	696	1153	21.9	23.50	107.31
	T13	241	172	17	0.842	138	696	1153	21.9	23.50	107.31
	T14	224	172	34	1.006	138	696	1153	21.9	23.50	107.31
	T15	206	172	52	0.516	138	696	1153	21.9	23.50	107.31
	T16	155	258	17	0.696	138	696	1153	21.9	23.50	107.31
	T17	138	258	34	0.344	138	696	1153	21.9	23.50	107.31
	T18	120	258	52	0.421	138	696	1153	21.9	23.50	107.31

2.2.2.2 Sample preparation and test methods

The rotating drum-type laboratory mixer was used in the production of FRC mixes. The FRC specimens were cast and covered with plastic sheets to maintain the moisture for the first 24 hours. After the initial curing period of 24 hours, the specimens were demoulded and kept in curing tank with 25 ± 2 °C for 7, 28 and 56 days. As per IS 10086-1982; three types of moulds, namely, the standard mild steel cubes of size 150 mm, cylindrical steel moulds measuring 150 mm diameter and 300 mm height and rectangular prism shaped steel moulds of size 100 mm × 100 mm × 500 mm, were used for the moulding of test specimens for determining the compressive strength (180 samples), split tensile strength (60 samples), modulus of elasticity (60 samples) and flexural strength (120 samples) of the designed concrete respectively. Further, all these tests were carried out as per IS-516 1991.

Among these mixtures, the original designed concrete strength grade was M40, and the slump of fresh concrete was controlled between 25 mm to 50 mm by superplasticizer (1.2% to 1.8% by weight of binder). Normally to know the workability parameter for any paving mixture commonly assessed test method is slump cone test, even though the test is of limited value and it does not reflect the characteristic of slip form paver. Hence, the present study includes box test method to evaluate the workability of FRC mixtures for slip formed pavements (i.e. the response of the FRC mixtures to vibration and simultaneously holding an edge). Cook et al. (2013) developed the box test method and evaluated the vibratory response of a concrete mixture and vertical edge slumping.

In this study box test was conducted for all the concrete mixtures under fresh state using 300 mm x 300 mm x 300 mm plywood box. The fresh concrete was uniformly hand scooped into the box up to a height of 200 mm. A 25 mm square head needle vibrator having 12,500 vibrations per minute were used to consolidate the mixtures. The needle vibrator was inserted into the center of the box and allowed to vibrate for three seconds at the bottom and top of the mixtures. The side clamps and side walls were removed and the response of concrete mixtures to vibrations was assessed by the surface voids (visually observed on the sides of the box). The average surface voids for each of the four sides was estimated with a number ranking. The

average of four side's surface voids from visual ranking was given to each test and it is shown in Table 2.7. Further, top or bottom edge slumping were measured using a steel scale. The box test apparatus is as shown in Fig. 2.3.

Table 2.7 Box test ranking for different surface voids

Type of surface voids	Ranking
Surface voids less than 10%	1
Surface voids less than 10-30%	2
Surface voids less than 30-50%	3
Surface voids greater than 50%	4

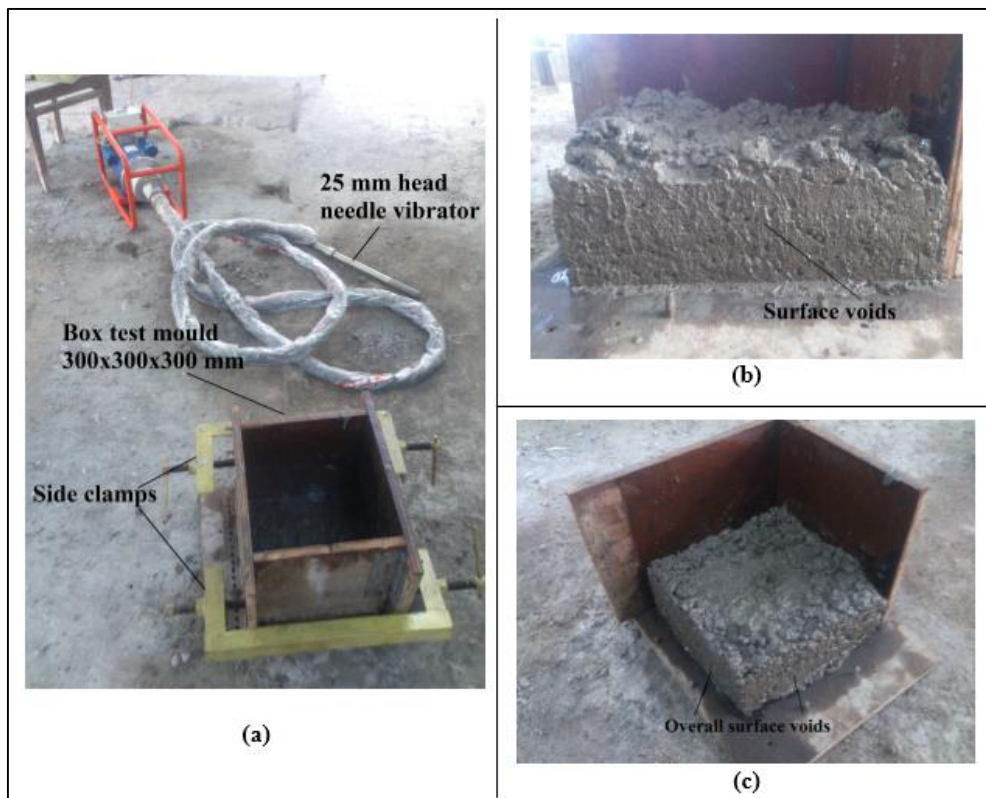


Fig. 2.3 Illustrates the surface voids ranking apparatus (a) Box test apparatus and needle vibrator (b) & (c) are surface voids of T17 mix

The fatigue test was performed using four point bending test method on the samples of size 100 mm × 100 mm × 500 mm in a 5000 kg capacity repeated load testing system. A frequency of 5 Hz with different stress ratios 0.55, 0.65, 0.75 and 0.85 was applied. The ratio is the load value applied in repeated load test to the maximum failure load value obtained from the static strength test. The loading waveform is a semi-sine wave and this waveform was relatively close to the traffic loading applied on

the pavement. For each load cycle, the applied stress was measured and the test was stopped once the permanent displacement reached.

Further, for the optimized mix proportion, three prism samples were casted and tested under static flexural condition. The maximum failure load obtained for each sample were recorded. Since concrete is a heterogeneous material, the flexural fatigue test data are scattered, even though the stress ratios are same. Therefore, for each failure load obtained for three samples during the static test were subjected to four different stress ratio and for each stress ratio, four samples were tested. The number of cycles required to failure the samples under different stress conditions was noted as fatigue life N . Since fatigue testing is time-consuming and a number of samples were proposed to be tested, an upper limit on the number of cycles to be applied were selected as 25 million. The test was stopped either sample failed within the upper limit or once it reaches the limit whichever is occurred first.

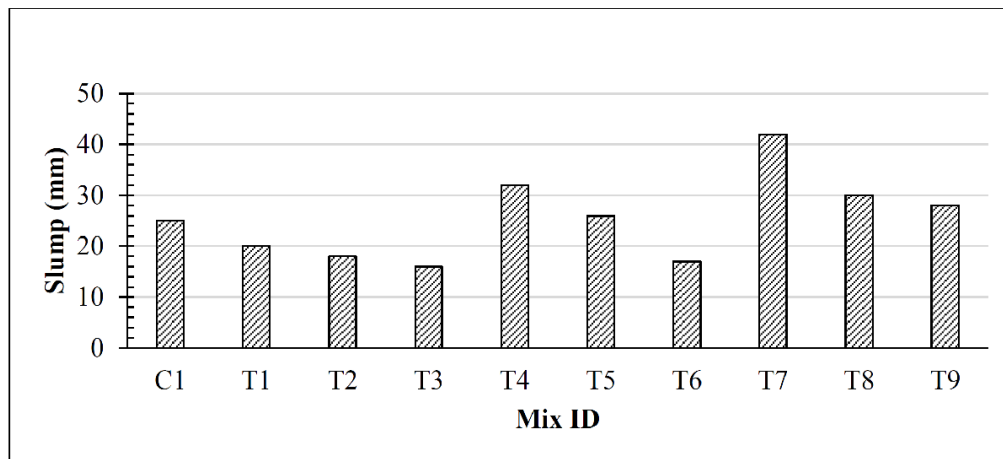
2.3 FRESH PROPERTY

2.3.1 Slump Cone

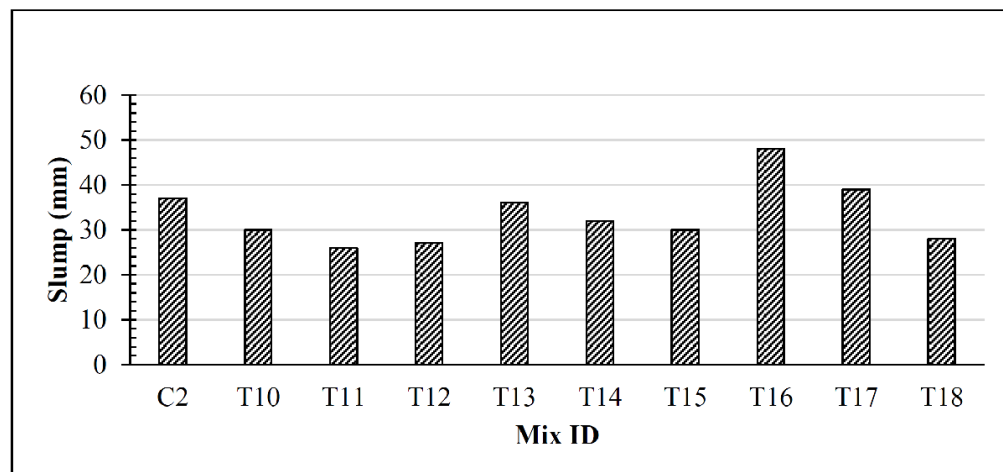
The test measures the downward movement of the concrete caused by its self-weight. The fresh property of two control mixtures and eighteen FRC mixes are shown in Fig. 2.4. The slump values for the control mixtures C1 and C2 are 25 mm and 37 mm respectively. It was observed from the Fig. 4, that in group A T4, T5, T7, and T8 mixtures had a higher slump value of 32, 26, 42 and 30 mm compared with other mixtures. In group A among nine mixes, only four mixture had shown better slump value and remaining mixes had a lower slump value than that of the control mix C1. From the Fig. 2.4, it was observed that T4 and T7 had a higher slump value of 32 and 42 mm than the control mix C1.

The lower slump value of 16 and 17 mm for T3 and T6 mixtures than the control mix C1 were observed. The decrease in slump value might be an increase in fiber dosage as well as SF content in the concrete mixture. Increase in fiber dosage consequences the snarling of fibers, which results, difficulty in dispersing the fiber in concrete mixture and create stronger interfacial fiber–matrix bond in the concrete. Also due to the presence of a high specific surface area of SF, increases the stickiness and viscosity of

the concrete mixture and finally restricts the distribution of the cement matrix. The percentage of slump value increased for the T7 mix in group A is around 68% compared to control mix C1. This may be due to lesser fiber dosage and SF content. In group B all the mixes had a slump value in the range of 26 to 48 mm and all these mixes were satisfying the slump values required for UTW pavements. This higher slump value in group B may be due to higher paste content compared with group A mixtures.



(a)









(b)

Fig. 2.4 Slump cone results for control mixes, (a) group A and (b) group B mixtures






2.3.2 Surface Voids Ranking

The overall surface voids for all the mixtures are shown in Fig. 2.5. From Fig. 2.5, it can be seen that box test ranking of 1 and 2 for the mixes T4, T5, T7, T8 and T9 in group A. However, in group A among nine mixes only five had shown box ranking of

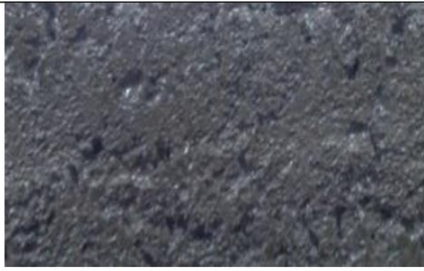
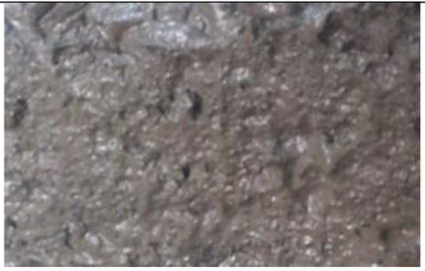

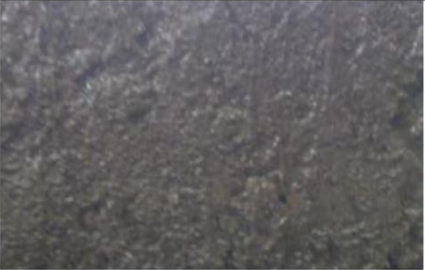


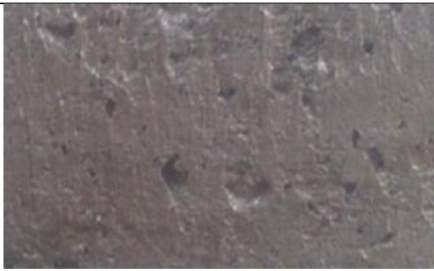
1 and 2 compared to the other mixes. This may be due to the influence of well-graded aggregates having a low void content, which minimizes the paste requirement. Further, all the void content is filled by paste, which results in the excess amount of paste and is helpful to coat the aggregate particles in the mix. This creates a gap between solid particles and concurrently reduces the overall surface voids. From Fig. 2.5, it can be seen that T1, T2, T3 and T6 in group A had box ranking of 3 and 4. This might be due to decreased paste thickness on the aggregate particle surface. This increases the degree of friction and interlocking of the solid particles by reducing the distance between the aggregate particles in the mix. Hence, overall surface voids increase by making the mixture too difficult in consolidation. Also, may be due to the effect of higher fiber dosages and SF content in the mixes. Higher fiber dosage results in poor fiber-matrix interaction or the formation of the multifilament structure due to insufficient dispersing of fibers in the concrete mixture. Due to the high specific surface area of SF, it leads to a reduction in workability of the concrete even though all the mixes are having the same volume of paste content. In group B all the mixes had shown box ranking of 1 and 2 except for the mix T10. The box ranking of 1 and 2 in group B may be due to higher paste content than that of group A. Hence, the minimum amount of paste is required between the aggregate particles to achieve desired surface voids for lesser vibration. It was observed that for the same amount of paste content T7, T13, T16, and T17 had shown edge slumping after removing the side clamps. Therefore, physical property of mineral admixture will play a significant role in the workability of concrete mixes even though all the mixes are having same paste content. Hence, type and amount of mineral admixture should be optimum in the concrete mixture.

Group A	
	
Mix ID T1, Box Ranking 4	Mix ID T2, Box Ranking 4
	
Mix ID T3, Box Ranking 4	Mix ID T4, Box Ranking 1
	
Mix ID T5, Box Ranking 2	Mix ID T6, Box Ranking 3

(a)

Group A	
	
Mix ID T7, Box Ranking 1 and edge slumping were observed	Mix ID T8, Box Ranking 1
	
Mix ID T9, Box Ranking 1	
Group B	
	
Mix ID T10, Box Ranking 3	Mix ID T11, Box Ranking 2

(b)

Group B	
	
Mix ID T12, Box Ranking 2	Mix ID T13, Box Ranking 2 and edge slumping were observed
	
Mix ID T14, Box Ranking 1	Mix ID T15, Box Ranking 1
	
Mix ID T16, Box Ranking 1 and edge slumping were observed	Mix ID T17, Box Ranking 1 and edge slumping were observed
Group B	
	
Mix ID T18, Box Ranking 2	

(c)

Fig. 2.5 (a), (b) and (c) represents overall surface void ranking for eighteen mixes

2.4 HARDENED PROPERTY

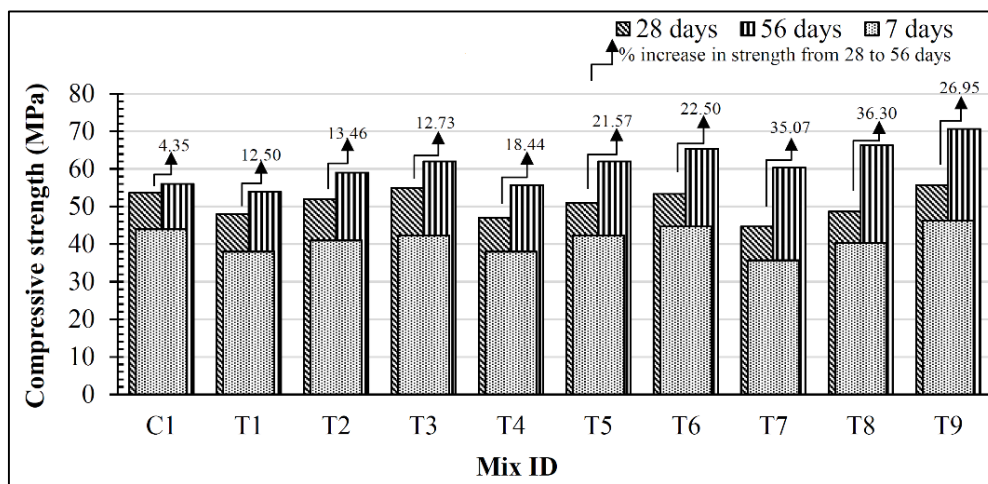
2.4.1 Compressive Strength

The variations of the compressive strength test results at the ages of 7, 28 and 56 days for control, group A and group B mixtures are illustrated in Fig. 2.6. From the Fig. 2.6, the increase in compressive strength for the T9 mix is 5%, 4% and 27% at 7, 28 and 56 days, in group A respectively, compared to the control mix C1. The mixture T18 in group B had a compressive strength of 2%, 2% and 29% at 7, 28 and 56 days, respectively which is higher than the control mix C2. It was observed from Fig. 2.6 that there is a significant increase in the strength from 28 days to 56 days in all the mixes. This might be due to concrete mixtures are blended with GGBS will hinder the early age strength. Because GGBS had a low degree of hydration at early ages compared with OPC, but in a later stage, it will exhibit strength equal or more than the control mixtures (Khokhar et al. 2010). Further, this behavior depends upon the dosages of GGBS in the concrete mixture (Abdelkader et al. 2010).

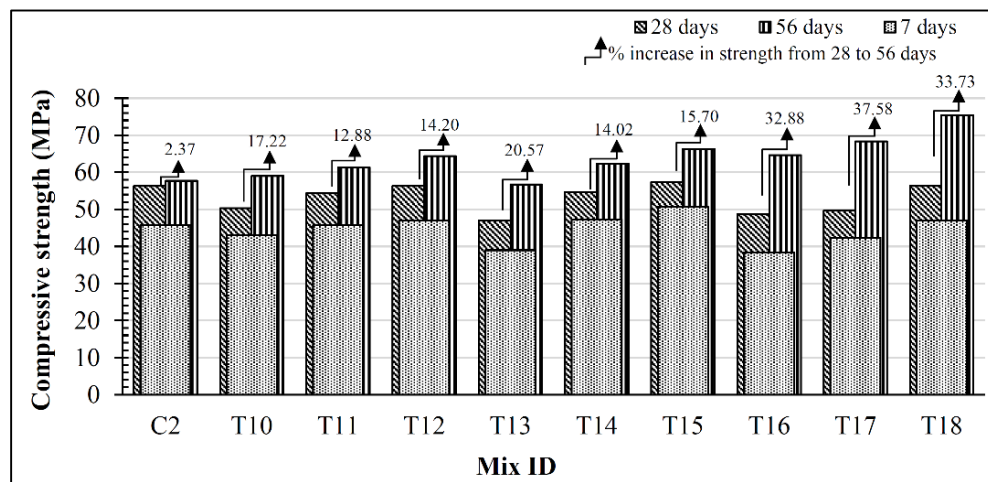
It can be seen from Fig. 2.6, two out of nine mixtures from group A and three out of nine mixtures in group B were developed the strength higher than that of control mixtures at 28 days. This may be due to the reaction of SF with calcium hydroxide liberated during hydration of cement. Further, this results in the formation of secondary calcium silicate hydrate that fills pore space formed during hydration reaction. This pozzolanic reaction makes the FRC matrix with SF stronger than the control mix. Also, it might be due to the presence of high dosage of SF and its specific surface area greater than the cement and GGBS that fills the void space exist between the particles of cement and GGBS and makes the concrete mixture denser. Further, in some of the mixtures, it can be seen that increasing paste content slightly decreased the compressive strength, this might be not all the cementitious materials participating in the pozzolanic reaction.

It can also see from Fig. 2.6 that mixtures T2 to T9 in group A and T10 to T12 and T14 to T18 mixes in group B had shown higher compressive strength than that of the control mixes at the age of 56 days respectively. This fact clearly shows that incorporation of Supplementary Cementitious Materials (SCMs) in the mixture has a positive effect on long-term compressive strength development. Further, it was

observed that the addition of fiber in concrete mixture reduce the crack enlargement compared to the control mixture. The results indicate that the pozzolanic properties of GGBS, SF and the crack restriction effect of polyester fiber may enhance the compressive strength of concrete considerably. During testing, it was noticed that the mixes having higher fiber dosages had a ductile failure i.e., the specimen is still intact after failure. This fact may due to the strong bond between polyester fibers and the concrete, which prevents the concrete from sudden failure (Han et al. 2012). Hence, there is a significant change in the failure mode of polyester FRC compared with the control mix.



(a)



(b)

Fig. 2.6 Compressive strength test results for control, (a) group A and (b) group B mixtures

2.4.2 Flexural Strength

The flexural strength test results at the ages of 7 and 28 days for control, group A and group B mixtures are presented in Fig. 2.7. From the Fig. 2.7, it was observed that by introducing fibers into the ternary mixture increased the flexural strength of all the mixes compared to the control mixes. The increase in flexural strength by 86% and 64% for T6 mixture in group A and 77% and 59% for T14 mixture in group B at the ages of 7 and 28 respectively, compared with the control mixes. This may be due to the combined effect of polyester fiber and SF dosage in the concrete mixture, yields a substantial improvement in the flexural strength for the FRC mixture. This may be endorsed to the fact that SF increases the strength of the transition zone in concrete, adhesive of the cement matrix-fiber, mortar aggregate interface area and finally improve the structural properties of the concrete. In addition to this, the dosage of polyester fibers acts as a crack arrestors. Hence, a substantial increase in flexural strength can be achieved, when polyester fiber and SF are used together, thereby more fully exploiting the advantages of SF and polyester fibers.

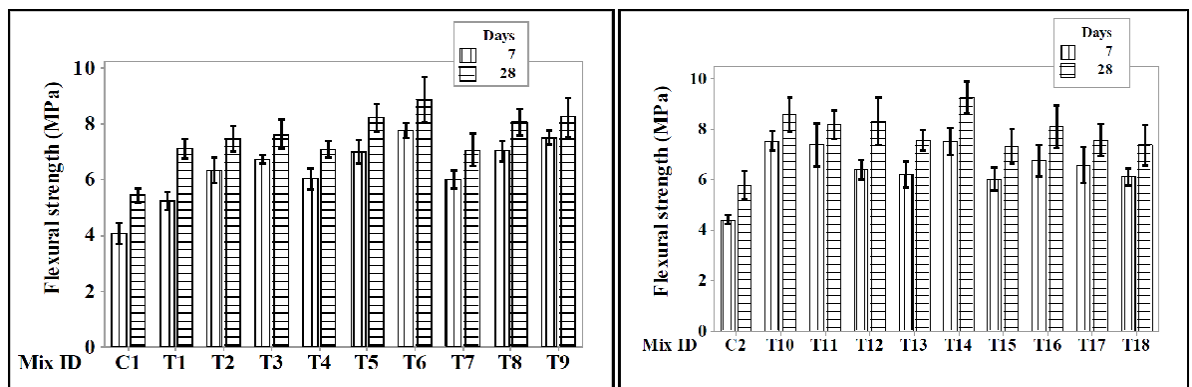


Fig. 2.7 Flexural strength test results for control, group A and group B mixtures

2.4.3 Split Tensile

The split tensile strength test results at the age of 28 days for control mixtures, group A and group B are shown in Fig. 2.8. From the Fig. 2.8, it was observed that the mixes T8 and T16 from group A and group B had shown 39% and 22% higher split strength than that of the control mixes. This may be due to the effect of polyester fibers in the concrete mixtures. However, it was observed that due to the effect of random orientation of polyester fibers in the concrete mixture, the splitting occurred and sustained. This

behavior influence the matrix can sustain entire load by transferring the stress from the matrix to the fiber through the connecting fibers across the split portions. Therefore, stress transfer improved the tensile strain capacity and finally increases the split tensile strength of the polyester FRC mixtures. The increased strength may also due to the formation of the extra dense calcium-silicate-hydrate gel obtained by the addition of SF. This improves the bond between fiber and matrix. From the Fig. 2.8, the mixes T1, T4 and T9 in group A and T11, T15 and T17 in the group had shown lesser splitting strength compared with the other mixes in group A and group B this may due to less number of polyester fibers intersecting across the fracture surfaces. Hence, the polyester fiber dosage and its isotropic behavior (i.e., random orientation in all the directions) in polyester FRC mixture may enhance the splitting strength compared to the control mixture.

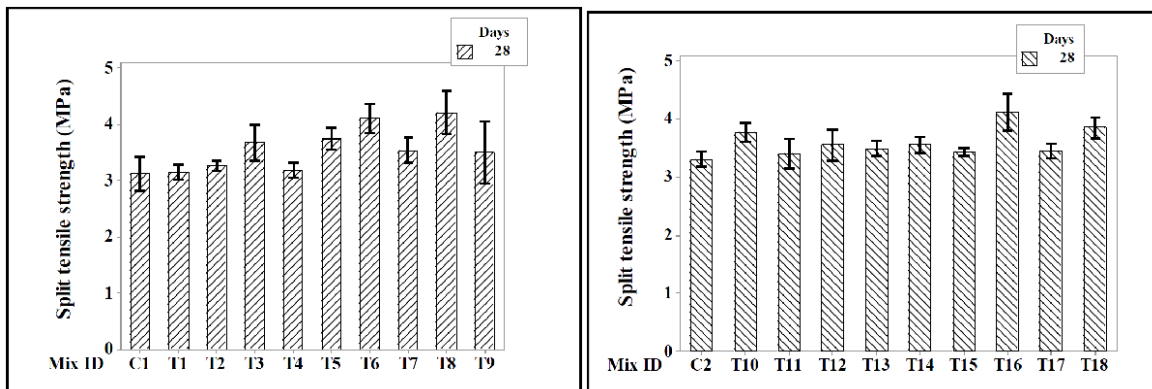


Fig. 2.8 Split tensile strength test results for control, group A and group B mixtures

2.4.4 Tangent Modulus

The modulus of elasticity test results at the age of 28 for control mixture, group A and group B are presented in Fig. 2.9. From the Fig. 2.9, it was observed that the mixes T6 in the group A and T12 in group B are having high modulus value than the control mixes. These values showed that polyester FRC mix T6 in group A and the mix T12 in group B produced about 6% and 3% of modulus values respectively, compared to the control mixes. The increment in results may due to the addition of SF enhance the cohesiveness of cement matrix (Alengaram et al. 2010) and fiber dosage subsidized to the crack bridging (Yap et al. 2013). Therefore, the combined effect of SF and polyester

fiber in the concrete mixture decreased the strain induced under compression loadings, and subsequently improved the modulus values of the mixes respectively.

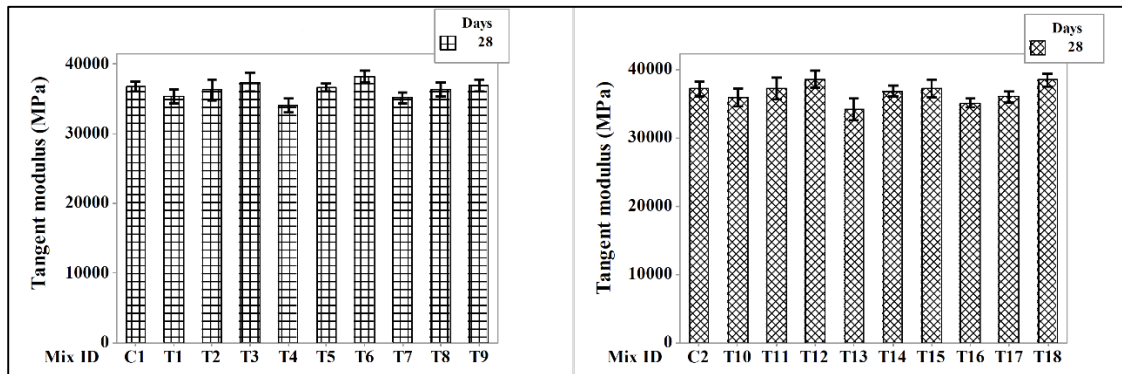


Fig. 2.9 Tangent modulus for control, group A and group B mixtures

2.4.5 Data Analysis of the *S/N* Ratios for Optimum Mix

The results obtained from experiments are analyzed as per Taguchi method using MINITAB v17, the mix proportions are set to best possible levels for the maximization of flexural strength. Table 2.7 shows the mean *S/N* ratios for 28 days flexural strength of UTW mixes. The optimal performance at the age of 28 days for flexural strength of UTW mixes was obtained at 0.45% fiber (Level 3), 8% SF (Level 2), 430 kg/m³ (Level 2) and 40% GGBS (level 2) settings. Fig. 10, represents the *S/N* ratio for the four control factors A, B, C and D studied at three levels for 28 days flexural strength values. Hence, T14 mix in group B is the optimum mix obtained from the Table 2.8.

Table 2.8 Response table mean signal-to-noise (*S/N*) ratio for flexural strength factor and significant interaction

Control factors	Unit	Level 1	Level 2	Level 3	Delta	Rank
Mean <i>S/N</i> ratio						
Cementitious Content (CC) (A)	kg/m ³	17.90	18.24 ^a	-	0.34	3
GGBS (B)	wt. %	18.08	18.19 ^a	17.95	0.24	4
SF (C)	wt. %	17.78	18.32 ^a	18.12	0.54	2
Fiber (D)	wt. %	17.68	17.84	18.70 ^a	1.02	1

^aOptimum level

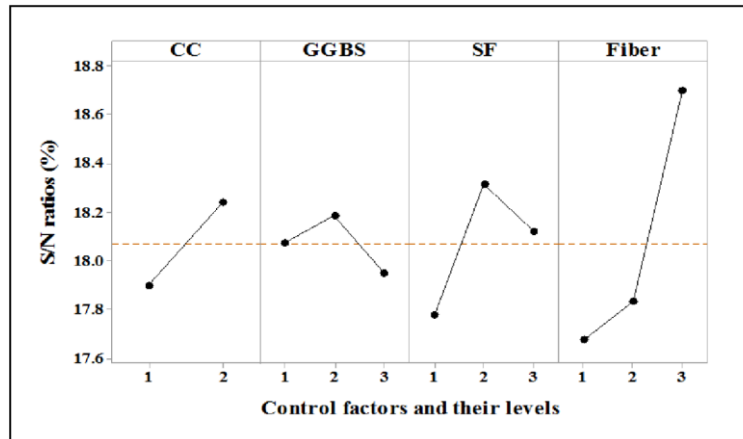


Fig. 2.10 S/N ratios of 28 days flexural strengths

2.4.6 Test Results for Optimum Mixture

For verifying the optimum mixture proportion results, FRC samples were casted and tested in accordance with the optimum condition as shown in Table 2.8. The fresh properties such as box test ranking and slump value of 1 and 35 mm were achieved. The average compressive strength at the ages of 7, 28 and 56 are 47, 56 and 64 MPa respectively, split tensile strength and young's modulus of elasticity at the age of 28 are 3.54 MPa and 37552 MPa is achieved, more than the control mixtures. The flexural strength test results for FRC are shown in Table 2.9.

Table 2.9 Static flexural failure load of individual samples

Specimen No.	Flexural Load (kN)
1	20.5
2	22.0
3	19.5

2.5 FLEXURAL FATIGUE LIFE

The test results for static and dynamic conditions are tabulated in Table 2.9 and Table 2.10. Since at 0.55 stress level all the samples were reached the upper limit, it was not considered for the analysis.

2.5.1 Analysis of Fatigue-Life Distribution Using Statistical Method

The present study incorporated a statistical method to evaluate the fatigue life distribution. Then independent variable X for applied stress level and the dependent

variable number of cycles at failure Y were considered. A linear regression analysis was performed using MS EXCEL v13 to calculate the regression coefficients and uncertainties for Y . Using LINEST function for X and Y values the slope (m), Standard Error SE_m , R^2 , intersect value (b), SE_b , SE_y , and degrees of freedom (n) are obtained respectively. At 95% confidence interval (CI) $\alpha = 0.05$ $t_{\alpha,y}$ -value and ΔY_{CI} were calculated and the equation for ΔY_{CI} is as follows.

$$\Delta Y_{CI} = \frac{t_{\alpha,y} \cdot SE_y}{\sqrt{n+2}} \quad (2.4)$$

Then $Y_{predicted}$ values were calculated using the Eq. (2.5)

$$Y_{predicted} = mX + b \quad (2.5)$$

Using Eq. (2.4) and Eq. (2.5) the both minimum and maximum values can be obtained for number of cycles at failure. The experimental data, calculated minimum and a maximum number of cycles at failure are plotted against applied stress and is shown in Fig. 2.11. It can be seen from the Fig. 2.11 that, as the stress level increased fatigue performance decreased. The R^2 value of 0.9025 represents the good correlation between the applied stress and number of cycles at failure.

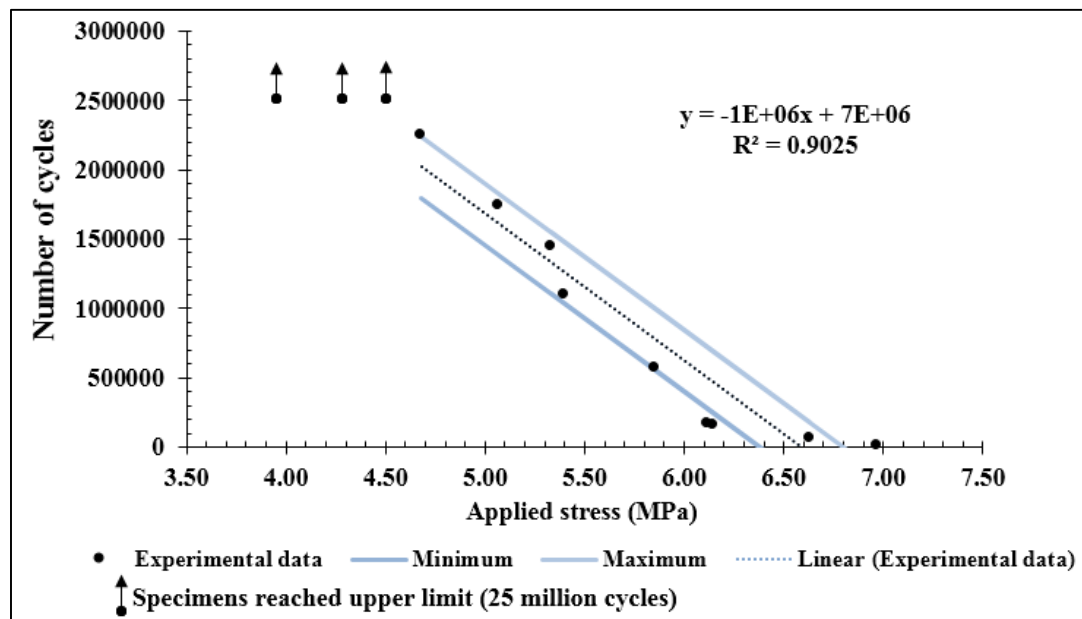


Fig. 2.11 Fatigue life distribution of optimized FRC mixture

Table 2.10 Summary of flexural fatigue test results

Flexural load (kN)	Stress ratio	Applied load (kg)	Applied stress (kg/cm ²)	Number of cycles at failure				Average number of cycles at failure	Number of samples tested
				Sample 1	Sample 2	Sample 3	Sample 4		
19.50	0.55	1094	44	All the samples have reached upper limit (25 million cycles)					4
	0.65	1292	52	2417871	1987124	2217014	2374870	2249220	4
	0.75	1491	60	1143150	1247836	1004806	1010239	1101508	4
	0.85	1690	68	231547	118974	155047	178014	170896	4
20.50	0.55	1150	46	All the samples have reached upper limit (25 million cycles)					4
	0.65	1359	54	1862310	1733109	1654780	1712452	1740663	4
	0.75	1568	63	578415	496790	610212	591456	569218	4
	0.85	1777	71	54005	64781	56874	65101	60190	4
22.00	0.55	1234	49	All the samples have reached upper limit (25 million cycles)					4
	0.65	1458	58	1543670	1357897	1417890	1463008	1445616	4
	0.75	1683	67	98756	154770	198002	174325	156463	4
	0.85	1907	76	14300	11256	11897	13254	12677	4
Total number of samples tested									64
Dimension of the specimens 100x100x500 mm									

2.5.2 Analysis of Fatigue-Life Distribution Using Weibull Distribution Parameters

The distributions of fatigue life were analyzed using experimental data shown in Table. 2.10. Further, earlier studies have evidenced that, the fatigue life distribution of concrete follow the Weibull distribution (Oh 1991). Therefore, the present investigation incorporated Weibull distribution for the description of fatigue life data at different stress ratio. The graphical method is employed to illustrate the distribution of fatigue life of FRC at a particular stress level. Then the Weibull distribution parameters i.e., (i) Shape factor ‘ α ’ – describes the shape of the distribution, (ii) Characteristic Life ‘ β ’ for the fatigue life will be determined using the graphical method. The Weibull probability density function $f_N(n)$ and its cumulative distribution function $F_N(n)$ for fatigue life may be written as follows (Oh 1991).

$$f_N(n) = \frac{\alpha}{u-n_o} \left(\frac{n-n_o}{u-n_o} \right)^{\alpha-1} \quad (2.6)$$

$$F_N(n) = 1 - \exp \left[- \left(\frac{n-n_o}{u-n_o} \right)^\alpha \right]; \quad n \geq n_o \quad (2.7)$$

Where, α = shape parameter; u = characteristic extreme value, and n_o = location parameter or minimum value.

Since the strength of concrete materials is random in nature, the value of n_o may be considered as zero (Oh 1991). This may yield two-parameter Weibull distribution.

The reliability function $L_N(n)$ may be written from Eq. (2.7) as follows,

The cumulative distribution function ‘ $F_N(n)$ ’ of the Weibull probability can be expressed as:

$$L_N(n) = 1 - F_N(n) = \exp \left[- \left(\frac{n}{u} \right)^\alpha \right] \quad (2.8)$$

Taking the double logarithm on both sides of Eq. (2.8), one obtains

$$\ln \left[\ln \left(\frac{1}{L_N} \right) \right] = \alpha \ln n - \alpha \ln \beta \quad (2.9)$$

The above Eq. (2.9) can be used to determine the statistical distribution of the fatigue life of FRC at different stress ratio. The fatigue life data at a given stress ratio are first

arranged in increasing order of cycles to failure and the empirical survivorship function can be calculated using Eq. (2.10).

$$L_N(n) = 1 - \frac{i}{k+1} \quad (2.10)$$

Where i =the failure order number and k =the number of fatigue data or sample size.

A graph is plotted between $Y = L_N(n)$ and $X = \ln(n)$. The plotted graphs are shown in Fig. 2.12. Further, the best fit straight line is drawn through the data. If data points fall approximately along the linear trend line, indicates that the two-parameter Weibull distribution is a reasonable assumption for the fatigue behavior of FRC. The slope of the line provides an estimate of the shape factor ' α ' and characteristic life ' β ' can be obtained by using the equation $B = \alpha \ln(\beta)$, where, B =is a constant of the straight line obtained from the graph. From the Fig. 2.12(a) it can be see that the slope of the line $\alpha = 0.8712$ and $B = 9.9315$, $B = \alpha \ln(\beta)$,

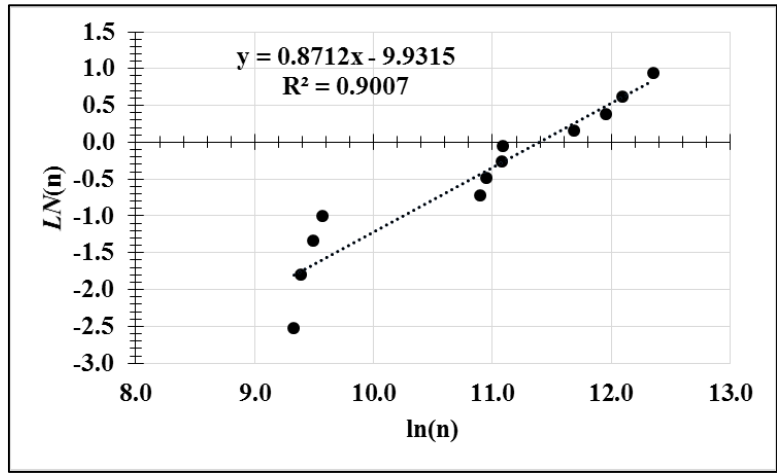
$$\ln(\beta) = \frac{B}{\alpha} = \frac{9.9315}{0.8712} = 11.3998,$$

$$\beta = \exp(11.3998) = 89303$$

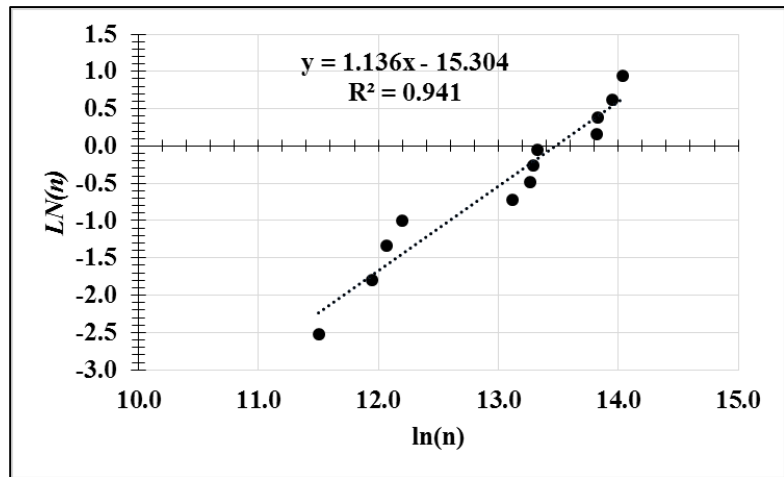
The parameters α and β obtained from the graph for different stress ratios are tabulated in Table 2.11. It can be seen from the Fig. 2.12, and Table 2.11 that the shape parameter ' α ' decreased at higher stress levels and increased at lower stress levels for the fatigue life of FRC. Hence the variability in the distribution of fatigue life of FRC becomes more at lower stress levels as compared with higher stress levels.

Table 2.11 Weibull parameters for fatigue of FRC

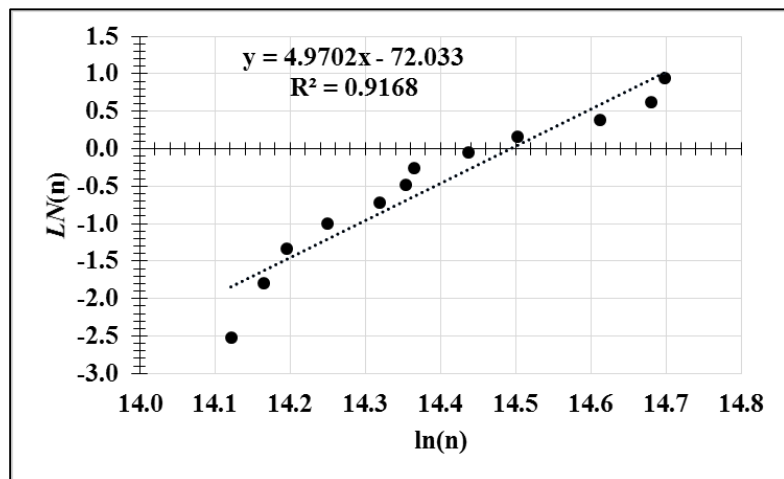
Stress ratio	Graphical method	
	α	β
S = 0.85	0.8712	89303
S = 0.75	1.1360	709156
S = 0.65	4.9702	1968885



(a)



(b)



(c)

Fig. 2.12 Graphical analysis of fatigue life data for FRC (a) stress ratio = 0.85 (b) stress ratio = 0.75 (c) stress ratio = 0.65

2.5.3 Failure Probability and Stress Ratio-Number of Cycles (S-N) Relationship

The Weibull distribution can be employed to incorporate the failure probability into the stress ratio-number of cycles (S-N) relationships of FRC. As the fatigue life data of FRC has been shown to follow the two-parameter Weibull distribution in the preceding section, this distribution can be used to calculate the fatigue lives corresponding to different failure probabilities. Rearranging the Eq. (2.8) and substituting the probability of failure $(1 - P_f)$ for L_N , the following expression can be obtained.

$$n = \ln^{-1} \left[\frac{\ln \left\{ \ln \left(\frac{1}{1-P_f} \right) \right\} + \alpha \ln(u)}{\alpha} \right] \quad (2.11)$$

Using the values of Weibull parameters α and β , as obtained previously for a given fatigue life data, Eq. (2.11), can be used to calculate fatigue lives of FRC corresponding to different failure probabilities (that is, $P_f = 0.05, 0.20, 0.50, 0.70, 0.90$ and 0.95). The calculated values of fatigue lives using Eq. (2.11) are listed in Table 2.12 for the optimized mix proportions of FRC. These values have been plotted to obtain the P_f -S-N relationships for FRC and shown in Fig. 2.13.

Table 2.12 Calculated fatigue lives of FRC mixtures for different probabilities of failure

Probability of failure (P_f)	S = 0.85	S = 0.75	S = 0.65
0.95	314643	1862939	2455231
0.90	232613	1477725	2328616
0.70	110510	835040	2043810
0.50	58635	513598	1828920
0.20	15964	189371	1455983
0.05	2953	51908	1083143

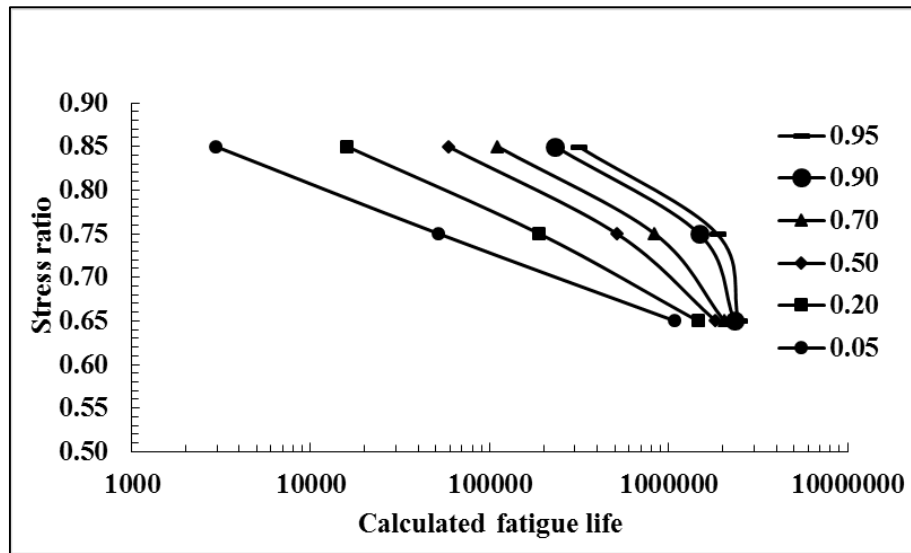


Fig. 2.13 Pr-S-N diagram for FRC mixture

It can be seen from the Fig. 2.11 that, the number of fatigue cycle values will fall within the minimum and maximum value lines. This represents almost similar to the values obtained for two-parameter Weibull distribution as P_f decreases the number of cycles also decreases (see Table 2.12). Therefore, the statistical method may be adopted to calculate the fatigue life. Fig. 2.11 can be used by design engineers to obtaining the flexural fatigue life of FRC for UTW overlays.

2.6 SUMMARY

The following conclusions are drawn, from the various experimental results reported in the present work.

- Material type and amount in the concrete mixture affect the slump and box ranking values.
- Box test method is one of the best test procedure to evaluate the mixture's response to vibration.
- The cementitious content of 430 kg/m^3 with 0.45% dosage of polyester fiber can produce good vibratory response for slip form paver and significantly improved hardened properties of the concrete mixture.
- The statistical method is more convincing than the two-parameter Weibull distribution and it is more appropriate to calculate the fatigue life.

CHAPTER 3

QUANTIFYING THE INTERFACE SHEAR BOND STRENGTH OF HMA- UTW COMPOSITES SUBJECTED TO DIRECT SHEAR TEST

3.1 BACKGROUND

UTW is one of the best alternative methods for resurfacing of asphalt pavements. The interface bond between the HMA-UTW layers reduces the bending stresses compared to unbonded overlays. The interface bond between existing asphalt layer and concrete is the major criteria for the performance of the UTW overlay. Specific construction techniques such as milling, chiseling and bonding agents are usually considered to ensure adequate bond is achieved. However, in UTW bonding can be achieved by milling the existing asphalt pavement to produce a clean and roughened surface for freshly laid concrete overlay (NCHRP 338 2004). The bonding between two layers causes monolithic action and share the load by shifting the neutral axis from the middle of the UTW slab to the bottom of UTW slab. This will bring the bending stresses into a range the UTW can withstand, but shear stresses will remain maximum at the neutral axis (Mack et al. 1998). Further, shear stresses will increase with the increase in the repeated application of traffic load. This will create an accumulation of strain at the interface resulting in failure of the monolithic or composite action. The same mechanism (internal stresses induced by gravity loads) will govern the interface debonding of the UTW from the HMA layer led to cracking and eventually surface distress problems. Finally this will affect the long-term service life of UTW overlays (Delatte and Sehdev 2003; Bissonnette et al. 2011). Therefore, UTW had better interface bond strength than the normal tensile stress and horizontal shear stress caused by traffic and environmental load.

The quality and strength of the bond between the layers depend on both the surface preparation i.e., specific construction technique (Kim and Lee 2013), the texture of HMA surface and the UTW placement procedure. Hence workmanship will play a

major role in achieving good quality and strength of the bond between the HMA and UTW overlay.

3.2 PREVIOUS STUDIES ON INTERFACE BOND STRENGTH

Several studies have been performed to determine the interface bond strength between the upper pavement layers using shear or tension mode. This is due to the fact that both the distress modes can cause pavement failure under traffic loading and is shown in Fig. 3.1. Since shear separation mode of failure is most commonly found in real pavement structures therefore most common test setup used is direct shear test mechanism, where load is applied to generate shear failure on the predefined interface plane. All such major studies have been briefly described in this section.

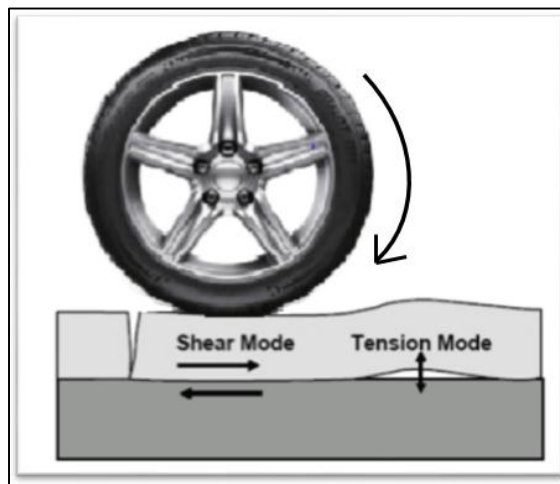


Fig. 3.1 Possible modes of pavement interface failure during service life

3.2.1 Asphalt-Asphalt Interface Bond Verification Test

To determine the shear stress between the asphalt layers many authors developed different kind of shear stress apparatus (Kruncheva et al. 2006; Felice et al. 2009; Tashman et al. 2008; Collop et al. 2009; Raab et al. 2009; Patel 2010; Raab et al. 2012; Raposeiras et al. 2012) such as shear box test, Layer Parallel Direct Shear (LPDS) test, Florida Department of Transportation (FDOT) shear test etc. Laboratory shear box test was adopted by Kruncheva et al. (2006) to evaluate the interface properties of asphalt layers. Dynamic cyclic horizontal loading at a frequency 2 Hz and a constant vertical load of 6 kN was applied and both horizontal and vertical displacements were measured using Linear Variable Displacement Transducers (LVDT). The shear stress at the

interface was calculated by multiplying vertical shear reaction modulus with relative vertical displacements.

Prasad (2011) carried out laboratory study to know the interface bond strength between HMA composites using direct shear test. Universal testing machine was used to evaluate the bond strength for 100 mm diameter samples; a tensile load at a deformation rate of 0.5 mm/min was applied till the specimen fails at interface. Interface shear strength was measured as maximum load to failure divided by its cross sectional area for different interface treatment.

LPDS test, Ancona Shear Testing Research and Analysis (ASTRA) and shear box test was developed by Swiss Federal Institute of Technology to evaluate the interlayer bonding properties. The shear strength properties between asphalt layers was carried out under field and laboratory conditions. The loading condition and deformation rate applied was found to be different for these three laboratory tests. In the case of LPDS test different deformation rate of 2.50 mm/min, 50 mm/min and 50.8 mm/min was applied, whereas in ASTRA test vertical normal load of 0.2 MPa was applied along with a horizontal deformation rate of 2.5 mm/min. In the Shear box test a horizontal deformation rate of 2.5 mm/min and a normal load perpendicular to the shear plane was applied. The test results obtained through LPDS and ASTRA were expressed in terms of peak interface shear stress, peak energy and equivalent shear displacement (peak energy/peak interface shear strength). The results of Shear box test were expressed in terms of shear stiffness (shear force/shear deformation) considering the different tack coat materials (Santagata et al. 2009; Raab et al. 2009 and Raab et al. 2012).

West et al. (2005) developed a modified National Center for Asphalt Technology (NCAT) shear tester to determine the bond strength between pavement layers. Marshal testing apparatus was used to evaluate the bond strength by applying a constant vertical load of 50.8mm/min which induces a normal stress under controlled environmental chamber. Bond strength was measured as maximum load to failure divided by its cross sectional area.

Louisiana Interlayer Shear Strength Tester (LISST) was used by Patel (2010) to study the interface shear strength properties of asphalt layers. The material testing system was used to apply a constant shear displacement of 0.1 mm/min and vertical confinement pressure (using normal actuator) of 138 kPa. Interface shear strength (ultimate shear load by cross sectional area of the specimen) and interface tangential modulus (function of the difference in horizontal displacements of the layers) was evaluated for different parameters such as tack coat material and surface treatment.

A laboratory based modified Leutner shear test method was developed (Collop et al. 2009) to evaluate the bond strength between asphalt layers. A constant vertical displacement rate of 50 mm/min was applied directly on the top layer, while the bottom layer was held in rest to produce displacement between layers. Shear strength, displacement and secant shear modulus were measured for different interface treatment.

The influence of various tack coats on the adhesive bond between the interfaces of pavement layer was studied using FDOT shear test, torque bond test and UTEP (University of Texas at El Paso) pull-off test (Tashman et al. 2008). Field studies were conducted using both torque bond test and pull off tests. Torque bond test was conducted by rotating a torque wrench in anticlockwise direction till the failure of bond. The pull off tests were carried out by applying a vertical tensile load till the plate get detached from the pavement layer. Shear test was carried out in laboratory for field core samples by applying a load of 50 mm/min. The responses obtained from the test were characterized into average shear strength, average torque bond and average tensile strength.

In Spain, Raposeiras et al. (2012) used Laboratorio de Caminos de Barcelona (LCB) shear tester to study the influence of surface macro-structure and adhesion properties between asphalt layers. A static deformation of 2.5 mm/min was applied over the top of the mold until the layer area gets separated at joint. Maximum load to failure, deformation and shear resistance were determined for different binder dosage rate.

An automatic torque bond testing machine was developed to measure the shear interface properties between asphalt layers. Tests were carried out with quasi static and repeated load interface testing with two different loading rates of constant torque rate

of 600 N m/min and constant rotation rate of 180⁰/min. Results were characterized in nominal shear strength and number of cycles to failure for different shear stress (Collop et al. 2011) for different testing temperature and tack coat materials.

Tschegg et al. (1995) and Tschegg et al. (2007) used wedge splitting tester to determine the fracture mechanical behaviour and fatigue crack growth in asphalt-asphalt interface. Parameters like temperature, tack coat materials and interface treatment were used to evaluate the fracture mechanical behaviour. A vertical load was applied with a wedge angle of 9.60⁰ over the samples prepared with groove at the interface to determine the fracture mechanical behaviour.

The pull push test method was utilized to determine the fatigue crack growth by applying a cyclic repeated vertical compressive force of frequency 2 Hz. The vertical force was applied on the wedge being placed over the groove which is already driven on the surface of the specimen. The fracture mechanical behaviour was determined in terms of vertical loading and horizontal loads using the vertical and horizontal displacements obtained. Here, the vertical loads are obtained directly and the horizontal loads were obtained based on the wedge angle. In order to know the fatigue behaviour number of cycles to failure were recorded.

A tensile type interface bond test called Interface bond test (IBT) was developed by Hakimzadeh et al. (2012) which was similar to “ASTM D7313-07a” to evaluate the interface properties in asphalt concrete. Here, a tensile load was applied through pins inserted into the loading holes at a constant Crack Mouth Opening Displacement (CMOD) rate of 0.5 mm/min. Fracture energy was evaluated using load versus CMOD curve for different tack coat application rate. Compact Tension test was conducted to study the fracture characteristics of thin bonded asphalt overlays. A “CMOD” load of 0.017 mm/sec was applied till the specimen failed. It was observed that specimen failed gradually with increase in CMOD rate. The fracture energy was measured as the amount of fracture work required to produce a unit crack on the surface area (Ahmed et al. 2012).

Chen et al. (2013) conducted composite specimen interface cracking (CSIC) test for laboratory prepared HMA overlay samples to evaluate the effect of interface

characteristics by applying a repeated load with a frequency of 1 Hz, rest period 0.9 sec and pressure of 4.03 MPa. Test results were interpreted as resistance to cracking and damage rate based on number of cycles to failure.

Hakim et al. (2000) developed non-destructive testing method to determine the bonding condition between the pavement layers using falling weight deflectometer (FWD) test data. Based on the data obtained in FWD a new software program called padal method was used to determine the stiffness in thin bonded pavement layers. Kruntcheva et al. (2004) developed Impulse hammer test method to evaluate the bond condition between asphalt concrete layers by applying an impulse force of 30-40 kN with a hammer having a mass of 3.92 kg and diameter 64 mm. The responses were measured using accelerometers. Results were characterized as qualitative by visual inspection of surface bonding condition and as quantitative by measuring the frequencies. A direct shear test with normal stress was adopted to evaluate the interface bonding between the cement concrete and asphalt overlays by Zhao et al. (2017). A shear displacement rate of 2.5 mm/min was applied at the interface under different type of interface, testing temperature and moisture.

3.2.2 PCC-Asphalt Interface Bond Verification Test

Cho and Koo (2006) developed an instrument called Heart Wheel Load Simulator (HWLS) to study the UTW behavior on asphalt pavements. A constant wheel pressure of 1.98 MPa was applied over an area of 40x50 mm². Compression strain and tensile strain were measured at top and bottom of the concrete layer for different testing temperature and layer thickness of asphalt and concrete. It was observed that load verses tensile curve showed linear behavior for larger thickness of asphalt and concrete overlay.

Tschegg et al. (2007) studied the fracture mechanical properties of asphalt-PCC interface overlays using pullout test and wedge splitting test method. A tensile force of 100 N/s and a horizontal splitting speed of 0.5 mm/min with a wedge angle of 10° were applied in pullout test and wedge splitting test. Responses were characterized into adhesive tensile strengths, crack propagation resistance and notched bar tensile strength for different testing temperature and interface pretreatment. The values of adhesive

tensile strength and crack propagation resistance were obtained directly, whereas the notched tensile strength was determined using linear elastic theory. The fracture energy curve was plotted and it was observed that it showed both the brittle and ductile behavior. Tia et al. (2007) and Wen et al. (2010) investigated the interface bond strength between the layers using Iowa shear test for field core samples. The average shear strength of 1.34-1.43 MPa was reported for different test sections and loading condition.

In Florida, Wu et al. (2007) carried out forensic investigation of UTW pavements. The interface shear strength properties for field samples were determined using Iowa DOT test procedure and average shear strength reported was about 2.11 MPa for different thickness, joint spacing and surface preparation. Samee (2010) investigated the bond strength of UTW overlay using modified immersion wheel tracking test machine. A repeated wheel loading by rolling a rubber wheel across the surface of composite slab of size 600x100x200 mm³ at a frequency of 25 to 40 Hz passes per min which carrying a load of 8 kg/cm² and 20 kg/cm² was applied. Deflections and number of repetitions were measured for different concrete admixtures.

Ozer et al. (2012) carried out laboratory direct shear test to evaluate the interface characteristics between hot mix overlay and concrete pavements. They were observed that for different tack coat materials specimen behavior was elastic and this elastic property was due to tensile strength and cohesion between the interfaces. Chabot et al. (2013) studied the debonding phenomenon of composite pavements using four point bending test. A static displacement of 0.7 mm/min was applied under controlled displacement condition. The maximum load to failure, displacement, strains at the bottom of bituminous layer and nature of debonding for different specimen geometry and interface treatment was determined.

Mu and Vandebossche (2017) utilized wedge splitting test to evaluate the interface fracture properties of asphalt to concrete overlays. The test was carried out for milled and unmilled asphalt surfaces at different temperature and moisture condition. A static crack mouth opening displacement load of 0.5 mm/min was applied. Suresha and Satish (2017) evaluated the interface bond strength between HMA-UTW layers under different interface treatments and test conditions. A special shear breaking- head

assembly was developed to perform direct shear test. Shear force was applied by pulling the handles in opposite direction at a shear displacement rate of 5mm/min.

3.2.3 PCC-PCC Interface Bond Verification Test

Flexural bending test was carried out under a controlled strain rate of 0.2 mm/min (Granju 1996) to know the debonding characteristics of fiber reinforced laboratory prepared composite beam specimens and it was found that for higher dosage of fiber, debonding was delayed and addition of fiber to the concrete resisted the crack formation. Zhang and Li (2002) carried out laboratory studies to know the effect of initial shrinkage, temperature change and traffic loading-induced reflective cracking on concrete-concrete overlays. Monotonic flexural bending test and fatigue test was used with a controlled displacement rate of 0.10 mm/min and 1-2 Hz. Modulus of rupture using simple linear elastic theory and fatigue life using stress verses number cycles to failure (S-N) diagram was determined for different interface treatment.

Lin et al. (2013) performed direct shear bond test and splitting tensile bond test to develop a new mix design concept for bonded overlays. The loading rates for shear test and splitting test was 0.39kN/sec and 1.4kN/sec was applied along the interface bond. Direct shear bond strength was obtained by dividing the maximum load to area and spit tensile bond strength was evaluated using an empirical equation. Kim and Lee (2013) evaluated the bond-fatigue behavior of bonded concrete overlays using indirect tensile test. A cyclic loading of frequency 15 Hz was applied at the interface. The number of cycles to failure were determined for different concrete overlay thickness.

The summary of literature review is shown in Table 3.1. It can be seen from the Table 3.1 that various agencies were adopted different surface preparation methods to achieve the degree of bonding. Later the bond strength was evaluated in the laboratory using Iowa shear test and their own measuring methods.

In India the degree of bonding is achieved as per IRC SP: 76 2008, between UTW overlay and the existing HMA layer to obtain 100 % bonding at the interface. In reality, the 100 % bonding is not always achieved, and the interface characteristics are unknown functions of the interface treatment, curing time and construction practices. From the literature (see Table 3.1) no work has been carried out on the interface shear

bond characteristics of UTW overlays subjected to repeated loading conditions for different interface treatment.

Therefore, it is essential to evaluate the interface bond condition of the UTW overlays for different interface treatment and its impact on long-term performance. In this study, a new interface treatment technique is developed. A laboratory direct shear test apparatus and method were used to evaluate the behavior of UTW overlays for different interface treatment techniques. The test was carried out under two different loading conditions such as static and dynamic loading.

Table 3.1 Summary of literature review

Authors	Tack coat		Samples obtained lab/field	Type of test	Loading rate	Test temperature °C	Type of sample used	Response characterized	Response values in range	Displacement
	Type	Application rate								
HMA-HMA interface bond strength										
Tschegg et al. (1995)	CE and PME	60% by weight of bitumen	Laboratory	Wedge splitting test	1 mm/min and wedge angle 9.60°	-21 – +10.5	Wedge samples	Horizontal force (N) and specific fracture energy (N/m)	750 – 3698 and 80 - 210	0.2 – 0.6 mm
Hakim et al. (2000)	NA	NA	Field	Indirect tensile stiffness test		20	NA	Layer stiffness	4000-11800 MN/m ²	NA
Kruntcheva et al. (2004)	CE	0.5 l/m ² and 1.0 l/m ²	Laboratory and Field	Impulse Hammer test	20kN and 30-40kN	NA	Slab-260mm thick, 105cm wide and 108cm long	Shear secant modulus (MPa/mm) Accelerometer Response (m/s ²) Frequency (Hz) Transfer function magnitude (m/s ² /N)	0.48-1.90 6.5-76 1000-6000 0.01-1.6	NA

Authors	Tack coat		Samples obtained lab/field	Type of test	Loading rate	Test temperature °C	Type of sample used	Response characterized	Response values in range	Displacement
	Type	Application rate								
West et al.(2005)	CRS-2	200-800 g/m ² residual bitumen	Laboratory and Field	Leutner test	50mm/min	+10,+ 25 and +60	NA	Force (kN)	1-11.6	2.7 - 3.3mm
	CSS-1			NCAT bond tester				Diameter -150mm Thickness - 115mm	Shear strength (psi)	25.6 - 735
Kruncheva et al. (2006)	PG-64-22	0.33 l/m ²	NA	Shear Box Test	40 kN Cyclic Horizontal load-2Hz & Vertical load-6 kN	NA	NA	Shear stress (kPa),	120-230	Horizontal (μ)- 9 -150 and Vertical (μ)- 2-18
	CE									
	CS									
	NE									
EE	1.0 l/m ²									
Tashman et al. (2008)	NA	0.00, 0.08, 0.22, 0.32 l/m ²	Field	FDOT Shear test	50mm/min	25	NA	Shear strength (kPa)	220-1400	NA
				Torque bond test	Upto failure of bond			20	Mean Torque bond (Nm)	320-400

Authors	Tack coat		Samples obtained lab/field	Type of test	Loading rate	Test temperature °C	Type of sample used	Response characterized	Response values in range	Displacement
	Type	Application rate								
				Pull off test	Upto failure of bond			Mean tensile strength (kPa)	18-Jul	
Collop et al. (2009)	CE	200 g/m ² residual bitumen	Laboratory and Field	Modified Leutner shear test	50mm/min	20	Dia-150mm Thickness - 100mm	Shear strength (MPa)	1.12-2.68	1.05-2.40mm
Raab et al. (2009)	NA	NA	NA	Modified LPDS Test	50.8 mm/min	20	Diameter -150mm	Shear force (kN) and shear stiffness (kN)	12 to 45	NA
Santagata et al. (2009)	CS	0.15 kg/ m ²	Laboratory & Field core	LPDS	50.8 mm/min	20	Diameter -150 mm	Normal Distribution	0.751-1.478	1.713-2.00 mm
	PME							Peak Shear stress (MPa),	0.886-3.681	
	NE							Peak Energy (N/mm)	0.467-0.668	
				ASTRA	Horizontal-2.5 mm/min Vertical - 0.2 MPa	20	Diameter -100 mm	Peak Shear stress (MPa),	0.676-1.258	1.506 - 2.388mm
Patel (2010)	PG-64-22	0.14-0.70 l/m ²	Laboratory and Field	(LISST)	0.1 inch/mm	NA	Diameter -100mm	Surface and tack rate –	76.1 - 654.8	NA

Authors	Tack coat		Samples obtained lab/field	Type of test	Loading rate	Test temperature °C	Type of sample used	Response characterized	Response values in range	Displacement
	Type	Application rate								
Prasad (2011)	SS-1h and SS-1 CRS-1				with 0,130 kPa		and 150mm	Interface shear strength	(kPa)	
	RS, MS & SC	0.2-0.4 kg/m ²	Laboratory	Direct shear	NA	+40,+ 50 and +60	Diameter -150mm, Thickness -65mm	Interface tangential modulus (k) Shear strength (N/mm ²)	129948-256755 (kN/m ³) 0.173 – 0.927	NA
Collop et al. (2011)	NE	150-300 g/m ²	NA	Automatic laboratory torque bond tester	180 ⁰ /min	+10,+20,and +30	Diameter -100mm, Thickness -60mm	Nominal Shear Strength (MPa)	0.9-2.9	NA
	ME	Residual bitumen			600 N m/min					
Hakimzadeh et al. (2012)	CSS-1h	0.45, 0.68, 0.9 l/m ²	Laboratory	Interface bond Test	0.5 mm/min	-12	Diameter -150 mm, Thickness -38mm	Fracture Energy (J/m ²)	97-131	Crack Mouth Opening Displacement (mm) 0.2-0.25
	PMAE	0.45,0.68 l/m ²	Field Core		NA					

Authors	Tack coat		Samples obtained lab/field	Type of test	Loading rate	Test temperature °C	Type of sample used	Response characterized	Response values in range	Displacement
	Type	Application rate								
Raab et al. (2012)	CSS	0.36, 0.45, 0.68 l/m ²	Laboratory	Superpa ve Shear test	2.5mm/ min	20	Diameter -150mm-175 mm	Shear force (kN) Shear stress (MPa) Stiffness (kN/mm) Reaction Modulus (MPa/mm)	11.9-16.2 0.7-0.9 9.7-11.7 0.6-0.7	1.6-1.8 mm
	NA	NA		LPDS			NA			
Raposeiras et al. (2012)	NA	125-750 g/m ²	Laboratory	LCB shear test	2.5 mm/min	20	Diameter -101.6 mm	Shear resistance (N)	4936-13489	NA
Chen et al. (2013)	UE	0.45 l/m ²	Laboratory	Repeate d load test	Pressure load of 4.03Mpa	NA	NA	Deformation and Number of cycles to failure	No. of cycles to failure	0.01-0.02 mm

Authors	Tack coat		Samples obtained lab/field	Type of test	Loading rate	Test temperature °C	Type of sample used	Response characterized	Response values in range	Displacement
	Type	Application rate								
	PMA E	0.9 l/m ²			Frequency 1Hz and Rest period-0.9s				25000-58000	
Zhao et al. (2017)	SBS, Cutback, anionic emulsion	0.4-0.8 kg/m ²	Laboratory	Direct shear	2.5 mm/min	10, 25 and 40	Diameter -150 mm and height-100 mm	Shear strength (kN)	300-1400	NA
PCC - PCC interface bond strength										
Granju (1996)	NA	NA	Laboratory	Three point bending test	Controlled strain-0.2 mm/min	20	100x100x500 mm ³	Max load (kN)	10	NA
Zhang and Li (2002)	NA	NA	Laboratory	Monotonic flexural bending and fatigue test	Controlled displacement of 0.10 mm/min and 1-2 Hz	NA	101.6x76.2x355.6 mm ³	Modulus of rupture (MPa), and	6.24-13.68	0.075 - 2.24 mm
Perez et al. (2009)	NA	NA	Laboratory	Static shear and	NA	20	Diameter -100mm Thickness	Bond strength (MPa)	5.77-5.88 and 1.8 - 2.7	NA

Authors	Tack coat		Samples obtained lab/field	Type of test	Loading rate	Test temperature °C	Type of sample used	Response characterized	Response values in range	Displacement
	Type	Application rate								
Lin et al. (2013)	NA	NA	Laboratory	tensile test Shear bond test and Splitting test	0.39kN/sec and 1.4kN/sec	NA	s - 100mm Diameter -100mm Thickness s - 180mm and 100x150x50 mm	Bond strength (MPa)	1.06 - 6.81 and 1.27 - 3.43	NA
Sahmaran et al. (2013)	NA	NA	Laboratory	Slant shear and Splitting prism test	0.25 MPa/s and 50 kN/min	NA	Diameter -100mm Thickness - 200mm and 76.2x50x30 mm	Bond strength (MPa)	7.1 - 21.7 and 1.82 - 3.58	NA
Kim and Lee (2015)	NA	NA	Laboratory	Indirect tensile test	Frequency 15 Hz	NA	Diameter -150 mm height- 300 mm	Bond strength (MPa) Number of cycle at failure	2.82 300-7000000	NA
HMA–PCC interface bond strength										
Cho and Koo (2006)	NA	NA	Laboratory	HWLS	Wheel weight 0.15 – 9.81 kN	+20 to +60	NA	Strain at interface (micro-strain/kN)	27 – 179	NA

Authors	Tack coat		Samples obtained lab/field	Type of test	Loading rate	Test temperature °C	Type of sample used	Response characterized	Response values in range	Displacement
	Type	Application rate								
Tia et al. (2007)	NA	NA	Field	Iowa shear test	NA	NA	Diameter -100mm Thickness -190 mm	Shear strength	NA	NA
Wu et al. (2007)	NA	NA	Field	Iowa shear test	NA	NA	Diameter -100mm	Shear strength (MPa)	1.13 – 2.11	NA
Tschegg et al. (2007)	Adhesion agents	> 0.2 mm thick	Laboratory	Tensile test and Wedge splitting test	100 N/s and 0.5 mm/min, wedge angle 10°	+20 and (-10) – (+22)	100x60x60 mm ³ and wedge specimen	Tensile strength (MPa) and specific fracture energy (J/m ²)	0.8 – 1.7 and 100 - 1000	NA
Samee (2010)	CPMA	5 mm thick	Laboratory	Modified immersion wheel tracking	25 to 40 passes per min	NA	600x100x200mm ³	Deflections (mm) and number of repetitions (cycles)	1.05 - 9.36 and 2x10 ⁵ -6x10 ⁵	NA
Wen et al. (2010)	NA	NA	Field	Iowa shear test	NA	NA	Diameter -100mm	Bond strength	NA	NA
Ozer et al. (2012)	NA	NA	Field	Direct shear test	NA	NA	NA	NA	NA	NA
Chabot et al. (2013)	NA	NA	Laboratory	Four point bending test	0.7 mm/min, 100	4 to 23	NA	Flexural strength (N)	4300 - 12190	NA

Authors	Tack coat		Samples obtained lab/field	Type of test	Loading rate	Test temperature °C	Type of sample used	Response characterized	Response values in range	Displacement
	Type	Application rate								
					N/s and 500 N/s					
Mu and Vandebosche (2017)	NA	NA	Laboratory	Wedge splitting test	0.03-0.5 mm/min	-13 and 23	Wedge split sample	Splitting force (kN)	22-Feb	0.025-0.045 mm
Suresha and Satish (2017)	NA	NA	Laboratory	Direct shear test	5 mm/min	40, 50 and 60	Diameter -100 mm Thickness 150	Interface shear strength (MPa)	0.22-1.29	NA

CPMA- cementitious polymer modified tile adhesive, NA-not available

3.3. INTERFACE SHEAR BOND STRENGTH TEST

A direct shear test apparatus has been fabricated which is a modified version of equipment developed by authors (Leutner 1979). The modified direct shear test apparatus was used to evaluate the interface bond strength of UTW overlay on HMA layer under laboratory condition.

3.3.1 Test Apparatus

The direct shear testing device consists of three segments, upper and lower cylindrical segments and a semicircular shearing head segment. The lower segment is fixed to the bottom plate and the upper segment is placed on the specimen. The upper and lower cylindrical segments act as a stationary sample holder, whereas the shearing head segment moves down during shear force application. A 5 mm gap was maintained between the stationary sample holder and shearing head segments, to allow the direct shear load at the interface. The effect of bending moment induced by the eccentricity of the vertical load was eliminated by using horizontal locking plate at the top is shown in Fig. 3.2. The Linear Variable Differential Transducers (LVDT's) are placed over the shearing head segment for measuring specimen deformation during shearing.

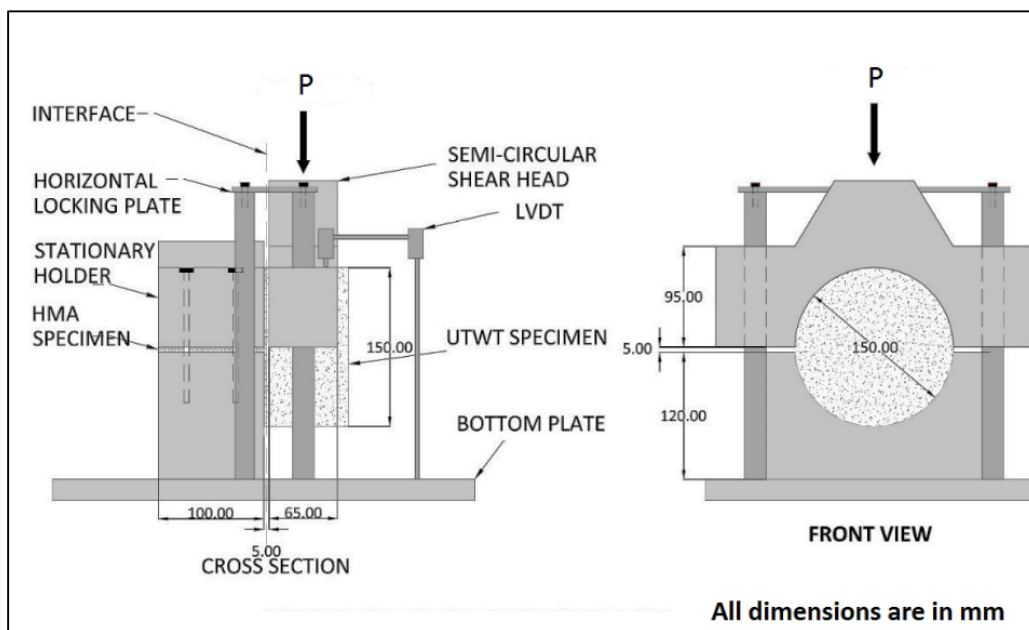
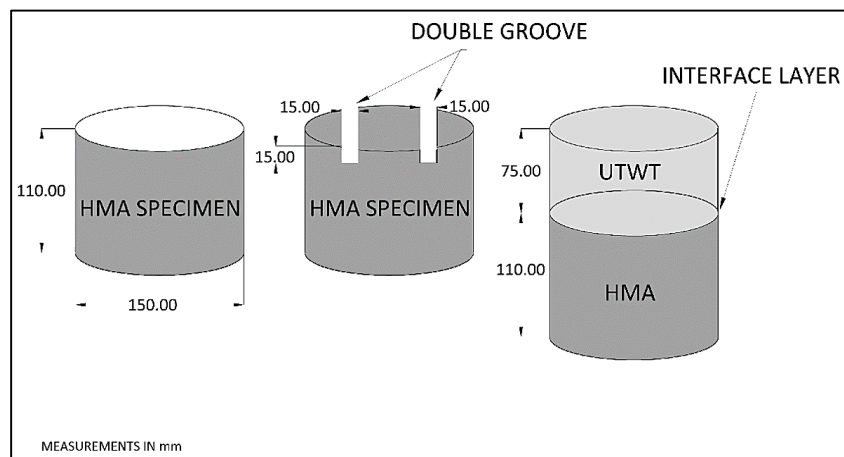


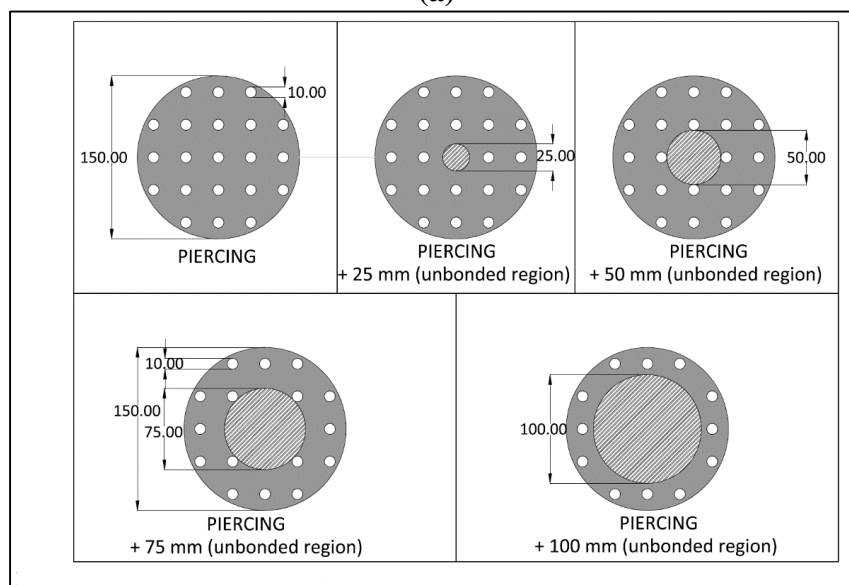
Fig. 3.2 Direct shear test apparatus

3.3.2 Interface Treatment

Milling is the most commonly used and recommended interface treatment technique for placing UTW overlay because it is the most effective method for rutting and shoving problems in the existing asphalt pavement and gives higher shear bond strength (NCHRP 338 2004; IRC: SP-76 2008). Present study incorporates different interface treatment techniques such as (i) NT (ii) SG (SG) (iii) DG (iv) Piercing interface and (v) Piercing with different percentage of bonding such as piercing+25, piercing+50, piercing+75 and piercing+100. The different interface techniques for HMA-UTW composites is shown in Fig.3.3.



(a)



(b)

Fig. 3.3 Different HMA-UTW interface treatments (a) DG (b) Piercing with different debonding (unbonded) region

3.3.3 Materials

The locally available crushed granite as coarse aggregate with 37.5 mm Nominal Maximum Aggregate Size (NMAS) were used for HMA specimens. The water absorption and saturated surface dry specific gravity of coarse aggregate values are 1.0% and 2.68. The optimum FRC mix proportion were used for UTW samples. The paving asphalt 60/70 grade was used and its physical properties are measured in the laboratory according to IS 73-2013 and are shown in Table 3.2. The percentage of combined flakiness and elongation index was less than 30%, which is the requirement for dense asphalt mixture. For dense asphalt mixture, the aggregates of different sizes were used in suitable proportions by trial and error method to obtain the average proportions of grading as specified by MoRTH (2013). The aggregate gradations for HMA mixtures are shown in Table 3.3.

Table 3.2 Physical Properties of Asphalt Binder (VG-30)

Tests	Test results
Penetration index (1/10 th of mm)	67
Softening point (°C)	58
Ductility (cm)	79
Viscosity at 135 ^o C, centipoise	175

Table 3.3 Aggregate Gradation for HMA Mixtures

Mixture type	HMA
NMAS (mm)	37.5
IS sieve sizes (mm)	Cumulative % by weight of total aggregate passing
45.0	100
37.5	95
26.5	78
20.0	--
19.0	--
13.2	65
10.0	--
9.5	--
4.75	46
2.36	35
1.18	--
0.6	--
0.3	14
0.15	--
0.075	5
Binder content	Min 4.5 percent by weight of total mix

3.3.4 Specimen Preparation

Three stages of HMA-UTW composite specimen preparation are as follows,

- (i) HMA mixture: Cylindrical specimens having a diameter of 150 mm and height 110 mm were prepared using Superpave gyratory compactor in the laboratory. Mixing and compaction temperature of 160⁰ C and 135⁰ C respectively was maintained. The superpave mix design are shown in Appendix B. The actual air voids for all mixtures are in the range of 4 ±0.1%. The specimens are allowed to cool for one day in room temperature 25±2⁰ C.
- (ii) Interface treatment: The compacted HMA mixture surface were subjected to groove and each groove having a cross section of 15 x 15 mm and each groove was separated with a distance of 40 mm apart as shown in Fig. 3.3(a). The groove and piercing interface method was carried out using a chop saw and driving tool. A partial bond method was introduced in piercing interface method by pasting a 0.15 micron PVC sheet at the center of HMA samples of varying diameter 25 mm, 50 mm, 75mm and 100 mm. The specimens with piercing interface treatment and different percentage of bonding are shown in Fig. 3.3(b). The groove interface treated specimens were placed inside an oven for drying at 40⁰C for a minimum of 24 hours due to the use of water as a lubricant.
- (iii) HMA-UTW composite: The HMA interface treated specimens were placed inside the cylindrical moulds of size 150 mm diameter and 300 mm height and made the treated surface wet by spraying water. Freshly prepared FRC mix was poured into the mould to achieve a total height of 185 mm HMA-UTW composite specimens.

The specimens were demould and allowed to water curing by immersing the 70 mm depth UTW portion till the date of testing. For each interface treatment, six specimens were prepared for static loading and five specimens for dynamic loading conditions to eliminate the experimental errors. The HMA-UTW cylindrical composite specimen preparation procedure for DG and piercing techniques is shown in Fig. 3.4.

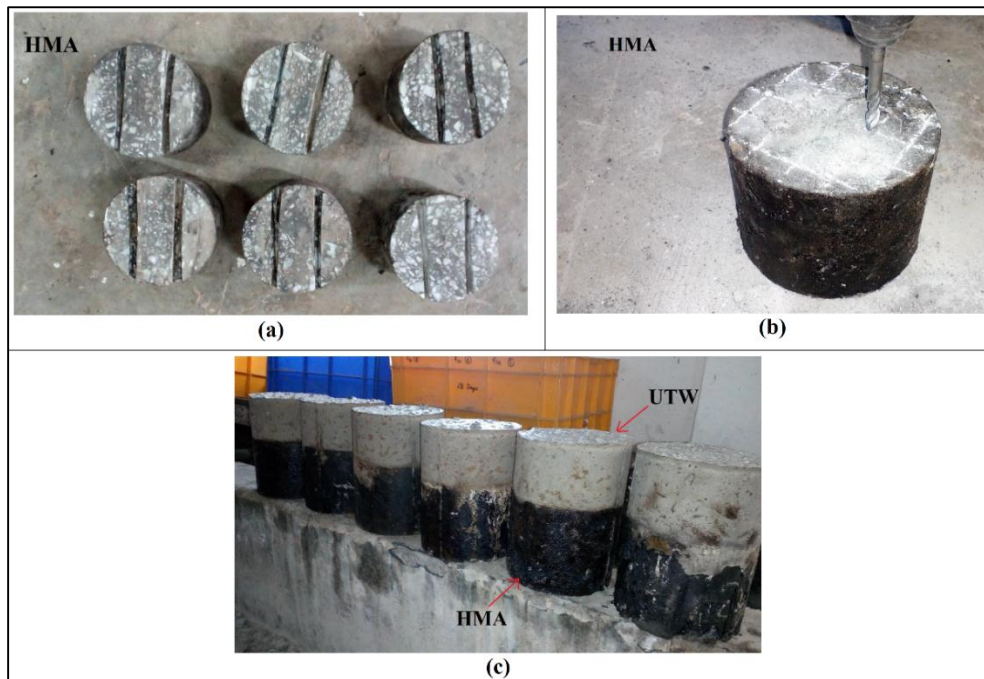


Fig. 3.4 Illustrates (a) DG interface treatment (b) piercing interface treatment and (c) HMA-UTW composite specimens

3.3.5 Test Procedure

Groove specimens were placed inside the direct shear apparatus and loading was carried out in three different modes, (a) groove parallel to loading, which simulates the existing milling interface treatment method (b) groove inclined at an angle of 45 degrees to loading and throughout the work this mode will be called as diagonal groove and (c) groove perpendicular to loading. The schematic representation of groove specimens subjected to different loading conditions as shown in Fig. 3.5. Groove, piercing and piercing with partially bond interface treated UTW composite specimens were placed horizontally inside the direct shear testing device as shown in Fig. 3.6. Once the test setup was established the direct shear test was carried out in two-phase,

- (i) Static loading: A constant vertical displacement of 6.0 mm/min was applied directly on the semicircular shearing head segment using strain controlled testing system and testing temperature of $25 \pm 2^{\circ} \text{C}$ was maintained.
- (ii) Dynamic loading: The HMA-UTW composite specimens exhibit higher shear bond strength were subjected to repeated load test by applying a frequency of 3 Hz with different stress ratios 0.05, 0.10, 0.15, 0.20, 0.25, 0.30, 0.35, 0.45, 0.55, 0.65, 0.75 and 0.85. The test was conducted using

stress controlled repeated loading testing machine as shown in Fig. 3.6. The repeated load was applied analogs to the semi-sine waveform and this waveform, relatively close to the traffic loading applied on the pavement. The stress ratio is the load value in a repeated load test to the ultimate shear bond strength value in the static shear bond strength test. For each load cycle, the applied stress and shear displacement at the interface were measured. The number of fatigue cycles at failure under shear load was identified, as suggested by Seo et al (2007).

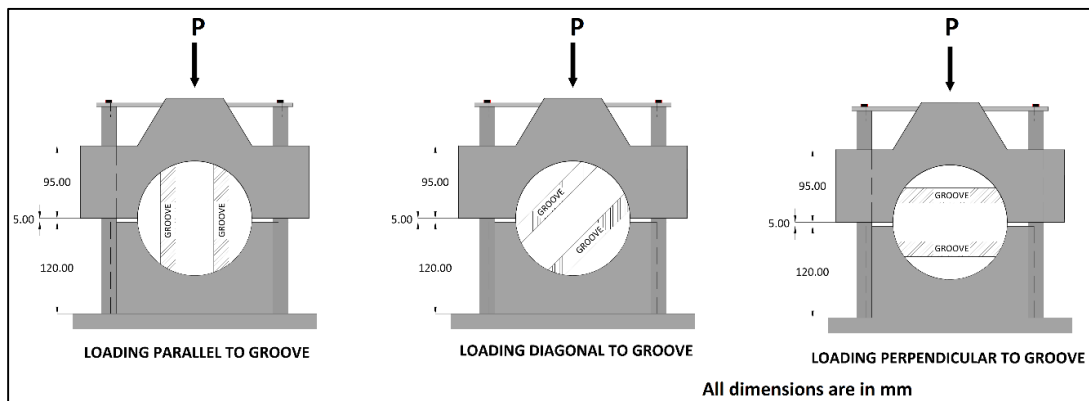


Fig. 3.5 Schematic diagram of groove interface treated samples subjected to different loading direction

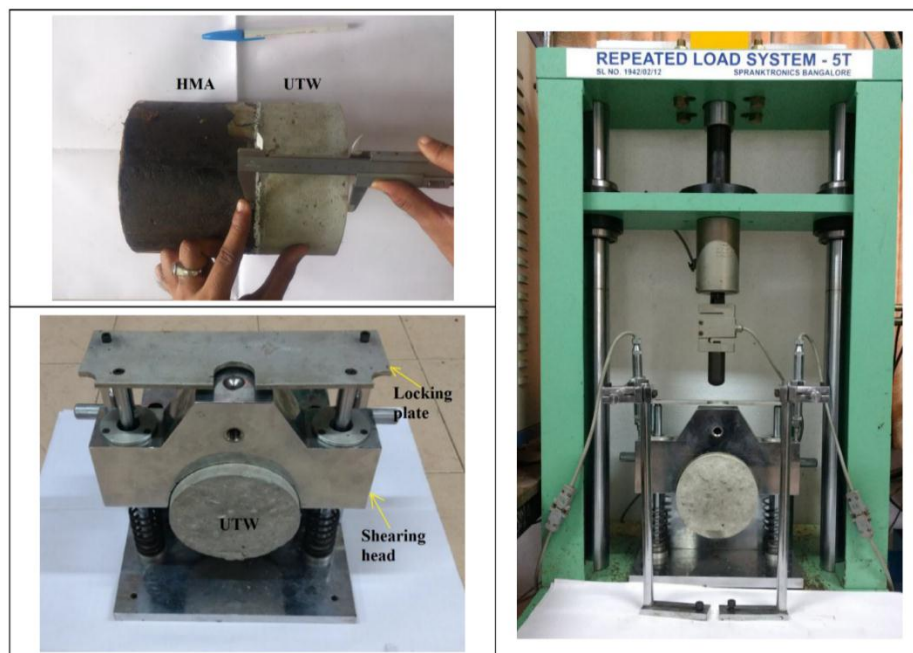


Fig. 3.6 Interface shear bond test procedure using direct shear test apparatus

3.3.6 Evaluation of Interface Shear Bond Strength (ISBS) and k-modulus Under Static Loading

The interface shear strength is considered the critical parameter for quantification of the influence of each test variable on interface bonding. Interface shear bond strength is calculated as the measured ultimate shear load divided by the contact area of the interface, as follows

$$ISBS = \frac{U_l}{A} \quad (3.1)$$

where, ISBS = interface shear bond strength (MPa), U_l = ultimate load applied to the specimen (N), and A = cross-sectional area of the specimen (mm^2).

The k-modulus was calculated using Goodman's constitutive law (Goodman et al. 1968) to describe the bond strength at the interface subjected to a direct shear load and it also represents the mechanical behavior of the pavement structure subjected to traffic loading. The equation is as shown below,

$$\tau = k\xi \quad (3.2)$$

where, τ = interface shear strength (MPa), k = interface tangential modulus (MPa/mm), and ξ = interface shear displacement (mm).

A typical interface shear stress versus displacement curve and k-modulus are shown in Fig. 3.7. The interface tangential modulus i.e., k-modulus is not a modulus in the classical sense, as this value can be easily seen from its units (MPa/mm).

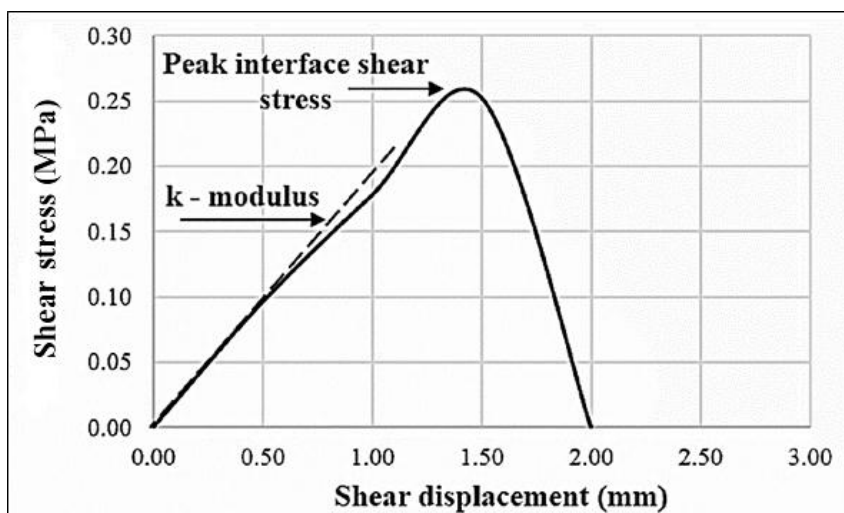


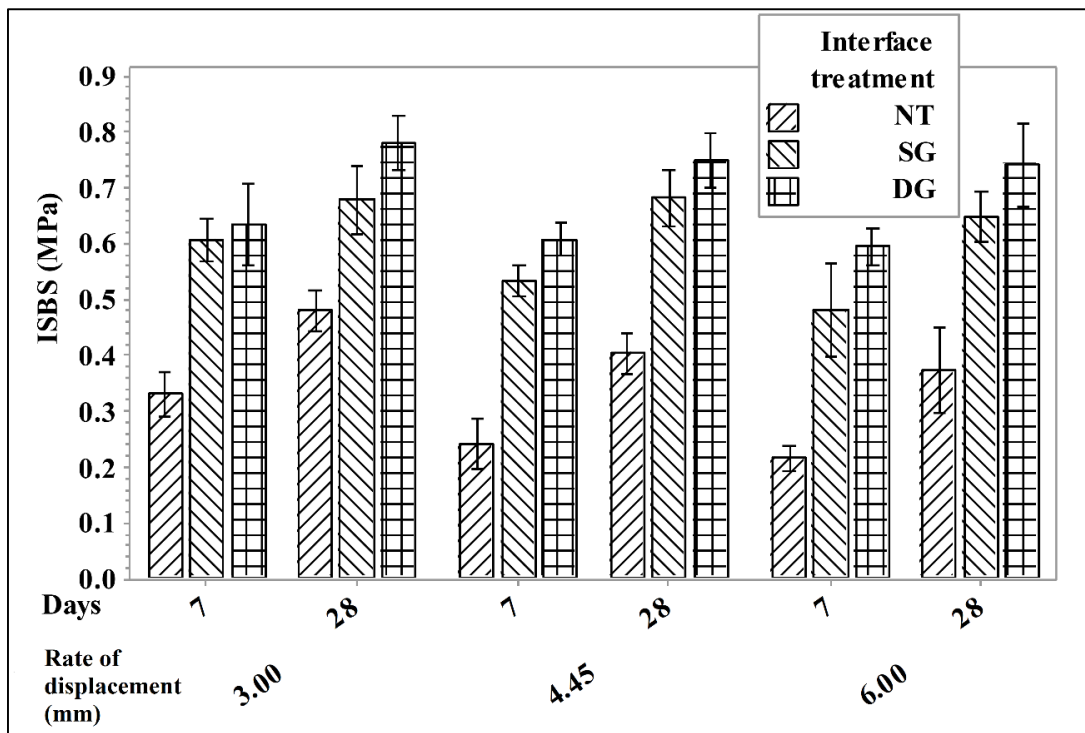
Fig. 3.7 Typical specimen interface response under the influence of shear load

3.4. RESULTS AND DISCUSSIONS

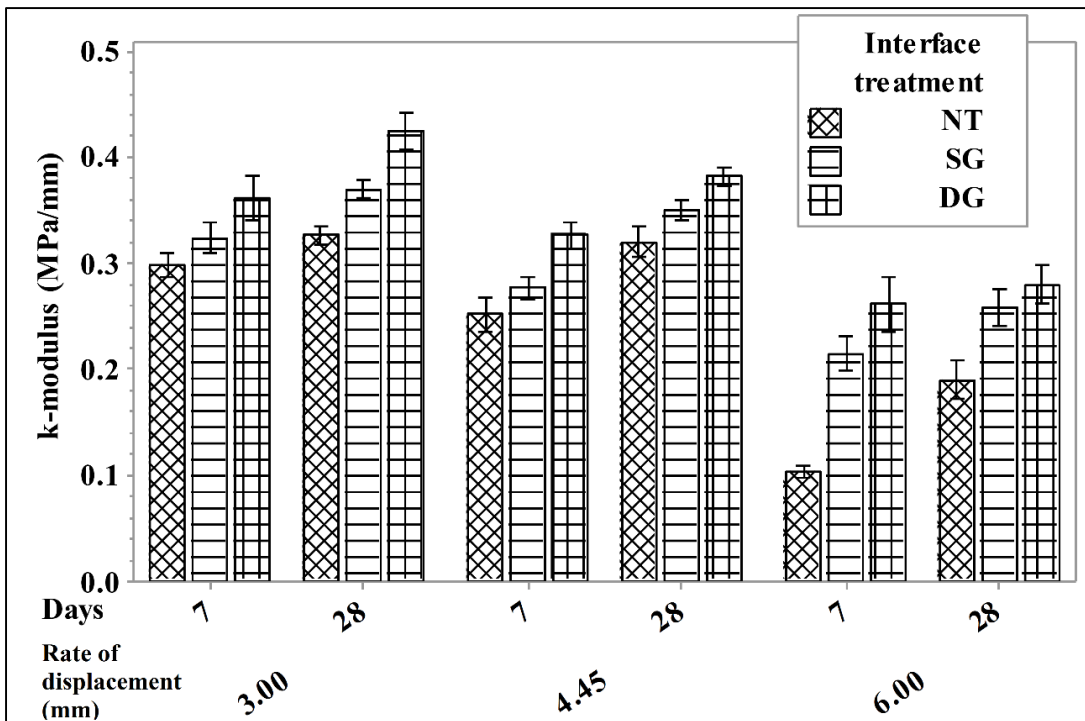
3.4.1 Effect of rate of displacement on ISBS and k-modulus

The test results of ISBS for NT, SG and DG samples are subjected to different rate of displacement are shown in Fig. 3.8 together with 95 % confidence interval. The samples with different interface treatment having a contact area of 17671 mm² were considered for calculating ISBS. It can be seen from the Fig.3.8 that for a different rate of displacement the ISBS is higher for DG compared to SG this may due to better resistance against shearing between HMA and UTW. As the groove number increases, interface bond strength increased from SG to DG this may also due to the better interlocking mechanism and a large amount of exposed aggregate surface area. For both the SG and the DG combinations the bond strength increases significantly overtime. It was observed from the test that the interface treatment and rate of displacement had an influence on the ISBS of the UTW overlay. The ISBS increased with the decrease in the rate of displacement from 6.0 mm/min, 4.45 mm/min and 3.0 mm/min. During test it was observed that for different rate of displacement the specimens were failed at the interface. The calculation of ISBS of NT specimens subjected to 6.0 mm/min rate of displacement is shown in Appendix C.

The k-modulus value for the different type of interface treatment was varied in the range of 0.10 to 0.36 MPa/mm for 7 days and 0.19 to 0.46 for 28 days. The k-modulus for different interface treatment is shown in Figure 3.8 together with 95% confidence limits. Fig. 3.8 shows that k value increases with increase in curing time. It was observed that DG treatment had higher k-modulus value compared to other interface treatment which shows that interface treatment had a significant effect on k-modulus. It can also see from Fig. 3.8 that the k modulus value decreases with the increase in the rate of displacement, which indicates that higher resistance to deformability at the interface for lower displacement rate and its value almost dependent on material characteristics of both HMA and UTW layers.



(a)



(b)

Fig. 3.8 Effect of different rate of displacement and interface treatment on (a) ISBS and (b) k-modulus

3.4.2 Effect of groove interface treatment on ISBS and k-modulus

Table 3.4 represents the test results of ISBS and k-modulus for groove interface samples subjected to the different loading direction. The interface shear strength with 95 % confidence interval is plotted against different loading conditions and shown in Fig. 3.9. Fig. 3.10 illustrates that all the samples were failed exactly at the interface, which indicates that no failure has occurred on the HMA layer. It can be seen from the Fig. 3.9 that the groove interface treatment subjected to loading perpendicular to the groove display the highest ISBS of 1.03 MPa at 7 days and 1.35 MPa at 28 days. But in practice, it is difficult to make groove or milling perpendicular to the direction of traffic. The samples subjected to diagonal and parallel loading to the groove had shown the ISBS of 0.77 MPa at 7 days and 1.27 MPa at 28 days and 0.58 MPa at 7 days and 0.74 MPa at 28 days respectively. It can also be seen from the Fig. 3.9 that the results for each interface treatment technique, ISBS increased with the increase in curing time by 22% and 39%. The ISBS for loading diagonal to the groove are 25% and 42% higher than the loading parallel to the groove at 7 and 28 days respectively. This shows that there is a better resistance to shear load between HMA and UTW layers for diagonal groove interface treatment. This indicates that specific interface treatment technique on HMA layer can significantly improve the ISBS.

The k values correspond to that observed for the peak shear stress as shown in Fig. 3.11. It can be observed from the Fig. 3.11 that the k-modulus values for different type of loading were varied in the range of 0.38 to 0.51 MPa/mm for 7 days and 0.36 to 1.10 MPa/mm for 28 days. It can also be seen from the Fig. 3.11 that the samples subjected to loading parallel to groove had shown higher k-modulus value at 7 days than 28 days, whereas in diagonal loading the k-modulus value increased over curing time by 40%. This is because the k-modulus values are measured for smaller displacements. Present finding leads to the conclusion that the potential of improvement of the k-modulus values in case of loading diagonal to the groove. Hence, k-modulus values seem to depend on the type of interface treatment technique.

From Fig. 3.11 the shaded area represents the k-modulus values at the interface ranging from 0.38 to 0.45 MPa/mm at 7 days and 0.36 to 0.63 MPa/mm at 28 days for the groove subjected to loading parallel and diagonal respectively. This shows that by

varying the direction of the groove on HMA layer increases the interface shear bond strength and k-modulus.

Table 3.4 Test Results of Interface Angle Groove

Sl No.	Direction of double groove	Area of contact (mm ²)	Average ISBS (MPa)		Average k-modulus (MPa/mm)	
			7 days	28 days	7 days	28 days
1	Parallel to loading	17671	0.58	0.74	0.45	0.36
2	Diagonal to loading	17671	0.77	1.27	0.38	0.63
3	Perpendicular to loading	17671	1.03	1.33	0.51	1.10

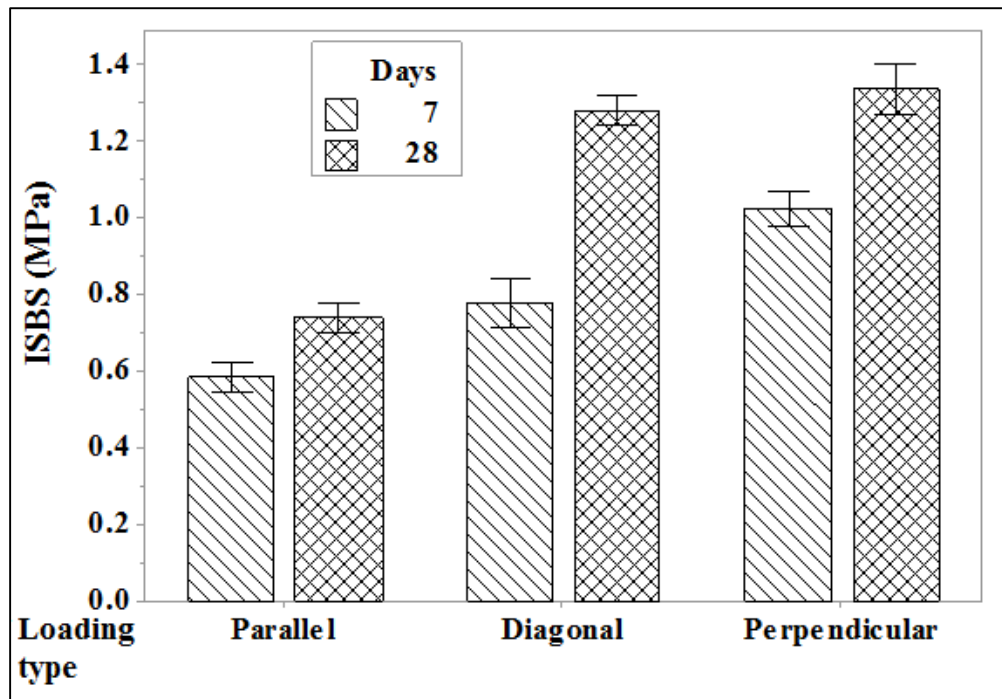


Fig. 3.9 Effect of groove interface treatment on ISBS

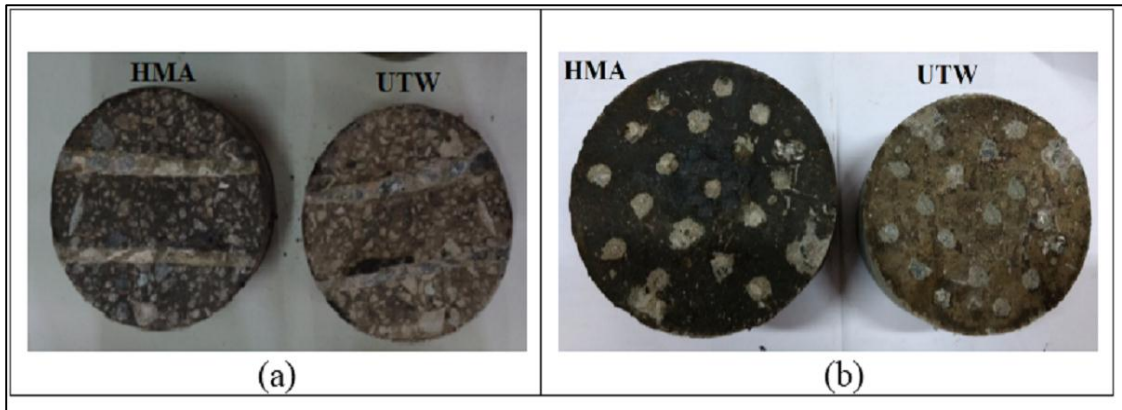
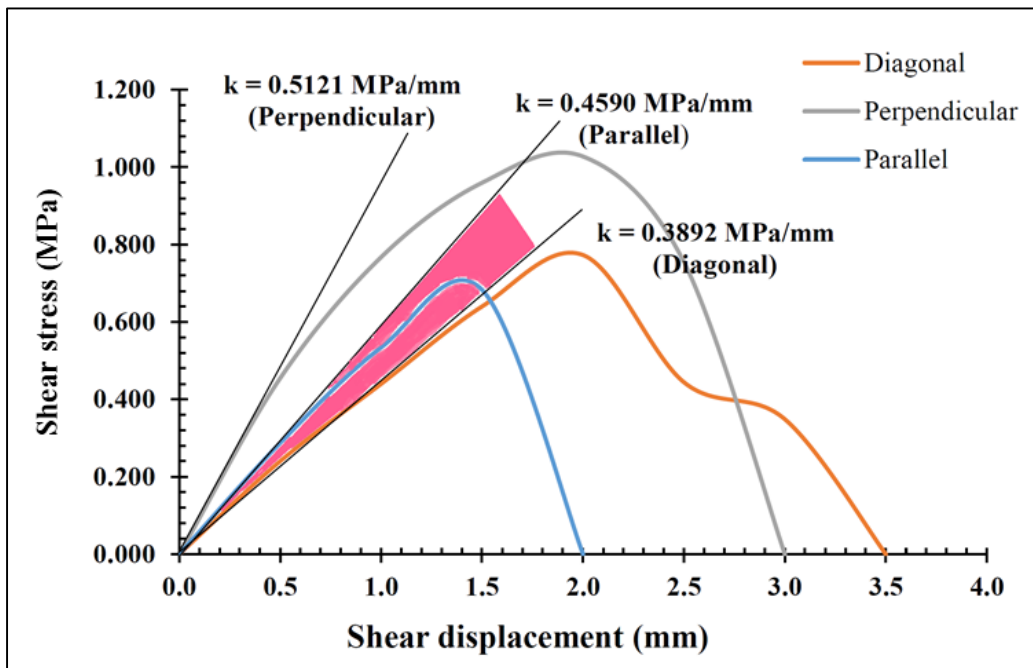
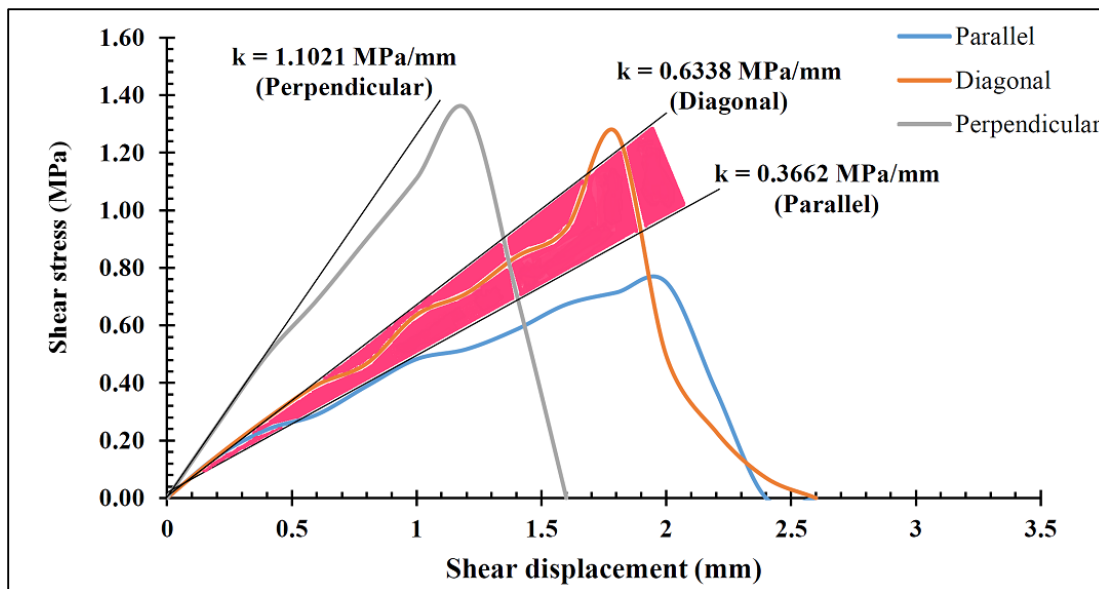


Fig. 3.10 Interface failure surfaces of the UTW shear strength specimens (a) groove interface treatment subject to parallel loading and (b) piercing interface treatment



(a)



(b)

Fig. 3.11 Effect of groove interface on k-modulus at (a) 7 days and (b) 28 days

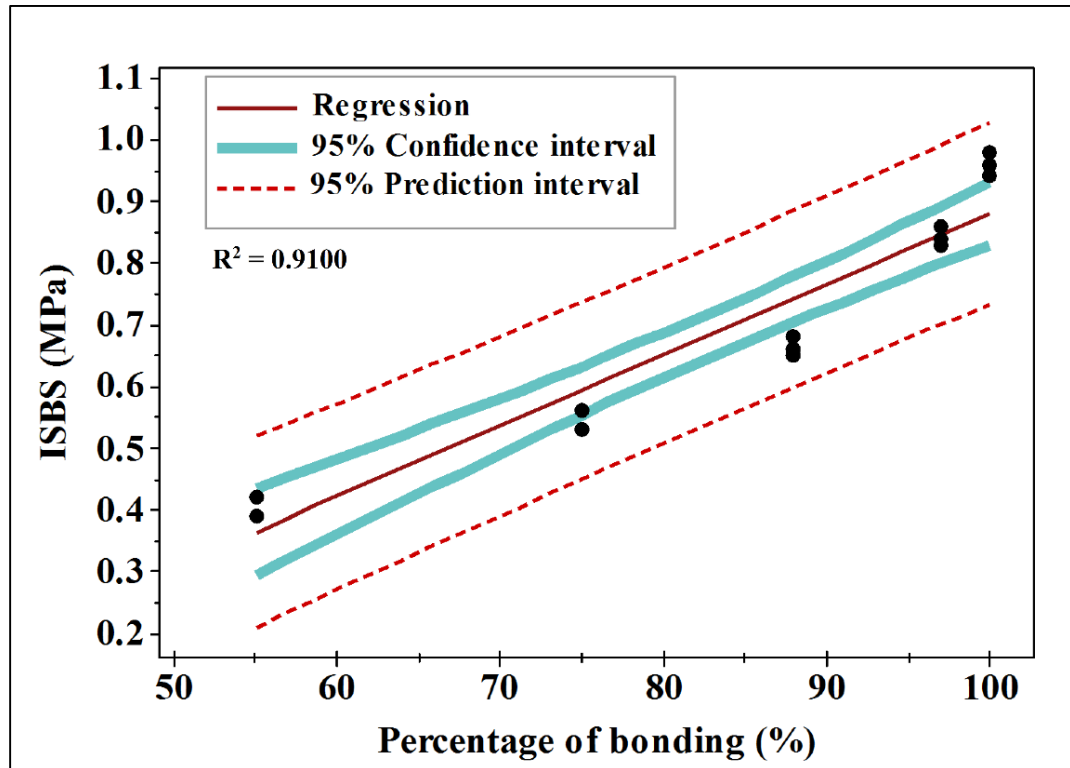
3.4.3 Effect of piercing interface treatment with different percentage of bonding on ISBS

The ISBS test results for the specimens provided with piercing interface treatment and different percentage of bonding are shown in Table 3.5. The ISBS test results are plotted against the percentage of bonding and shown in Fig. 3.12. The shaded area in the Fig. 3.12 illustrates the 95% confidence interval and 95% prediction intervals of ISBS. This represents that the ISBS values will remain within the predicted limits for piercing treatment having 55 to 100% bonding. The data presented in the Fig. 3.12 shows that the ISBS values decreased from 0.98 MPa to 0.48 MPa at 7 days and 1.17 MPa to 0.73 MPa at 28 days. This finding shows that the ISBS values decreased gradually over the interface bonding from fully bonded to partially bond.

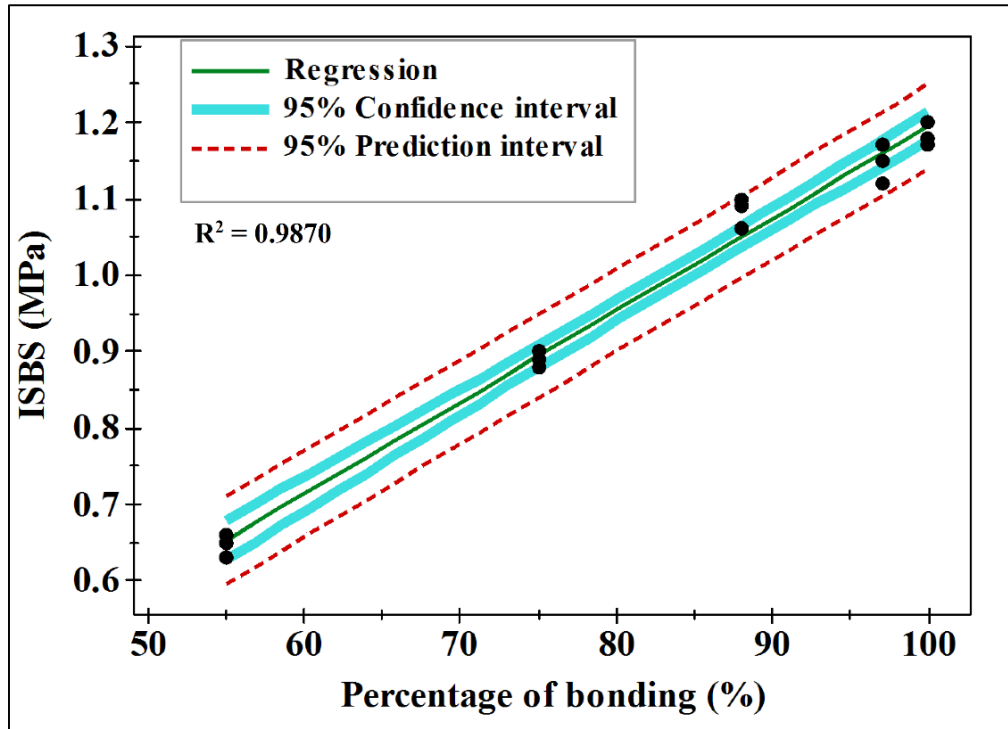
Table 3.5 ISBS Test Results of Different Percentage of Bonding

Sl No.	% of bonding	Type of interface treatment	Area of contact (mm ²)	Average failure load (kN)		Average ISBS (MPa)	
				7 days	28 days	7 days	28 days
1	100	Piercing	17671	17.52	20.58	0.98	1.17
2	97	Piercing+25	17180	13.95	19.23	0.81	1.12
3	88	Piercing+50	15708	10.73	17.50	0.68	1.11
4	75	Piercing+75	13253	7.73	13.79	0.58	1.04

Sl No.	% of bonding	Type of interface treatment	Area of contact (mm ²)	Average failure load (kN)		Average ISBS (MPa)	
				7 days	28 days	7 days	28 days
5	55	Piercing+100	9871	4.76	7.22	0.48	0.73



(a)



(b)

Fig. 3.12 ISBS for piercing and different percentage of bonding at (a) 7 days and (b) 28 days

Comparing Fig. 3.9 and Fig. 3.12 the specimens of interface treated with piercing technique had obtained higher ISBS at 7 days and 28 days compared to, the groove interface method subjected to loading towards the direction of traffic. The higher ISBS value in piercing treatment may due to the presence of visible roughness i.e., macro-texture is more and larger amount of an exposed aggregate surface. The roughness and exposed aggregate surface will provide sufficient bonding area between the two materials, thus, indicating good bonding between two layers. Using the test data presented in Table 3.5, a generalized linear equation was determined through analyzing the reduction in ISBS versus percentage of bonding (see Fig. 3.13) at 7 and 28 days, as shown in following equations Eq. (3.3) and Eq. (3.4).

At 7 days,

$$RSSB = -1.1938P_B + 127.7 \quad [R^2 = 0.9146] \quad (3.3)$$

At 28 days,

$$RSSB = -1.023P_B + 101.42 \quad [R^2 = 0.9922] \quad (3.4)$$

Where, $RSSB$ = Reduction in shear bond strength (MPa), P_B = Percentage of bonding (%)

It can be seen from the Fig. 3.13 that the piercing interface treatment technique can reduce the ISBS compared to NT in the range of 0.0 to 57.3 % at 7 days and 0.0 to 45.4% at 28 days for 100 to 55% bonding respectively. It was also observed that the interface shear bond strength increased with the increase in age at a rate of 16 to 44% for 100 to 55% bonding. Hence the specific type of interface treatment method and curing time are the key factors to improve the interface shear bond strength of UTW overlays.

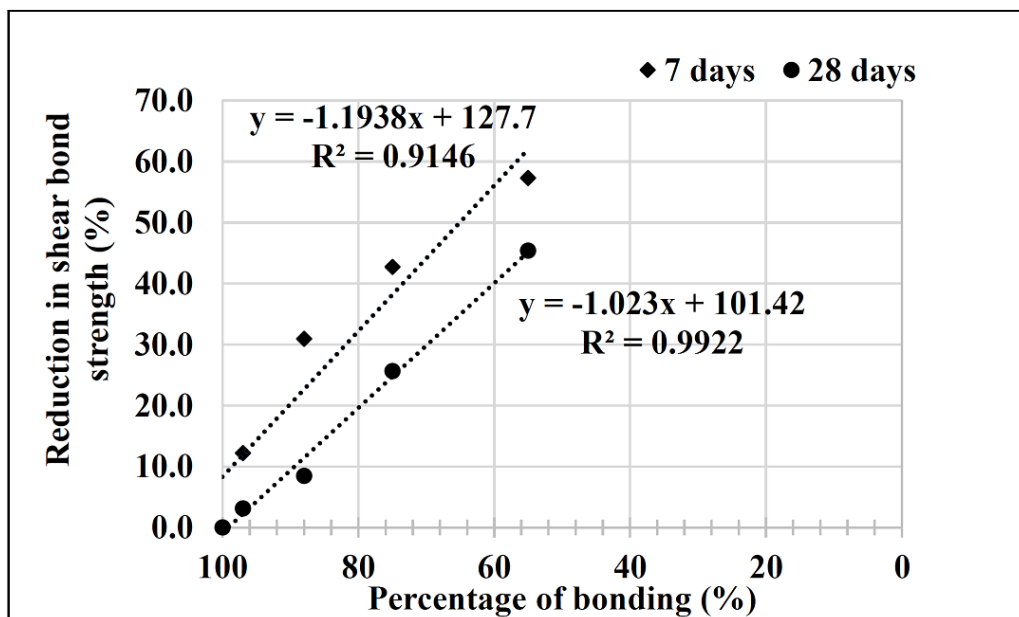


Fig. 3.13 Reduction in ISBS at 7 and 28 days

3.4.4 Effect of piercing interface treatment with different percentage of bonding on k-modulus

The k-modulus values for piercing interface treatment with different percentage of bonding were analyzed from the test data and shown in Table 3.6. Fig. 3.14 shows the calculated interface k-modulus versus percentage of bonding at 7 and 28 days with 95% confidence limits respectively. In Fig. 3.14 the k-modulus value for piercing technique with different percentage of bonding was varied in the range of 0.12 to 0.33 MPa/mm for 7 days and 0.16 to 0.36 MPa/mm for 28 days. It can be seen from the Fig. 3.14 that the piercing treatment appears to have increased k-modulus values with age at a rate of

8 to 26 %. Comparing Fig. 3.11 and Fig. 3.14 the k-modulus value of 0.36 at 28 days for 100% bonding is similar to the k-modulus value obtained in the groove interface technique. The k-modulus values for the piercing interface are similar to parallel groove interface treatment at the age of 28 days, whereas diagonal groove interface exhibit highest value of 43% compared to the piercing interface. This reveals that the interface k- modulus values almost dependent on the interface treatment.

Table 3.6 Interface k-modulus Test Results of Different Percentage of Bonding

Sl. No.	% of bonding	Type of interface treatment	Area of contact (mm ²)	Average k- modulus (MPa/mm)	
				7 days	28 days
1	100	Piercing	17671	0.33	0.36
2	97	Piercing+25	17180	0.31	0.34
3	88	Piercing+50	15708	0.24	0.27
4	75	Piercing+75	13253	0.17	0.23
5	55	Piercing+100	9871	0.12	0.16

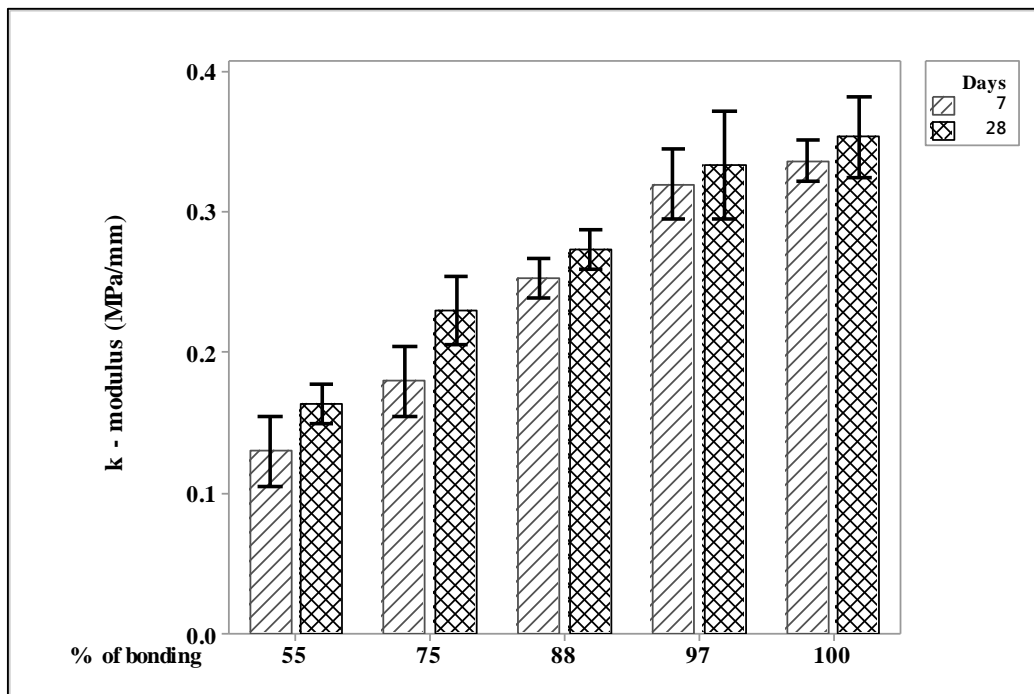


Fig. 3.14 Effect of percentage of bonding on k-modulus

3.5 INTERFACE SHEAR BOND FATIGUE

The direct shear fatigue test was adopted to evaluate the fatigue response of HMA-UTW composites. The interface treatment that had highest interface shear bond strength i.e. piercing interface treatment was subjected to interface shear bond fatigue test. During interface shear bond fatigue test, vertical displacements on either side were measured and averaged and then plotted against the number of cycles. Seo et al (2007) studied the fatigue life of asphalt concrete using indirect tensile fatigue test. They graphically determined the number of cycles at failure using bisection method. This method finds a straight line that bisects the angle between two tangent lines of the displacement curve. The straight line that crosses the displacement curve results in a number of cycles at failure. Present study consists of similar bisection method and one of the specimens fatigue life data is explained in Fig. 3.15. It can be seen from Fig. 3.15 that the last four points were discarded owing to the reason of HMA-UTW composite interface detaching. The interface shear bond fatigue test results for piercing interface treatment are shown in Table 3.7. The interface shear bond fatigue test results for different percentage of bonding are shown in Appendix D. During interface shear bond fatigue test it was observed that the specimens treated with 75, 88, 97 and 100 % of bonding had shown HMA mode of failure. The specimen had attained HMA mode of failure is shown in Fig. 3.16.

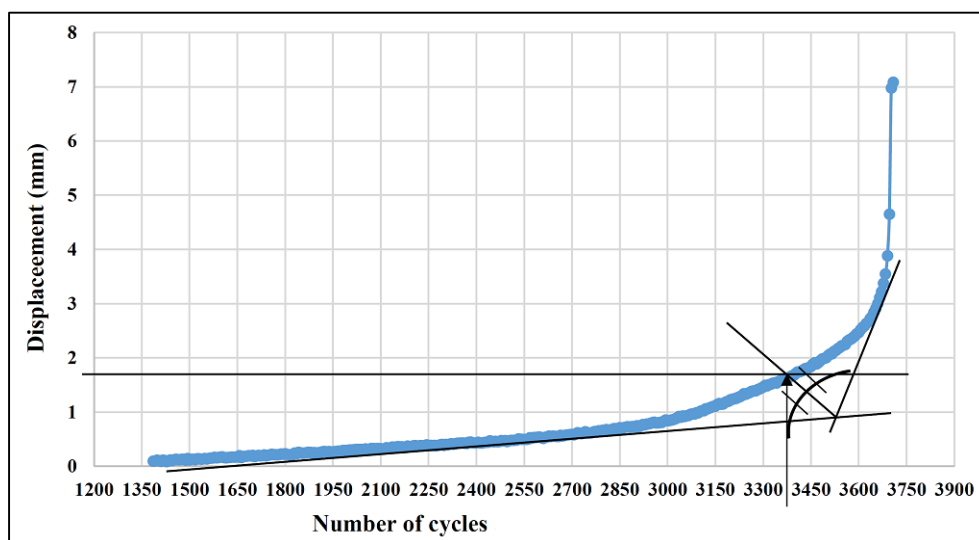


Fig. 3.15 Schematic representation of determining displacement and number of cycles at failure under the influence of shear bond fatigue

Table 3.7 Interface Shear Bond Fatigue Test Results for 100% Bonding (Piercing)

Stress ratio	Applied load (kN)	Applied stress (MPa)	Number of cycles at failure					Average number of cycles at failure
			Sample 1	Sample 2	Sample 3	Sample 4	Sample 5	
0.05	1.04	0.06	5438520	4854385	4287704	5613596	5076230	5054087
0.10	2.07	0.12	3641170	3846117	2872824	3152075	3202910	3343019
0.15	3.11	0.18	1664176	2214352	1524315	1231160	916640	1510129
0.20	4.14	0.23	632880	763280	315800	512657	494962	543916
0.25	5.18	0.29	135516	85020	320327	233870	101355	175218
0.35	7.25	0.41	62897	61132	59805	66706	64356	62979
0.45	9.32	0.53	34258	35478	33123	36780	34515	34831
0.55	11.39	0.64	22951	21587	24178	20143	22310	22234
0.65	13.46	0.76	10923	10109	10487	11325	9658	10500
0.75	15.53	0.88	5012	5148	6120	4781	4632	5139
0.85	17.60	1.00	1256	1010	1125	1796	982	1234



Fig. 3.16 Represents one of the HMA failed specimens with 100 % bonding interface

Fig. 3.17 represents the calculated number of cycles at failure for each specimen versus applied stress on a double logarithmic scale. In order to obtain a generalized interface shear bond fatigue equation, statistical regression modeling was performed and shown in Fig. 3.17. Among all the regression models, negative power model had furnished highest regression coefficient value R^2 values in the range of 0.86 to 0.94. A negative power model is shown in the following equation Eq. (5) and its statistical coefficient 'a' and 'b' obtained from analyses are summarized in Table 3.8.

$$N_{sf} = aI_c\tau^{-b} \quad (5)$$

Where, N_{sf} = is the interface shear fatigue life, I_c = is the coefficient of the interface type ($I_c = 1$), τ = interface shear stress, and a and b are coefficients.

It can be seen from this Fig. 3.17 that, as expected, the fatigue life of HMA-UTW composite specimen increased as the stress level is reduced. It is also observed that early bond failure will occur at a number of load repetition around 1200 cycles if the shear stress exceeds 85, 75, 65 and 55 % of the bond strength at the interface had 100, 97, 88, 75 and 55 % bonding.

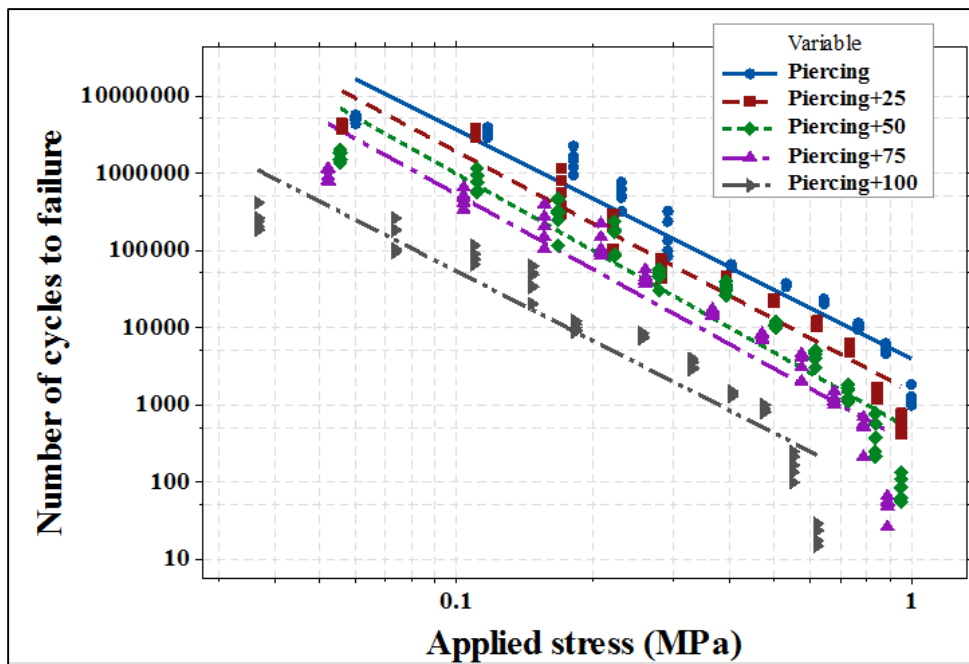


Fig. 3.17 Relationship between shear bond fatigue life and applied stress for piercing technique and different percentage of bonding

3.6 SUMMARY OF FINDINGS

Focusing towards research on the interface shear bond strength of UTW overlays, many researchers either studied the performance of UTW overlays under normal laboratory static loading conditions or investigated the performance of UTW overlays in the field for interface treated with different methods. The current research work carried out focused towards exploring the role of specific interface treatment technique with different percentage of bonding for the performance of UTW overlays. The following

conclusions are drawn from the various experimental results reported in the present work.

- The rate of loading had significant effect on the interface shear bond strength for both 7 and 28 days.
- All the HMA-UTW composite samples subjected to static loading exhibited a pure shear failure mode at the interface.
- For different interface treatment technique the interface shear bond strength was varied in the range of 0.12 to 1.17 MPa.
- Diagonal groove interface and piercing interface method ensured highest interface shear bond strength and interface k-modulus values.
- Interface treatment techniques and degree of bonding had a significant effect on the interface shear bond strength.
- The interface shear bond strength increased with the increase in curing time for groove and piercing interface method.
- A good correlation exists between applied stress and number of cycles at failure, which follows a negative power model.
- From the interface shear bond fatigue test, two million number of cycles required to fail the HMA-UTW composites with a maximum stress of 25, 20, 15 and 5% for 100, 97, 88, 75 and 55% contact area.

CHAPTER 4

QUANTIFYING THE EFFECT OF HMA THICKNESS ON FLEXURAL BOND STRENGTH OF HMA-UTW COMPOSITES UNDER FLEXURAL LOADING

4.1 BACKGROUND

The bond between UTW overlay and existing HMA pavement is immensely important for achieving design service life. Bond between the layers will be achieved by adopting different interface treatment technique.

Milling is the most effective method for rutting and shoving problems in the existing asphalt pavements. Therefore, it is most commonly used and recommended interface treatment technique for placing UTW overlays. This technique increases the surface texture of the HMA layer at macro and micro scale and gives higher shear bond strength (Delatte and Chen 2005; Mu and Vandebossche 2017). Different agencies and authors suggested that a depth of 75 to 100 mm milling operation can be carried out on the existing HMA pavement (Pereira et al. 2006). Authors also suggested that even after milling the HMA layer should have an adequate thickness and stiffness. Because UTW overlay engages the HMA layer in carrying the load (Pereira et al. 2006; Barman et al. 2017). In addition to this the thickness of HMA layer is lesser than the expected, increases the UTW panel stresses, this will lead to higher flexural stresses and early fatigue failure (Delatte and Chen 2005). Hence thickness of HMA layer had a significant effect on the performance of UTW overlays.

Further the UTW overlays has been developed for low volume roads (Li et al. 2004; IRC SP: 76 2008). Whereas the design thickness of HMA layer for low volume roads is found to be 75 to 100 mm (IRC SP: 72 2015). However milling operation may remove the HMA layer and expose the base layer, which should be avoided. Therefore a study is required to quantify the HMA thickness for UTW overlays. Present study evaluates the effect of HMA thickness and variation in stress at bottom of UTW overlay for different percentage of bonding.

4.2 SAMPLE PREPARATION

The UTW prism specimens were casted using an optimized FRC mix proportion (see chapter 2). Properties of asphalt and aggregates for HMA mix are explained in chapter 2. The aggregate gradation adopted for HMA prism specimens is shown in Table 4.1.

Table 4.1 Aggregate composition for HMA mixture (MoRTH, 2013)

Designation	DBM grading-2	
NMAS (mm)	26.5	
Layer thickness (mm)	50-75	
IS sieve (mm)	Cumulative % by weight of total aggregate passing	
	Specified Limits	Adopted
37.5	100	100
26.5	90-100	95
19.0	71-95	83
13.2	56-80	68
9.5	--	--
4.75	38-54	46
2.36	28-42	35
1.18	--	--
0.6	--	--
0.3	7-21	14
0.15	--	--
0.075	2-8	5
Binder content	Min 4.5 percent by weight of total mix	

Three stages of HMA-UTW composite prism specimen preparation are as follows,

- (i) HMA mixture: The prism specimens having a cross section of 77 x 77 x 380 mm were casted by compacting the hot asphalt mixture in a rectangular mold by kneading action to get the required density. The mixing and compaction temperature of 160⁰ C and 135⁰ C was maintained. The specimens are allowed to cool for one day in room temperature 25±2⁰ C.
- (ii) Interface treatment: The compacted HMA mixture were demould and two types of interface treatment was carried out such as (a) no treatment and (b) different percentage of bonding. The different percentage of bonding at the interface were introduced by pasting a 0.15 micron PVC sheet at the center of HMA samples. The 50 % interface bonding specimens are shown in Fig. 4.1.

- (iii) HMA-UTW composite flexural beam: The HMA interface treated specimens were placed inside the wooden beam moulds of size 77 x 180 x 380 mm and made the HMA surface wet by spraying water. Freshly prepared FRC mix was poured into the mould to achieve a total height of 155 mm HMA-UTW composite specimens (see Fig. 4.2).

The specimens were demould and allowed to water curing by immersing the 70 mm depth UTW portion till the date of testing. For each interface treatment, six specimens were prepared for static loading and four specimens for dynamic loading conditions to eliminate the experimental errors.

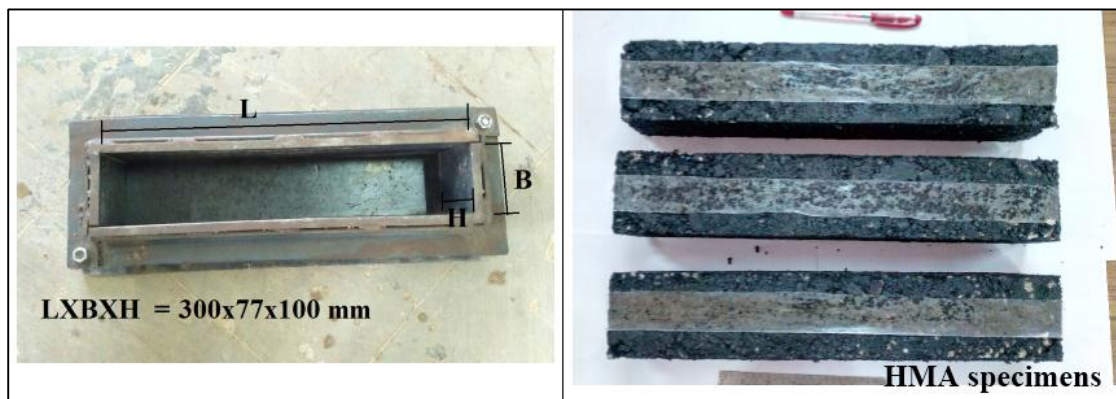


Fig. 4.1 Represents the prism mould and HMA specimens with 50 % interface treatment

4.3 TEST PROCEDURE

HMA-UTW composite flexural beam specimens were placed horizontally inside the testing machine as shown in Fig. 4.2. Once the test setup was established four point bending test was carried out in two-phase,

- (i) Static loading: A constant vertical displacement of 6.0 mm/min was applied directly on the steel plate segment using strain controlled Material Testing System (MTS) and testing temperature of $25 \pm 2^{\circ} \text{C}$ was maintained.
- (ii) Dynamic loading: Flexural fatigue load had a frequency of 3 Hz with different stress ratios was applied on HMA-UTW composite specimens. The test was conducted using stress controlled repeated loading testing machine as shown in Fig. 4.2. The repeated load was applied analogs to the semi-sine waveform and this waveform, relatively close to the traffic loading applied on the pavement. The stress ratio is the load value in a repeated load test to

the ultimate load value in the static flexural strength test. For each load cycle, the applied stress and vertical displacement were measured.



Fig. 4.2 Represents the repeated load test for HMA-UTW composite prism specimens and 50 % interface bonding failure specimen

4.4 RESULT AND DISCUSSIONS

4.4.1 Effect of HMA Thickness and Percentage of Bonding on Flexural Bond Strength

The static flexural test was performed on 50% and 100% bonding HMA-UTW composite prism specimens. Fig. 4.3 represents the flexural bond strength of HMA-UTW composite specimens. The flexural bond strength test results are plotted against the percentage of bonding and different HMA thickness. Fig. 4.3 illustrates the 95% confidence interval limits of flexural bond strength at 7 and 28 days. The data presented in the Fig. 4.3 shows that the flexural bond strength values decreased from 1.01 MPa to 0.31 MPa at 7 days and 1.71 MPa to 0.64 MPa at 28 days for 75 mm HMA thickness. Also 50 mm HMA had shown the same trend 0.63 MPa to 0.13 MPa at 7 days and 1.06 MPa to 0.28 MPa at 28 days. This finding shows that the interface flexural bond

strength values decreased gradually over the interface bonding from fully bonded to partially bond. From the Fig. 4.3 the specimens of 75 mm HMA thickness had the higher flexural bond strength of 1.01 MPa at 7 days and 1.71 MPa at 28 days; in contrast, the specimens of 50 mm HMA thickness of 0.63 MPa at 7 days and 1.06 MPa at 28 days. The higher flexural bond strength value in 75 mm HMA may due to the higher flexural rigidity. This will improve flexural stiffness of the HMA-UTW composites.

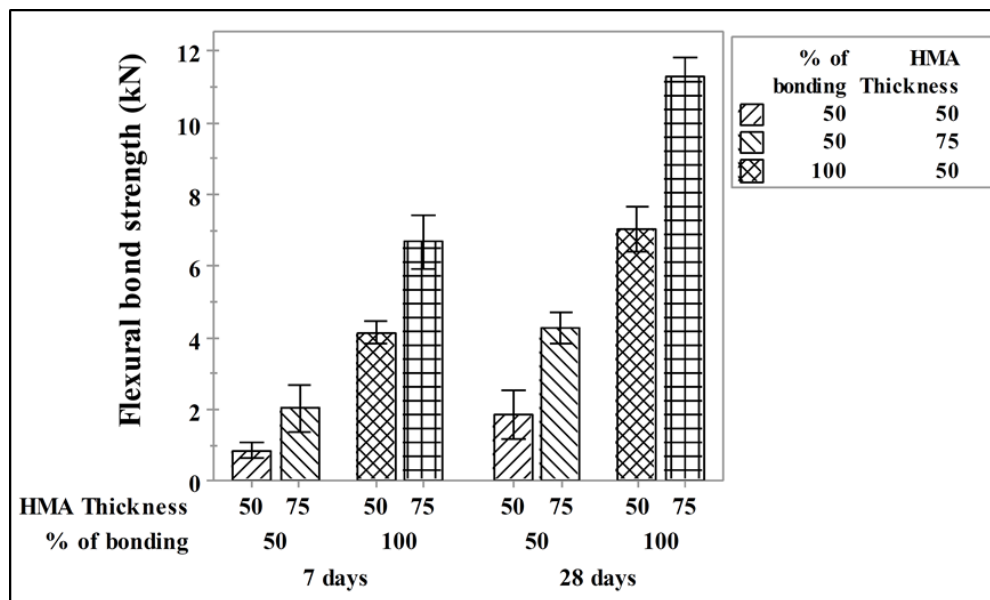


Fig. 4.3 Flexural bond strength of HMA-UTW prism composites at 7 and 28 days for 50 and 100 percent bonding

4.4.2 Effect of HMA Thickness and Percentage of Bonding on Flexural Fatigue Life

The flexural fatigue test was adopted to evaluate the fatigue response of HMA-UTW prism composites. The HMA thickness of 75 mm had shown highest interface flexural bond strength than the 50 mm HMA thickness. Therefore HMA-UTW composite specimens had a HMA thickness of 75 mm was subjected to interface flexural fatigue test. During flexural fatigue test, the vertical displacements on either side were measured and averaged and then plotted against the number of cycles. Fig. 4.4 represents the calculated number of cycles at failure for each specimen versus stress ratio on a logarithmic scale. The summary of number of fatigue cycles to failure is shown in Table 4.2. In order to obtain a generalized interface flexural bond fatigue

equation, statistical regression modeling was performed and shown in Fig. 4.4. Among all the regression models, exponential model had furnished highest regression coefficient values. The exponential model is shown in the following equation Eq. (4.1).

$$N_f = ae^{-b(SR)} \quad (4.1)$$

Where, N_f = is the flexural fatigue life, SR = stress ratio, and a and b are coefficients.

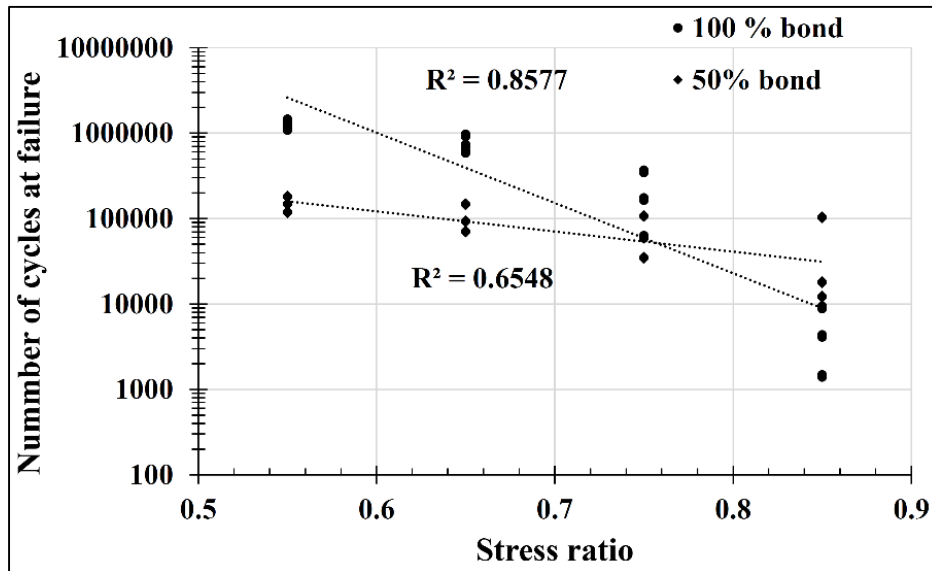


Fig. 4.4 Relationship between stress ratio and fatigue life of 75 mm HMA thickness HMA-UTW prism composites

4.4.3 Analysis of Fatigue-Life Distribution Using Weibull Distribution Parameters

The distributions of fatigue life were analyzed using experimental data. The present investigation incorporated Weibull distribution for the description of fatigue life data at different stress level. The graphical method is employed to illustrate the distribution of fatigue life of HMA-UTW prism composites had a 75 mm HMA thickness with 100 and 50% bonding at a particular stress level. Then the Weibull distribution parameters i.e., (i) Shape factor ‘ α ’ – describes the shape of the distribution, (ii) Characteristic Life ‘ μ ’ for the fatigue life will be determined using the graphical method. The Weibull probability density function $f_N(n)$ and its cumulative distribution function $F_N(n)$ for fatigue life were determined. Weibull distribution parameters and equations are explained in the chapter 2.

Table 4.2 Summary of flexural fatigue life of HMA-UTW prism composites

75 mm HMA Thickness									
% of bonding	Failure load (kg)	Stress ratio	Applied load (kg)	Applied stress (kg/cm ²)	Number of cycles to failure				Average number of cycles
					Sample 1	Sample 2	Sample 3	Sample 4	
100	1152	0.55	634	9.59	1266578	1209582	1234914	1184250	1223831
		0.65	749	11.33	737424	704240	718988	689491	712536
		0.75	864	13.08	175000	167125	170625	163625	169094
		0.85	979	14.82	4365	4169	4256	4081	4218
	1090	0.55	600	9.07	1458762	1393118	1422293	1363942	1409529
		0.65	709	10.72	972415	928656	948105	909208	939596
		0.75	818	12.37	368710	352118	359492	344744	356266
		0.85	927	14.02	9417	8993	9182	8805	9099
	1236	0.55	680	10.29	1157216	1105141	1128286	1081997	1118160
		0.65	803	12.16	623870	595796	608273	583318	602814
		0.75	927	14.03	63218	60373	61638	59109	61084
		0.85	1051	15.90	1486	1419	1449	1389	1436
50	300	0.55	165	2.50	186945	178532	182271	174794	180636
		0.65	195	2.95	152108	145263	148305	142221	146974
		0.75	225	3.41	110860	105871	108089	103654	107118
		0.85	255	3.86	106748	101944	104079	99809	103145
	465	0.55	256	3.87	122860	117331	119789	114874	118713
		0.65	302	4.57	73015	69729	71190	68269	70551
		0.75	349	5.28	35864	34250	34967	33533	34654
		0.85	395	5.98	12587	12021	12272	11769	12162
	415	0.55	228	3.45	153121	146231	149293	143168	147953
		0.65	270	4.08	96172	91844	93768	89921	92926
		0.75	311	4.71	61796	59015	60251	57779	59710
		0.85	353	5.34	18657	17817	18191	17444	18027

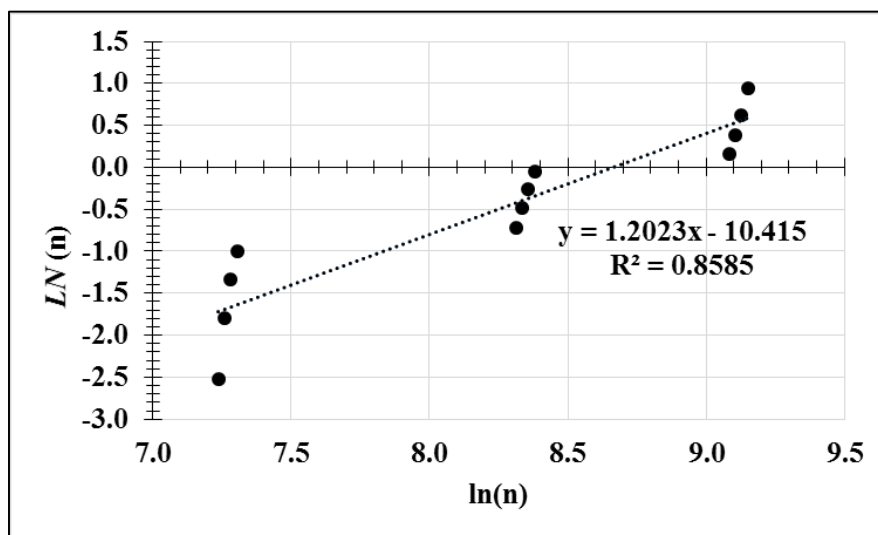
A graph is plotted between $Y = L_N(n)$ and $X = \ln(n)$. The plotted graphs are shown in Fig. 4.5. Fig 4.5 (a) and (b) represents the data for 0.85 stress ratio. Similar graphs were plotted for 0.75, 0.65 and 0.55 stress ratios and it is shown in Appendix E. Further, the best fit straight line is drawn through the data. If data points fall approximately along the linear trend line, indicates that the two-parameter Weibull distribution is a reasonable assumption for the fatigue behavior of HMA-UTW prim composites. The slope of the line provides an estimate of the shape factor ' α ' and characteristic life ' β ' can be obtained by using the equation $B = \alpha \ln(\beta)$, where, B= is a constant of the straight line obtained from the graph. From the Fig. 4.5(a) it can be see that the slope of the line $\alpha = 1.2023$ and $B = 10.415$,

$$B = \alpha \ln(\beta)$$

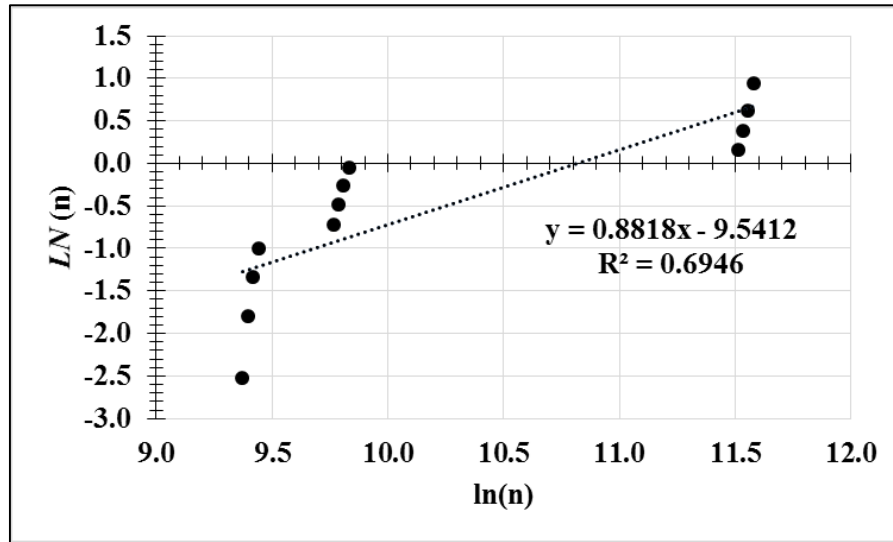
$$\ln(\beta) = \frac{B}{\alpha} = \frac{10.415}{1.2023} = 8.6625$$

$$\beta = \exp(8.6625) = 5782$$

The parameters α and β obtained from the graph for different stress ratios are tabulated in Table 4.3. It can be seen from the Fig. 4.5, that the shape parameter ' α ' decreased at higher stress levels and increased at lower stress levels for the fatigue life of 75 mm HMA thickness. Hence the variability in the distribution of fatigue life of 75 mm HMA thickness with 100% bonding becomes more at lower stress levels as compared with higher stress levels.



(a)



(b)

Fig. 4.5 Graphical analysis of fatigue life data for (a) 100% and (b) 50% bonding HMA-UTW prism composites

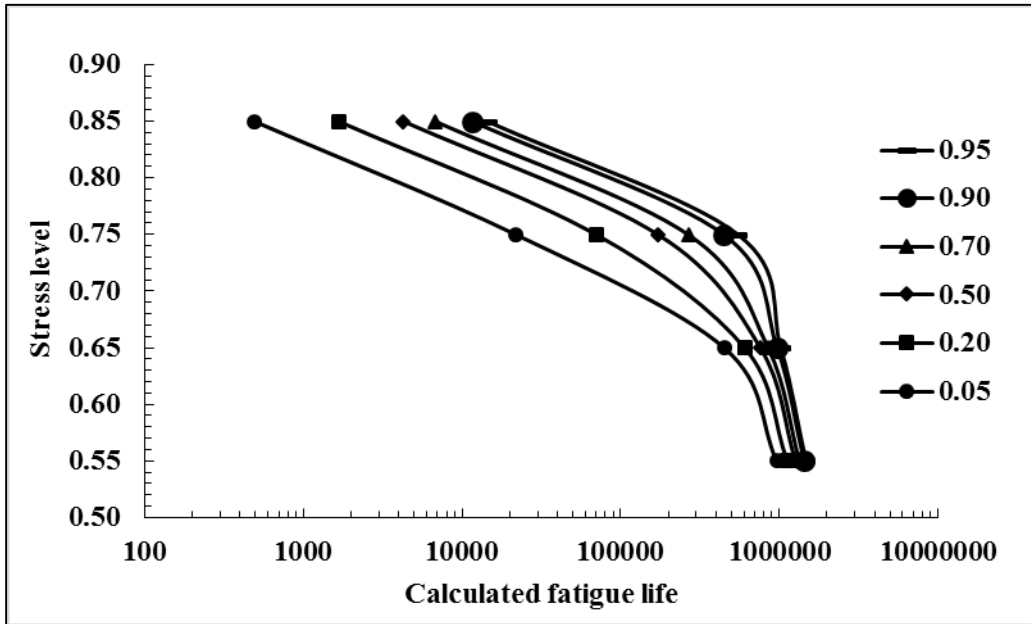
Table 4.3 Weibull parameters for fatigue lives of HMA-UTW composites with 50 and 100% bonding interface

Stress Ratio	Graphical method	
	100% bonding	
	α	β
0.85	1.2023	5782
0.75	1.2604	230056
0.65	4.9523	817889
0.55	9.5490	1312362
	50% bonding	
0.85	0.8818	50018
0.75	1.9748	78076
0.65	2.9634	117013
0.55	5.4287	161161

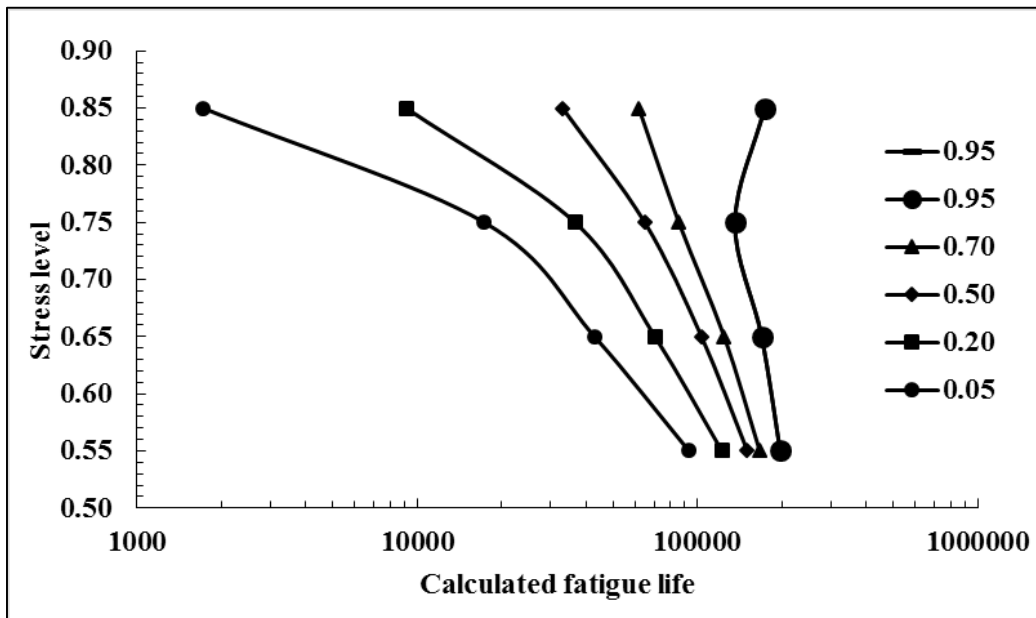
4.4.4 Failure Probability and S-N Relationship

The Weibull distribution can be employed to incorporate the failure probability into the S-N relationships of HMA-UTW prism composites. Using the values of Weibull parameters α and μ , as obtained previously for a given fatigue life data, were used to calculate fatigue lives of FRC corresponding to different failure probabilities (that is, $P_f = 0.05, 0.20, 0.50, 0.70, 0.90$ and 0.95). Further, these values have been plotted to obtain the P_f -S-N relationships for 75 mm HMA thickness with 100 and 50% bonding

and shown in Fig. 4.6. This represents almost similar to the values obtained for two-parameter Weibull distribution as P_f decreases the number of cycles also decreases.



(a)



(b)

Fig. 4.6 P_f -S-N diagram for (a) 100% and (b) 50% bonding HMA-UTW prism composites

4.5 SUMMARY OF FINDINGS

In this study HMA-UTW prism composite specimens with different HMA thickness and percentage of bonding were subjected to static and dynamic loading conditions. The following conclusions were drawn.

- Based on the flexural bond strength test the interface flexural bond strength was varied between 0.13 to 1.71 MPa. Therefore HMA thickness had a significant effect on flexural bond strength.
- Irrespective of HMA thickness and percentage of bonding the flexural bond strength was increased with curing time of UTW layer.
- The flexural bond fatigue equation was developed between the applied stress and number of cycles at failure, which follows a negative exponential model. The coefficient of determination was in the range of 0.65 to 0.85, which means the flexural bond fatigue test was reliable.
- The fatigue-life distributions of HMA-UTW prism composite specimens at a given stress level is shown to approximately follow the two-parameter Weibull distribution.
- Stress levels and percentage of bonding had a significant effect on the fatigue life of HMA-UTW prism composite specimens. Because HMA failure were observed at higher stress level in 50 and 100 % bonding.
- From flexural bond fatigue test, five million number of cycles required to fail the HMA-UTW prism composites with a maximum stress of 0.65 for 100 percentage of bonding.

CHAPTER 5

SIMULATING HMA-UTW INTERFACE FRACTURE BY SUPERIMPOSING CONTACT FRICTION MODEL USING DIRECT SHEAR AND FLEXURAL LOADING TEST DATA

5.1 BACKGROUND

Interface bond strength between HMA and UTW layer plays an important role towards the service lives of UTW overlays. Adequate interface bond strength is necessary to resist the stress caused by traffic loading. The present work includes a three-dimensional (3-D) FE approach to evaluate the effect of different percentage of bonding on interface shear bond strength as measured by the direct shear and flexural test. From the literature it can be seen that authors have adopted different interface model to evaluate interface bond strength. The summary of literature is shown in Table 5.1.

5.2 EXPERIMENTAL DESIGN

The commercial FE software ANSYS Version 14.0 was used to simulate the test results. The contact friction model available in ANSYS was used to simulate interface bond strength of UTW overlays. The element type SOLID185 has been found to provide sufficiently accurate results for structural analysis. Therefore present work includes 3D brick elements SOLID185, having eight nodes with three degrees of freedom at each node and the nodal translations in x, y, and z directions. This element was used to model both HMA and UTW layers.

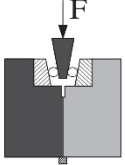
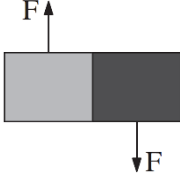
In order to connect the HMA and UTW layers surface-to-surface contact elements of CONTA174 were used to model the contact and sliding between 3-D target surfaces TARGE170. It has three degrees of freedom at each node: translations in the nodal x, y, and z directions. The modulus of elasticity of HMA layer was assumed to be 3500 MPa. For UTW layer modulus of elasticity of 37552 MPa was considered from the experimental test results explained in chapter 2. The Poisson's ratio for HMA layer 0.35 and UTW layer 0.15 was adopted. The coefficient of friction $\mu = 0.35$ was assumed.

Five separate models were developed for the direct shear test, such as 100 %, 97 %, 88 %, 75 % and 55 % bonding between HMA and UTW layer. The interface properties presented in Table 5.1 were used in the simulation of the direct shear test. HMA layer had a diameter of 150 mm and 100 mm thickness and UTW layer of 150 mm diameter and 75 mm thickness were considered for modeling. The mesh size for HMA and UTW layer of 50 x 50 x 50 mm was adopted. The degrees of freedom in x, y and z direction was fixed in HMA layer. Whereas, in UTW layer x and z degrees of freedom was fixed and y component is set to displace in loading direction. Further, to solve the simulated model, displacement values obtained from experimental were applied on the UTW layer. The simulated HMA-UTW cylindrical composites model subjected to ISBS is shown in Fig. 5.1.

Four separate models were developed for interface flexural bond strength test. Each model had different percentage of bonding at the interface and HMA layer thickness. In all the models UTW layer thickness of 75 mm was kept constant.

Two different bonding conditions were adopted for 50 and 75 mm HMA thickness. The UTW layer thickness of 75 mm was kept constant. A 50 x 50 x 50 mm mesh was adopted for HMA-UTW prism composites. Further to solve the simulated model displacement values were applied in the direction of loading. The simulated HMA-UTW prism composites model subjected to flexural bond strength is shown in Fig. 5.2.

Table 5.1 Summary of literature for simulation of interface bond strength in FEM

Sl. No.	Test method	Type of model	Element type	Interface element type	Assumptions	References
1	 <p>Wedge splitting test (mode I)</p>	Damage simulation, cohesive zone model	8 node brick solid element	NA	NA	Tschegg et al. (1995), Mu and Vandebossche (2017)
2	 <p>Direct shear test (mode II)</p>	2D, 3D fracture based elastoplastic.	8 node brick solid element	Zero thickness interface element, Hyperbolic Mohr's-Coulomb theory, contact elements.	Tensile strength equal to cohesion. The friction angle and the residual friction angle of 35 and 30 degrees	Romanoschi and Metcalf (2001), Kruntcheva et al. (2005), Kruntcheva et al. (2006), Ozer et al. (2008), Ozer et al. (2012)
3	NA	3D	20 nodes	NA	All the materials were modeled as linearly elastic and isotropic	Kumara et al. (2003)
4	Indirect tensile test	3D	NA	Spring element	NA	Nishiyama et al. (2005)
5	Compact tension test	2D plane-strain cohesive zone elements	NA	NA	NA	Ahmed et al. (2012)
6	NA	3D	8-node brick element with reduced integration	NA	Assuming full bonding behavior	Kim and Lee (2013)
7	NA	2D and 3D	3 node CONTACT48	Contact elements	NA	Kruntcheva et al. (2005), Li et al. (2014)
8	NA	Cohesive contact model	NA	Contact elements	NA	Skar and Poulsen (2015)

Sl. No.	Test method	Type of model	Element type	Interface element type	Assumptions	References
9	NA	NA	27 node isoparametric brick elements	Spring elements	NA	Barman et al. (2015), Barman et al. (2017)

Bituminous material;
 Cement concrete material

Table 5.2 Interface properties from direct shear test

Sl. No.	Percentage of bonding	ISBS (MPa)	Tangential stiffness (MPa/mm) ^a
1	100	1.17	0.36
2	97	1.12	0.34
3	88	1.11	0.27
4	75	1.04	0.23
5	55	0.73	0.16

^a Tangential stiffness values were assumed in both transverse and longitudinal directions

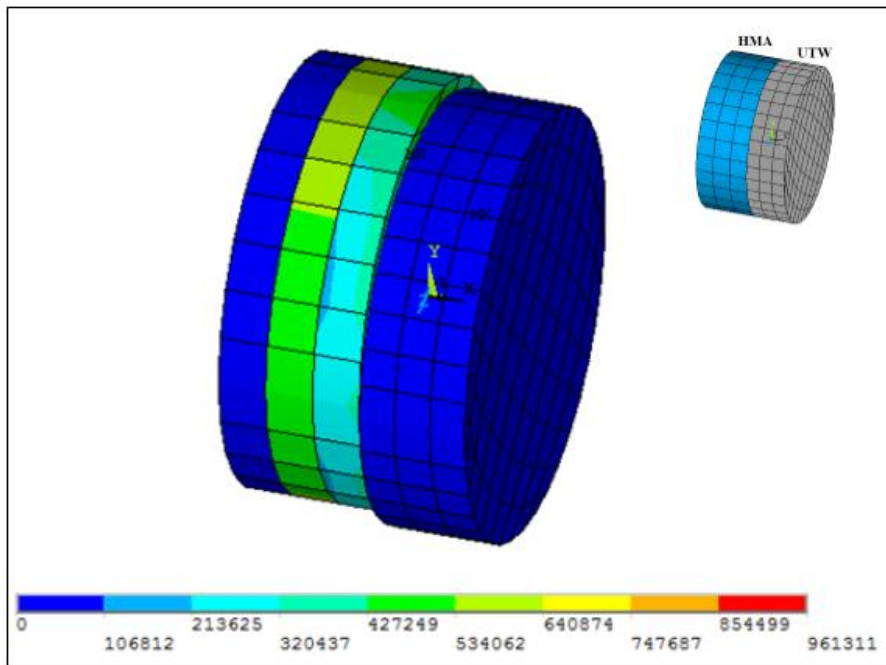


Fig. 5.1 The stress variation at the interface for 97 % bonding specimen subjected to direct shear loading.

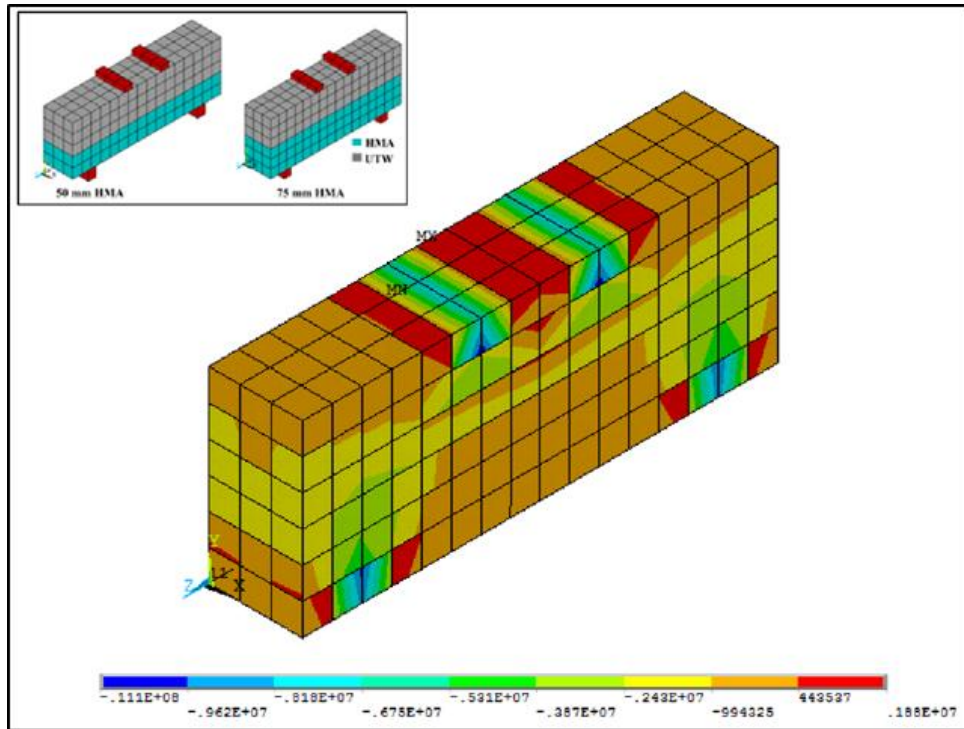


Fig. 5.2 Stress variation at the interface for 75 mm HMA thick with 100% bonded interface subjected to flexural loading.

5.2 RESULTS AND DISCUSSION

The experimental and simulation results for ISBS and flexural bond strength are shown in Fig. 5.3 and Fig. 5.5. From the Fig. 5.3 it can be seen that simulated models results are comparable with the experimental results. An error of 4% obtained in 100 and 55% bonding compared to 97, 88 and 77 % bonding. The lesser error may be due to area of contact elements at the interface is almost similar to the laboratory specimens. A statistical regression modeling was performed for ISBS verses percentage of bonding and is shown in Fig. 5.4. Among all the regression models, power model had furnished highest regression coefficient value for experimental ($R^2 = 0.94$) and simulated model ($R^2 = 0.90$).

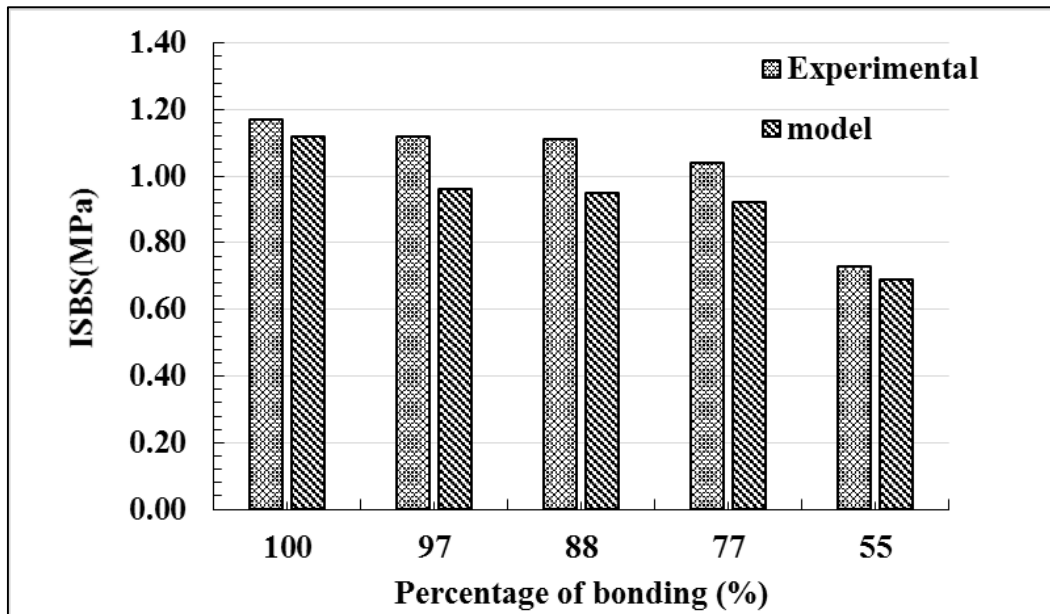


Fig. 5.3 Comparison of experimental and model ISBS of piercing interface treatment and piercing with different percentage of bonding

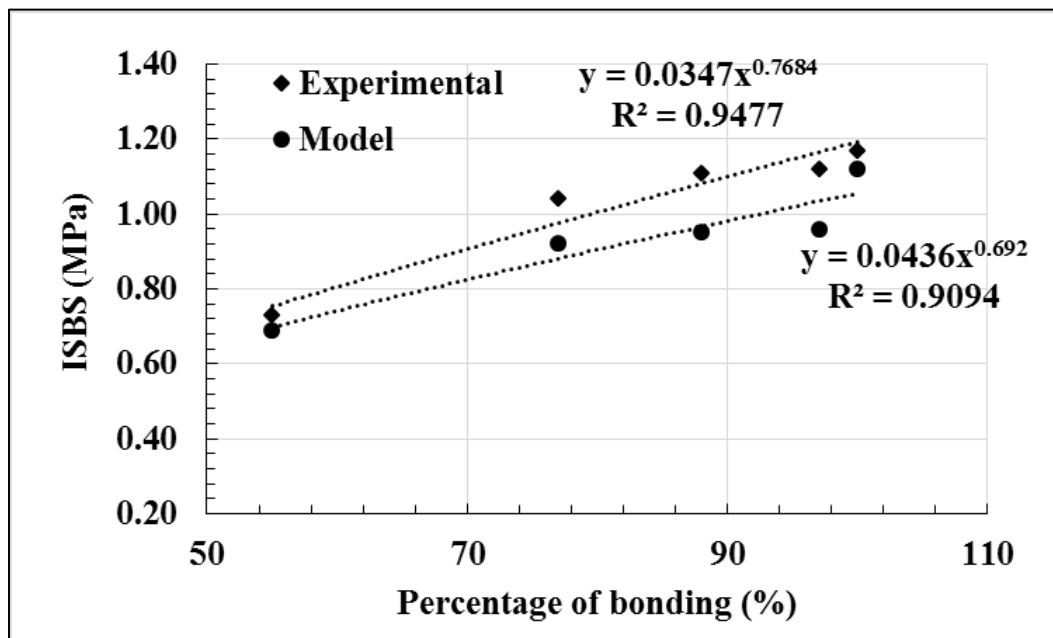


Fig. 5.4 Regression coefficient values for simulated model and experimental result for ISBS.

It can be seen from the Fig. 5.5 that flexural bond strength values are comparable with the experimental and simulated model. An error of 5 to 14 % was achieved between experimental and simulated model.

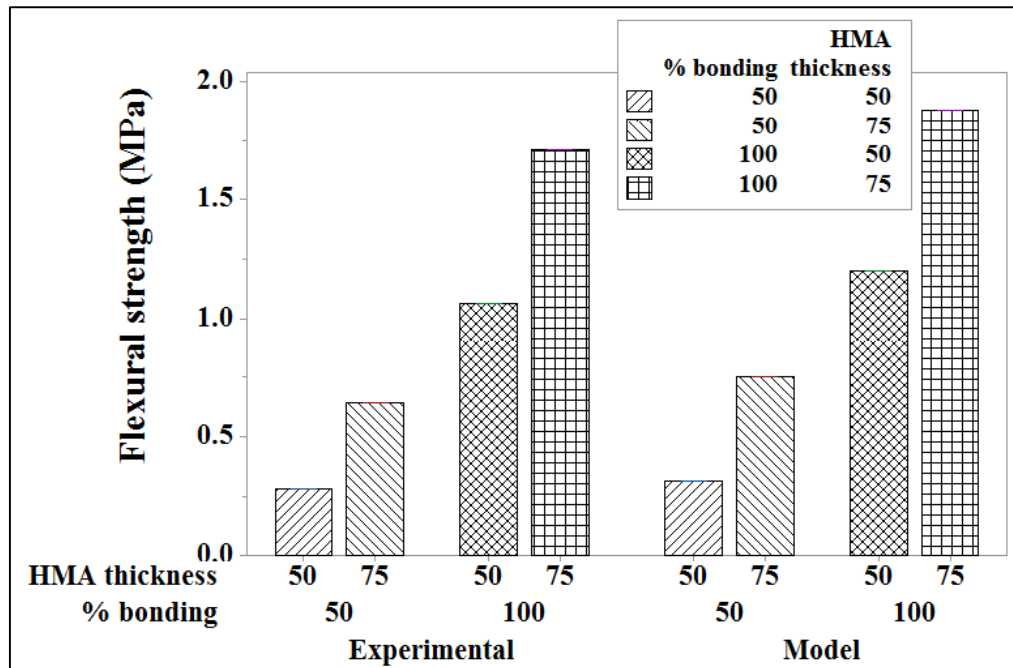


Fig. 5.5 Comparison of experimental and simulated model for the samples subjected to interface flexural bond strength

5.3 SUMMARY OF FINDINGS

A contact friction model was successfully simulated the test data's obtained for HMA-UTW cylindrical and prism composites. An acceptable error of 4 to 15 % were obtained in both the cases. Therefore direct shear test and flexural bond strength test methods can utilized to evaluate interface bond strength of UTW overlays.

CHAPTER 6

CONCLUSION AND FUTURE WORK

The laboratory-based framework has been developed and simulated to determine the interface bond strength of UTW overlays under static and dynamic loading conditions. The percentage of bonding is defined as the delaminated area at the interface of HMA-UTW composites. The framework includes different interface treatment techniques and modified laboratory test methods. For different interface treatment techniques, the direct shear test was conducted to investigate the interface bond strength and k-modulus of UTW overlays. Later, interface treatment technique obtained highest interface bond strength was subjected to interface shear bond fatigue test under different stress levels. To evaluate the effect of HMA thickness on UTW overlays, different HMA thickness with different percentage of bonding at the interface were subjected to the flexural test. A contact friction model was adopted in the finite element analysis to simulate the laboratory test results.

A direct shear test was conducted for all the interface treatment technique specimens. An interface failure was observed in the specimens when subjected to direct shear test under static loading condition. Based on direct shear test, groove interface treatment with an inclination of 45 degrees and piercing had obtained higher ISBS compared to NT and DG interface treatment. Therefore interface treatment techniques had a significant effect on the ISBS. A generalized linear equation was determined for a reduction in shear bond strength for piercing interface treatment with different percentage of bonding. When the percentage of bonding decreased at the interface HMA failure were identified for 5 million number of cycles at 5, 10, 20 and 25 % stress levels. A negative power model was established for piercing interface treatment with different percentage of bonding subjected to fatigue loading.

The flexural bond test strength was conducted for different percentage of interface bonding and HMA thickness to determine effective HMA thickness and its behavior. It

was found HMA thickness had a significant effect on the flexural bond strength of UTW overlays. The HMA failure was observed for 50 and 100 percentage of bonding when subjected to flexural fatigue test. The percentage of bonding increases the fatigue life of UTW overlays. An exponential model was obtained between stress ratio and a number of cycles at failure. In order to determine the probability of failure at different stress levels a two-parameter Weibull distribution was adopted. The calculated number of fatigue cycles will follow a two-parameter Weibull distribution. Therefore Weibull distribution method is suitable for calculating the number of fatigue cycles for HMA-UTW composites subjected to flexural fatigue test. The obtained models from direct shear and flexural bond strength test can be used in the design of UTW overlays for different percentage of bonding. A contact friction model can be used for the simulation of HMA-UTW composites subjected to direct shear and flexural test under static loading.

Based on the experimental studies following suggestions were made,

1. Direct shear test method is suggested for the evaluation of ISBS for UTW overlays under static and dynamic loading conditions.
2. Groove interface treatment with an inclination of 45 degrees and piercing interface treatment techniques is suggested.
3. Statistical models were drawn from static and dynamic loading conditions is suggested for determining the reduction in bond strength and fatigue life of UTW overlays subjected to different percentage of bonding.
4. A minimum HMA thickness of 75 mm is suggested for placing UTW overlays.
5. It was found that percentage of bonding at the interface was very sensitive to static and dynamic loading. Therefore the percentage of bonding at the interface under dynamic loading can be taken into account for the design of UTW overlays.
6. Contact friction model is proposed for simulating the different percentage of bonding at the interface.

The testing methods and obtained models had certain limitations such as uniaxial loading, test was conducted for single temperature, no variation in binder content (asphalt content) and UTW thickness.

Finally, additional works to be carried out to make the laboratory-based framework more mechanistically sound and applicable to field conditions. The interface shear bond strength of HMA-UTW composites in the presence of different normal stress under static and dynamic loading conditions to be investigated. The effect of moisture induced damage at the interface to be determined for different binder content. A study is required on the predefined failure on HMA samples (notch) subjected to static and dynamic loading. Also, there is a need to investigate the finite element modeling for dynamic loading condition.

APPENDIX A

Example: Calculation of FRC mix proportion using IS: 10262-2009

DESIGN STIPULATIONS

- i) Characteristic compressive strength required in the field at 28 days of curing : 40 N/mm²
- ii) Nominal maximum size of aggregate : 20 mm
- iii) Degree of workability (Slump test) : 25 to 50 mm
- iv) Degree of supervision : Good

TEST DATA FOR MATERIALS

- i) Cement used : Ordinary Portland Cement of 43 grade conforming to IS: 8112
- ii) Specific gravity of cement : 3.14
- iii) Specific gravity of fine aggregate (sand) : 2.53
- iv) Specific gravity of coarse aggregate : 2.68
- v) Coarse aggregate : 20 mm and down size
- vi) Fine aggregate (natural sand) conforming to zone-II

DESIGN PROCEDURE FOR SPECIMEN MIX M40

TARGET MEAN STRENGTH FOR MIX PROPORTIONING

It is given by the relation

$$f'_{ck} = f_{ck} + 1.65 S$$

Where,

f'_{ck} = target average compressive strength at 28 days,

f_{ck} = characteristic compressive strength at 28 days,

S = standard deviation and it is 5.0 for M40 concrete from

Table 1 of IS: 10262-2009,

Thus, $f_t = 40 + 1.65 \times 6.0 = 49.90 \text{ N/mm}^2$

SELECTION OF WATER CEMENT RATIO

From Table 5 of IS 456, maximum water-cement ratio = 0.50

Based on IRC SP 76-2008, adopt water-cement ratio as 0.32, $0.32 < 0.5$, hence O.K.

SELECTION OF CEMENT CONTENT

Water-cement ratio = 0.32

As per IS: 10262-2009 cement content should not exceed 425 kg/m^3 .

Therefore two cement content were selected 350 kg/m^3 and 430 kg/m^3 .

SELECTION OF WATER CONTENT

Water content = $350 \times 0.32 = 112$ litre

DETERMINATION OF VOLUME OF COARSE AGGREGATE AND FINE AGGREGATE CONTENT

From the literature volume of coarse aggregate 0.61 is selected

Volume of fine aggregate content = $1 - 0.61 = 0.39$

MIX CALCULATIONS

The mix calculations per unit volume of concrete shall be as follows:

- a) Volume of concrete (a) = 1 m^3
- b) Volume of cement (b) = $\frac{\text{mass of cement}}{\text{specific gravity of cement}} \times \frac{1}{1000}$
 $\frac{350}{3.14} \times \frac{1}{1000}$
 0.111 m^3
- c) Volume of water (c) = $\frac{\text{mass of water}}{\text{specific weight of water}} \times \frac{1}{1000}$
 $\frac{112}{1} \times \frac{1}{1000}$
= 0.112 m^3
- d) Volume of super plasticizers (d) = $\frac{\text{mass of super plasticizers}}{\text{specific gravity of plasticizers}} \times \frac{1}{1000}$
(0.5 % of cementitious mass) = $\frac{1.75}{1.05} \times \frac{1}{1000}$

$$\begin{aligned}
&= 0.0016 \text{ m}^3 \\
\text{e) Volume of all in aggregate} &= [a - (b + c + d)] \\
&= (1-0.02) - (0.111+ 0.112 + 0.0016) \\
&= 0.756 \text{ m}^3 \\
\text{f) Mass of coarse aggregate} &= \text{volume of all in aggregate} \times \text{volume of coarse aggregate} \\
&\quad \times \text{specific gravity of coarse aggregate} \times 1000 \\
&= 0.756 \times 0.61 \times 2.68 \times 1000 \\
&= 1236 \text{ m}^3 \\
\text{g) Mass of fine aggregate} &= \text{volume of all in aggregate} \times \text{volume of fine aggregate} \times \\
&\quad \text{specific gravity of fine aggregate} \times 1000 \\
&= 0.756 \times 0.39 \times 2.53 \times 1000 \\
&= 746 \text{ m}^3
\end{aligned}$$

Ingredients	Quantity
Cement	350 kg/m ³
Fine aggregate	746 kg/m ³
Coarse aggregate	1236 kg/m ³
Water	112 Litres
Mix Proportion Ratio C : F.A : C.A : W\C	1 : 2.13: 3.53 : 0.32

CALCULATION OF FIBERS

From IRC- SP46 2013 gives the nominal fibre dosages in kg/m³ for different volume fractions of fibre.

Dosages in kg/m³ = 10 x (fibre volume in %) * (specific gravity of fibre material)

$$= 10 \times (0.25) \times (1.36)$$

$$= 3.4 \text{ kg/m}^3$$

APPENDIX B

Example: Calculation of Superpave mix design properties of HMA samples (NMAS 37.5) compacted at 90 °C and designed at 205 gyrations.

Consider mixture with 5.5% asphalt content by weight of mixture

- Weight of Aggregate (Including mineral filler) = 4700 g
- Weight of the bitumen = 221 g
- Total weight of the mixture = 1269.63 g
- Bulk specific gravity of aggregates, G_{sb} = 2685 kg/m³
- Maximum theoretical density of loose mixture, G_{mm} = 2518 kg/m³
- Bulk Density of Specimen, G_{mb} = 2435 kg/m³
- Air Voids, VTM (%)
$$= \frac{G_{mm} - G_{mb}}{G_{mm}} \times 100$$

= 3.29
- Aggregate content (% by total weight of mix), P_s = $100 \times [4700 / (4700 + 221)]$
= 95.5
- Voids in Mineral Aggregate, VMA (%)
$$= 100 - \frac{G_{mb} \cdot P_s}{G_{sb}}$$

= 13.4
- Voids Filled with Asphalt, VFA (%)
$$= \frac{VMA - VTM}{VMA} \times 100$$

= 75.44

APPENDIX C

Example: Calculation of ISBS of NT specimens subjected to 6.0 mm/min rate of displacement. The data obtained from static test are tabulated in Table C.1 and shown in Fig. C.1

Table C.1 ISBS test results of NT specimens

Displacement (mm)	Load (kN)					
	Sample 1	Sample 2	Sample 3	Sample 4	Sample 5	Sample 6
0.0	0.011	0.011	0.011	0.011	0.011	0.011
0.5	0.252	0.735	0.976	0.493	0.915	0.554
1.0	0.614	1.398	2.544	0.976	2.302	1.096
1.5	1.699	2.182	3.388	2.724	3.388	2.664
2.0	3.147	3.448	0.011	3.991	0.011	3.086
2.5	4.473	3.930		0.011		3.448
3.0	0.011	0.071				0.011
3.5		0.011				

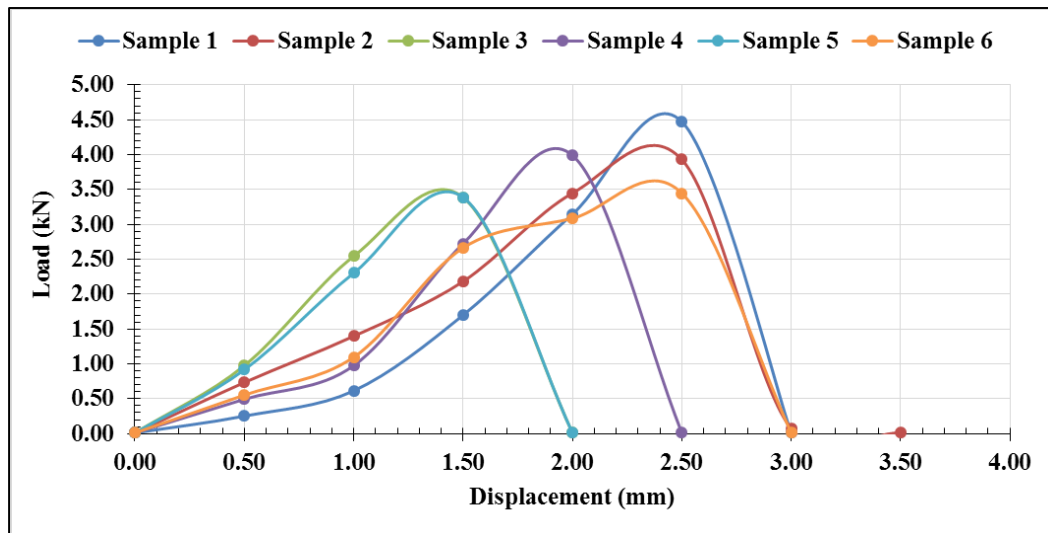


Fig. C.1 Load versus displacement curve for groove interface treatment specimens subjected to 6.0 mm/min rate of loading

$$\text{ISBS} = \frac{U_l}{A}$$

Where, ISBS = interface shear bond strength (MPa), U_l = ultimate load applied to the specimen (N), and A = cross-sectional area of the specimen (mm^2).

$$\text{ISBS} = \frac{4.2 \times 1000}{17671.46} = 0.237 \text{ N/mm}^2$$

APPENDIX D

Example: Test results for interface shear bond fatigue of piercing samples with different percentage of bonding.

Table D.1 Interface Shear Bond Fatigue Test Results for 97% Bonding (Piercing+25)

Stress ratio	Applied load (kN)	Sample 1	Sample 2	Sample 3	Sample 4	Sample 5	Average number of cycles at failure
0.05	0.96	4254721	4263830	4085092	4423368	3812115	4167825
0.10	1.92	2980510	3150810	3744706	2861590	3074512	3162426
0.15	2.88	377734	813565	1166242	575462	309448	648490
0.20	3.85	102015	202015	94530	285265	102556	157276
0.25	4.81	64327	78432	42905	58654	66818	62227
0.35	6.73	40187	41567	46313	44102	42578	42949
0.45	8.65	22568	22654	23265	21787	21301	22315
0.55	10.58	10762	10589	11478	12009	11432	11254
0.65	12.50	5147	6254	4780	5365	5651	5439
0.75	14.42	1500	1547	1632	1247	1305	1446
0.85	16.35	784	601	580	698	415	616

Table D.2 Interface Shear Bond Fatigue Test Results for 88% Bonding (Piercing+50)

Stress ratio	Applied load (kN)	Sample 1	Sample 2	Sample 3	Sample 4	Sample 5	Average number of cycles at failure
0.05	0.88	1317256	1825617	1975884	1526340	1329315	1594882
0.10	1.75	783154	554318	1171235	584617	957885	810242
0.15	2.63	300480	248006	328507	460052	113765	290162
0.20	3.50	181860	172900	86650	91727	236478	153923
0.25	4.38	48372	30480	56255	45744	54930	47156
0.35	6.13	26890	29872	34781	32542	39125	32642
0.45	7.88	12139	10235	10982	9874	11456	10937
0.55	9.63	4754	3875	5127	3128	4587	4294
0.65	11.38	1560	1875	1105	1228	1678	1489
0.75	13.13	254	758	368	215	561	431
0.85	14.88	136	62	84	110	58	90

**Table D.3 Interface Shear Bond Fatigue Test Results for 75% Bonding
(Piercing+75)**

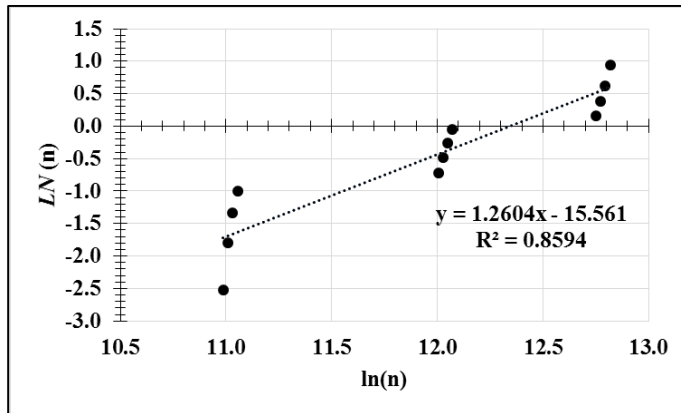
Stress ratio	Applied load (kN)	Sample 1	Sample 2	Sample 3	Sample 4	Sample 5	Average number of cycles at failure
0.05	0.69	913860	1086130	770900	1182510	822846	955249
0.10	1.38	492292	506390	338720	412584	645230	479043
0.15	2.07	205790	386850	279570	104115	151385	225542
0.20	2.76	153015	96348	229225	106030	85538	134031
0.25	3.45	36684	55260	45076	39730	41362	43622
0.35	4.83	16012	16487	17878	14231	14701	15862
0.45	6.21	7235	7012	8740	7456	8032	7695
0.55	7.58	3104	3012	4564	2015	4212	3381
0.65	8.96	1007	1212	1078	982	1470	1150
0.75	10.34	504	689	213	556	547	502
0.85	11.72	54	66	27	58	48	51

**Table D.4 Interface Shear Bond Fatigue Test Results for 55% Bonding
(Piercing+100)**

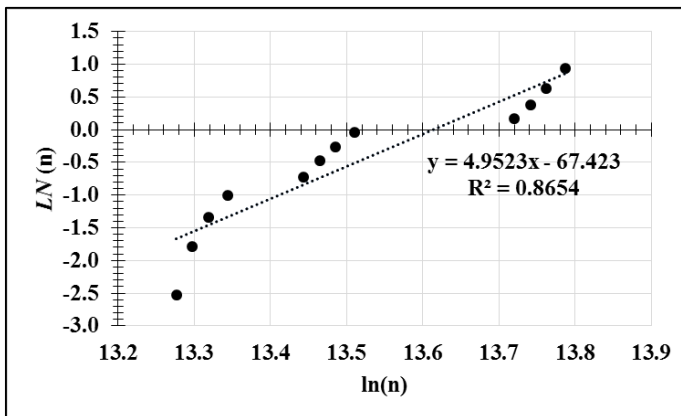
Stress ratio	Applied load (kN)	Sample 1	Sample 2	Sample 3	Sample 4	Sample 5	Average number of cycles at failure
0.05	0.36	412456	231784	198470	265651	182516	258175
0.10	0.72	185956	265412	98289	105973	92738	149674
0.15	1.08	91045	113806	87560	64257	75090	86352
0.20	1.44	61781	48675	20262	34453	52121	43458
0.25	1.80	11890	10134	8798	10987	9521	10266
0.35	2.52	7578	7547	7272	8086	8554	7807
0.45	3.24	3504	2916	3036	3654	3912	3404
0.55	3.97	1326	1254	1398	1488	1500	1393
0.65	4.69	810	846	990	792	918	871
0.75	5.41	168	210	246	138	102	173
0.85	6.13	15	30	24	30	18	23

APPENDIX E

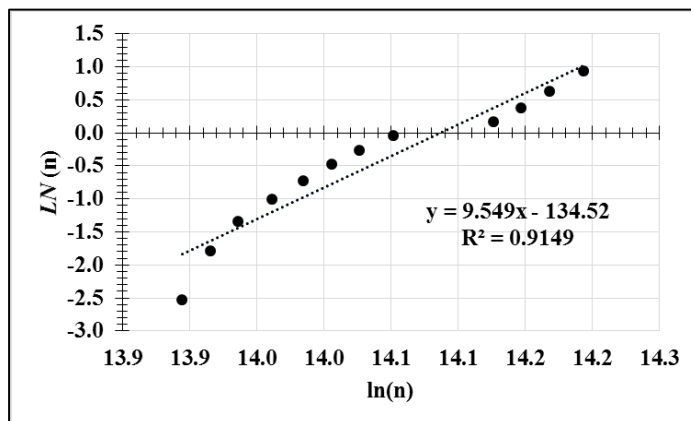
Example: Calculation of flexural bond fatigue for HMA-UTW prism composite samples subjected to dynamic loading.



(a)

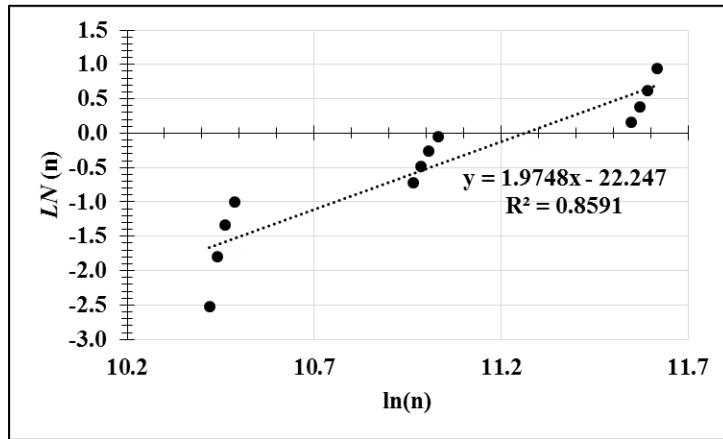


(b)

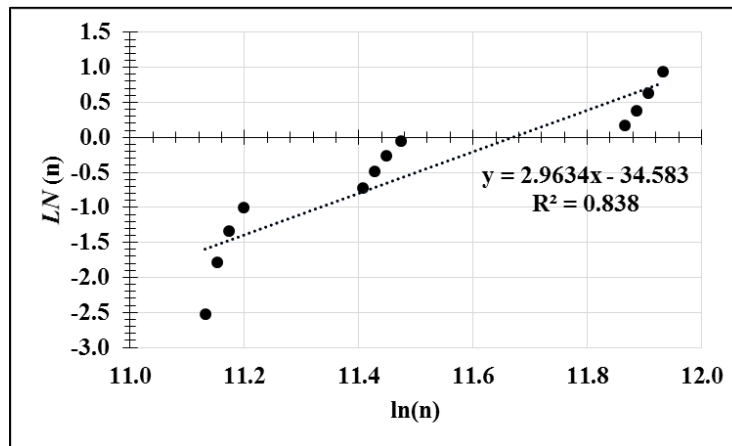


(c)

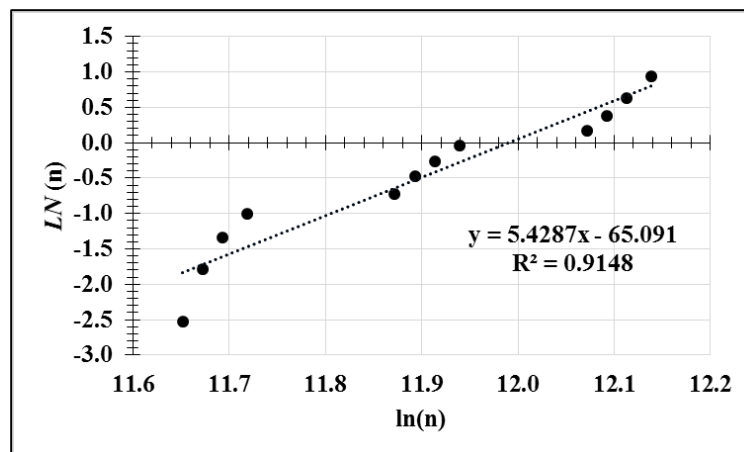
Fig. D.1 Graphical analysis of fatigue life data for 100% bonding at different stress ratios (a) 0.75 (b) 0.65 (c) 0.55



(a)



(b)



(c)

Fig. D. 2 Graphical analysis of fatigue life data for 50% bonding at different stress ratios (a) 0.75 (b) 0.65 (c) 0.55

REFERENCES

- Abdelkader, B., El-Hadj, K., and Karim, E. (2010). “Efficiency of granulated blast furnace slag replacement of cement according to the equivalent binder concept”. *Cement and Concrete Composites*, 32(3), 226-231.
- Ahmed, S., Dave, E. V., Buttlar, W. G., and Behnia, B. (2012). “Compact tension test for fracture characterization of thinbonded asphalt overlay systems at low temperature.” *Road Materials and Pavement Design*, 45, 1207–1220.
- Alengaram. U. J., Mahmud. H., and Jumaat M. Z. (2010). “Comparison of mechanical and bond properties of oil palm kernel shell concrete with normal weight concrete”. *Physics and Science*, 5(8):1231–9.
- Altoubat, S. A., Roesler, J. R., Lange, D. A., and Rieder, K. A. (2008). “Simplified method for concrete pavement design with discrete structural fibers”. *Construction and Building Materials*, 22(3), 384-393.
- ANSYS (2014). *ANSYS Theory Manual (14.1)*
- ASTM. (2003). “Standard test method for bulk density and voids in aggregate.” C-29, West Conshohocken, Pa.
- Bagheri, A., Zanganeh, H., Alizadeh, H., Shakerinia, M., and Marian, M. A. S. (2013). “Comparing the performance of fine fly ash and silica fume in enhancing the properties of concretes containing fly ash”. *Construction and Building Materials*, 47, 1402-1408.
- Barbhuiya, S. A., Gbagbo, J. K., Russell, M. I., and Basheer, P. A. M. (2009). “Properties of fly ash concrete modified with hydrated lime and silica fume”. *Construction and Building Materials*, 23(10), 3233-3239.
- Barman, M., Vandenbossche, J. M., and Li, Z. (2015). “Characterization of load transfer behavior for bonded concrete overlays on asphalt”. *Transportation Research Board*, 2524, 143-151.

- Barman, M., Vandenbossche, J. M., and Li, Z. (2017). Influence of Interface Bond on the Performance of Bonded Concrete Overlays on Asphalt Pavements. *Transportation Engineering, Part B: Pavements*, 143(3), 04017008.
- Bentur, A. (1989). "Silica fume treatments as means for improving durability of glass fiber reinforced cements". *Materials in Civil Engineering*, 1(3), 167-183.
- Bentur, A., and Goldman, A. (1989). "Curing effects, strength and physical properties of high strength silica fume concretes". *Materials in Civil Engineering*, 1(1), 46-58.
- Bissonnette, B., Courard, L., Beushausen, H., Fowler, D., Trevino, M., and Vaysburd, A. (2013). "Recommendations for the repair, the lining or the strengthening of concrete slabs or pavements with bonded cement-based material overlays." *Materials and Structures*, 46, 481–494.
- Bissonnette, B., Courard, L., Fowler, D. W., and Granju, J. L. (Eds.). (2011). "Bonded Cement-Based Material Overlays for the Repair, the Lining Or the Strengthening of Slabs Or Pavements: State-of-the-Art Report of the RILEM Technical Committee 193-RLS, 3, *Springer Science & Business Media Proceedings*.
- Bordelon, A. C. (2011). "Flowable fibrous concrete for thin pavement inlays". Doctoral dissertation, University of Illinois at Urbana-Champaign, USA.
- Burnham, R. T. (2005). "Forensic investigation report for MN/road ultrathin whitetopping test cells 93, 94, and 95." *Rep. No. MN/RC - 2005-45, Minnesota Department of Transportation*.
- Carlsward, J. (2006). "Shrinkage cracking of steel fibre reinforced self compacting concrete overlays: test methods and theoretical modelling." Doctoral dissertation, Lulea University of Technology, Lulea, Sweden
- Cervantes, V., and Roesler, J. (2009). "Performance of Concrete Pavements with Optimized Slab Geometry." Doctoral Dissertation, University of Illinois at Urbana-Champaign, Urbana, IL.

- Chabot, A., Hun, M. and Hammoum, F. (2013). “Mechanical analysis of a mixed mode debonding test for composite pavements.” *Construction and Building Materials*, 40(12), 1076–1087.
- Chen, H. J., Huang, S. S., Tang, C. W., Malek, M. A., and Ean, L. W. (2012). “Effect of curing environments on strength, porosity and chloride ingress resistance of blast furnace slag cement concretes: A construction site study”. *Construction and Building Materials*, 35, 1063-1070.
- Chen, Y., Tebaldi, G., Roque, R., Lopp, G. and Exline, M. (2013). “A mechanistic test to evaluate effects of interface condition characteristics on hot-mix asphalt overlay reflective cracking performance.” *Road Materials and Pavement Design*, 14, 262-273.
- Cheng, A., Huang, R., Wu, J. K., and Chen, C. H. (2005). “Influence of GGBS on durability and corrosion behavior of reinforced concrete”. *Materials Chemistry and Physics*, 93(2), 404-411.
- Cho, Y. H., and Koo, H. M. (2006). “UTW behavior on asphalt pavements tested with HWLS.” *Transportation Engineering*, 132(11), 880-887.
- Chunhua, H. (2005). “Synthesis of current minnesota practices of thin and ultra-thin whitetopping.” *Rep. No. MN/RC-2005-27, Minnesota Department of Transportation*.
- Collop, A.C., Sutanto, M. H., Airey, G.D., and Elliott, R.C. (2009). “Shear bond strength between asphalt layers for laboratory prepared samples and field cores.” *Construction and Building Materials*, 23 (01), 2251–2258.
- Collop, A.C., Sutanto, M.H., Airey, G.D., and Elliott, R. C. (2011). “Development of an automatic torque test to measure the shear bond strength between asphalt.” *Construction and Building Materials*, 25(7), 623–629.
- Cook, M. D., Ley, M. T., and Ghaeezadah, A. (2014). “A workability test for slip formed concrete pavements”. *Construction and Building Materials*, 68, 376-383.
- Delatte, N., and Chen, S. E. (2005). “Investigation of sasw as evaluation technique to evaluate asphalt pavement with UTW”. *Experimental Techniques*, 29(2), 38-42.

- Delatte, N., and Sehdev, A. (2003). “Mechanical properties and durability of bonded-concrete overlays and ultrathin whitetopping concrete”. *Transportation Research Board*, 1834, 16-23.
- Erdoğan, Ş., Arslantürk, C., and Kurbetci, Ş. (2011). Influence of fly ash and silica fume on the consistency retention and compressive strength of concrete subjected to prolonged agitating. *Construction and Building Materials*, 25(3), 1277-1281.
- Galeota, D., and Giammatteo, M. M. (1989). “Stress-strain relations of normal and lightweight concrete with silica fume under uniaxial compression”. *Special Publication*, 114, 991-1012.
- Goel, S., Singh, S. P., and Singh, P. (2012). “Fatigue analysis of plain and fiber-reinforced self-consolidating concrete”. *ACI Materials Journal*, 109(5), 573.
- Goodman, R. E., Taylor, R. L., and Brekke, T. L. (1968). “A model for the mechanics of jointed rocks”. *Soil Mechanics and Foundations Div*, 94, 637-659.
- Granju, J.L. (1996). “Thin bonded overlays, about the role of fiber reinforcement on the limitation of their debonding.” *Advance Cement Base Materials*, 4(01), 21-27.
- Haddad, R. H., and Smadi, M. M. (2004). “Role of fibers in controlling unrestrained expansion and arresting cracking in Portland cement concrete undergoing alkali-silica reaction”. *Cement and Concrete Research*, 34(1), 103-108.
- Hadjsadok, A., Kenai, S., Courard, L., Michel, F., and Khatib, J. (2012). “Durability of mortar and concretes containing slag with low hydraulic activity”. *Cement and Concrete Composites*, 34(5), 671-677.
- Hakim, B. A., Cheung, L. W., and Armitage, R. J. (2000). “Use of FWD data for prediction of bonding between pavement layers.” *Pavement Engineering*, 01(01), 49-59.
- Hakimzadeh, S., Kebede, N. A., Buttler, W. G., Ahmed, S., and Exline, M. (2012). “Development of fracture-energy based interface bond test for asphalt concrete.” *Road Materials and Pavement Design*, 13(6), 76-87.

- Han, T. Y., Lin, W. T., Cheng, A., Huang, R., and Huang, C. C. (2012). “Influence of polyolefin fibers on the engineering properties of cement-based composites containing silica fume”. *Materials and Design*, 37, 569-576.
- Hasçalık, A., and Çaydaş, U. (2008). “Optimization of turning parameters for surface roughness and tool life based on the Taguchi method”. *Advanced Manufacturing Technology*, 38(9), 896-903.
- Hilsdorf, H. K., and Kesler C. E. (1966). “Fatigue strength of concrete under varying flexural stresses”. *In Journal Proceedings*, 63(10), 1059-1076.
- Hogan, F. J., and Meusel, J. W. (1981). “Evaluation for durability and strength development of a ground granulated blast furnace slag”. *Cement, Concrete and Aggregates*, 3(1), 40-52.
- IRC SP: 72-2015. “Guidelines for design of flexible pavement for low volume rural roads”.
- IRC:SP-76. (2008). “Tentative guidelines for conventional, thin and ultrathin whitetopping.”
- IS: 10086-1982. “Indian standard specification for moulds for use in tests of cement and concrete”. Bureau of Indian Standards, New Delhi, India.
- IS: 10262 (2009). “Indian standard guidelines for concrete mix design”. Bureau of Indian Standards, New Delhi, India.
- IS: 12089-1987. “Indian standard specification for granulated slag for the manufacture of Portland slag cement”. Bureau of Indian Standards, New Delhi, India.
- IS: 15388-2003. “Indian standard specification for silica fume”. Bureau of Indian Standards, New Delhi, India.
- IS: 383-1970 “Indian standard specification for coarse and fine aggregates from natural sources for concrete”. Bureau of Indian Standards, New Delhi, India.
- IS: 516-1991. “Indian standard methods of tests for strength of concrete”. Bureau of Indian Standards, New Delhi, India.

- IS: 73-2013. “Indian standard specification for paving bitumen”. Bureau of Indian Standards, New Delhi, India.
- IS: 8112-2001. “Ordinary Portland Cement, 43 grade-specification (second revision)”. Bureau of Indian Standards, New Delhi, India.
- IS: 9103-1999. “Indian standard specification for concrete admixtures”. Bureau of Indian Standards, New Delhi, India.
- Jun, Z., and Stang, H. (1998). “Fatigue performance in flexure of fiber reinforced concrete”. *ACI Materials Journal*, 95(1), 58-67.
- Keleştemur, O., Arıcı, E., Yıldız, S., and Gökçer, B. (2014). “Performance evaluation of cement mortars containing marble dust and glass fiber exposed to high temperature by using Taguchi method”. *Construction and Building Materials*, 60, 17-24.
- Khedr, S. A., and Abou-Zeid, M. N. (1994). “Characteristics of silica-fume concrete”. *Materials in Civil Engineering*, 6(3), 357-375.
- Khokhar, M. I. A., Rozière, E., Turcry, P., Grondin, F., and Loukili, A. (2010). “Mix design of concrete with high content of mineral additions: Optimisation to improve early age strength”. *Cement and Concrete Composites*, 32(5), 377-385.
- Khorami, M., and Ganjian, E. (2013). “The effect of limestone powder, silica fume and fibre content on flexural behaviour of cement composite reinforced by waste Kraft pulp”. *Construction and Building Materials*, 46, 142-149.
- Kim, Y. K., and Lee, S. W. (2013). “Performance evaluation of bonded concrete overlay”. *Construction and Building Materials*, 49, 464-470.
- Kim, Y. K., and Lee, S. W. (2015). “Bond-fatigue behavior of bonded concrete overlay”. *Testing and Evaluation*, 44(4), 1724-1732.
- Kruntcheva, M. R., Collop, A. C., and Thom N. H. (2004). “Feasibility of assessing bond condition of asphalt concretelayers with dynamic nondestructive testing.” *Transportation Engineering*, 130(04), 510-518.
- Kruntcheva, M. R., Collop, A. C., and Thom. N. H. (2006). “Properties of asphalt concrete layer interfaces.” *Materials in Civil Engineering*, 18(07), 467-471.

- Kruntcheva, M. R., Collop A. C., and Thom, N. H. (2005). “Effect of bond condition on flexible pavement performance.” *Transportation Engineering*, 131(11), 880-888.
- Kumara, M. W., Tia, M., Wu, C. L., and Choubane, B. (2005). “Analysis of Composite Pavements Under Moving and Static Wheel Loads From a Heavy-Vehicle Simulator”. In International Conference on Best Practices for Ultrathin and Thin Whitetoppings.
- Kumara, W., Tia, M., Wu, C. L., and Choubane, B. (2003). “Evaluation of applicability of ultrathin whitetopping in Florida”. *Transportation Research Board*, 1823, 39-46.
- Leutner, R. (1979). “Investigation of the adhesion of bituminous pavements”. *Bitumen*, 3, 84-91.
- Li, S., Li, Y., Way, G., and Noureldin, S. (2004). “Mechanistic-Empirical characterization of bonding between ultra-thin white-topping and asphalt pavement”. *Testing and Evaluation*, 32(4), 274-281.
- Li, S., Liu, X., and Liu, Z. (2014). “Interlaminar shear fatigue and damage characteristics of asphalt layer for asphalt overlay on rigid pavement”. *Construction and Building Materials*, 68, 341-347.
- Limbachiya, V., Ganjian, E., and Claisse, P. (2016). “Strength, durability and leaching properties of concrete paving blocks incorporating GGBS and SF”. *Construction and Building Materials*, 113, 273-279.
- Lin, D. F., and Wang, H. Y. (2005). “Forensic investigation of ultra-thin whitetopping failures in Taiwan”. *Performance of Constructed Facilities*, 19(2), 165-171.
- Lin, Y., Karadelis, J. N., and Xu, Y. (2013). “A new mix design method for steel fibre-reinforced, roller compacted and polymer modified bonded concrete overlays.” *Construction and Building Materials*, 48(07), 333–341.

- Mack, J., Hawbaker, L., and Cole, L. (1998). “Ultrathin whitetopping: state-of-the-practice for thin concrete overlays of asphalt”. *Transportation Research Board*, 1610, 39-43.
- Mccall, J. T. (1958). “Probability of fatigue failure of plain concrete”. *In Journal Proceedings*, 55(8), 233-244.
- Ministry of Road Transport and Highways (2013). “Manual for Construction and Supervision of Bituminous Works”, 1-98.
- Mu, F. (2014). “Laboratory and numerical investigation of interface debonding of bonded concrete overlay of asphalt and its effect on the critical stress in the overlay”. Doctoral dissertation, University of Pittsburgh, USA.
- Mu, F., and Vandebossche, J. (2017). “A superimposed cohesive zone model for investigating the fracture properties of concrete–asphalt interface debonding”. *Fatigue and Fracture of Engineering Materials and Structures*, 40(4), 496-511.
- Mu, F., and Vandebossche, J. M. (2011). “Development of Design Guide for Thin and Ultra-Thin Concrete Overlays of Existing Asphalt Pavements, Task 2: Review and Selection of Structural Response and Performance Models (No. MN/RC 2011-25). *Transportation Research Board*, (1532), 15-20.
- NCHRP Synthesis 338. (2004). “Thin and ultrathin whitetopping.” <http://www.trb.org/Main/Public/Blurbs/155409.aspx>.
- Nili, M., and Afroughsabet, V. (2010). “Combined effect of silica fume and steel fibers on the impact resistance and mechanical properties of concrete”. *Impact Engineering*, 37(8), 879-886.
- Nishiyama, T., Lee, H., and Bhatti, M. (2005). Investigation of bonding condition in concrete overlay by laboratory testing, finite element modeling, and field evaluation. *Transportation Research Board*, 1933, 15-23.
- Nordby, G. M. (1958). “Fatigue of concrete-A review of research”. *In Journal Proceedings*, 55(8), 191-219.
- Oh, B. H., (1991) “Fatigue-Life Distributions of Concrete for Various Stress Levels,” *ACI Materials Journal*, 88(2), 122-128.

- Oner, A., and Akyuz, S. (2007). “An experimental study on optimum usage of GGBS for the compressive strength of concrete”. *Cement and Concrete Composites*, 29(6), 505-514.
- Ozbay, E., Oztas, A., Baykasoglu, A., and Ozbebek, H. (2009). “Investigating mix proportions of high strength self compacting concrete by using Taguchi method”. *Construction and Building materials*, 23(2), 694-702.
- Ozer, H. (2011). “Development of domain integral and generalized finite element methods for three dimensional analysis of near-surface cracking in flexible pavements”. Doctoral Dissertation, University of Illinois at Urbana-Champaign.
- Ozer, H., Al-Qadi, I. L., Wang, H., and Leng, Z. (2012). “Characterisation of interface bonding between hot-mix asphalt overlay and concrete pavements modelling and in-situ response to accelerated loading.” *Pavement Engineering*, 13(02), 181–196.
- Ozer, H., Al-Qadi, I., and Leng, Z. (2008). “Fracture-based friction model for pavement interface characterization”. *Transportation Research Board*, 2057, 54-63.
- Patel, B. N. (2010). “Factors affecting the interface shear strength of pavement layers.”MS Dissertation, Louisiana State University,USA.
- Pereira, D. D. S., Balbo, J. T., and Khazanovich, L. (2006). “Theoretical and field evaluation of interaction between ultra-thin whitetopping and existing asphalt pavement”. *Pavement Engineering*, 7(4), 251-260.
- Perez, F., Bissonnette, B., and Gagné, R. (2009). “Parameters affecting the debonding risk of bonded overlays used on reinforced concrete slab subjected to flexural loading. *Materials and Structures*, 42(5), 645-662.
- Poon, C. S., Lam, L., and Wong, Y. L. (1999). “Effects of fly ash and silica fume on interfacial porosity of concrete”. *Materials in Civil Engineering*, 11(3), 197-205.
- Raab, C., and Partl M. N. (2009). “Interlayer bonding of binder, base and sub-base layers of asphalt pavements Long-term performance.” *Construction and Building Materials*, 23(03), 2926–2931.

- Raab, C., Halim, A.O. A. E., and Partl M. N. (2012). “Interlayer bond testing using a model material.” *Construction and Building Materials*, 26(07), 190-199.
- Rajan, S., and Olek, J. (2002). “Concrete Overlay as a Rehabilitation Option for Distressed Asphalt Pavements”. Joint Transportation Research Program, 37.
- Raposeiras, A. C., Vega-Zamanillo, Á., Calzada-Pérez, M. Á., and Castro-Fresno, D. (2012). “Influence of surface macro-texture and binder dosage on the adhesion between bituminous pavement layers”. *Construction and Building Materials*, 28(1), 187-192.
- Rasmussen, R. O., and Rozycki, D. K. (2004). “*Thin and ultra-thin whitetopping: A synthesis of highway practice*”. *Transportation Research Board*, 338.
- Risser Jr, R.J., Lahue, S.P., Voigt, G.F. and Mack, J.W., (1993). “Ultra-thin concrete overlays on existing asphalt pavement”. In Fifth International Conference on *Concrete Pavement Design and Rehabilitation* (Vol. 2).
- Roesler, J., Bordelon, A., Ioannides, A., Beyer, M., and Wang, D. (2008). “Design and concrete material requirements for ultrathin whitetopping.” *Rep. No. FHWA-ICT-08-016, Illinois Center for Transportation*.
- Roesler, J., Bordelon, A., Ioannides, A., Beyer, M., and Wang, D. (2008b). "Design and concrete material requirements for ultra-thin whitetopping." *Rep. No. FHWA-ICT-08-016, Research Report for the Illinois Center of Transportation R27-3A, Urbana, IL*.
- Romanoschi, S., and Metcalf, J. (2001). “Characterization of asphalt concrete layer interfaces”. *Transportation Research Board*, 1778, 132-139.
- Sahmaran, M., Yücel, H. E., Yildirim, G., Al-Emam, M., and Lachemi, M. (2013). “Investigation of the bond between concrete substrate and ECC overlays”. *Materials in Civil Engineering*, 26(1), 167-174.
- Santagata, F. A., Ferrotti, G., Partl, M. N., and Canestrari, F. (2009). “Statistical investigation of two different interlayer shear test methods.” *Materials and Structures*, 42, 705–714.

- Seo, Y., El-Haggan, O., King, M., Joon Lee, S., and Richard Kim, Y. (2007). “Air void models for the dynamic modulus, fatigue cracking, and rutting of asphalt concrete”. *Materials in Civil Engineering*, 19(10), 874-883.
- Shi, C., Wu, Z., Lv, K., and Wu, L. (2015). “A review on mixture design methods for self-compacting concrete”. *Construction and Building Materials*, 84, 387-398.
- Singh, S. P., and Kaushik, S. K. (2001). “Flexural fatigue analysis of steel fiber-reinforced concrete”. *ACI materials Journal*, 98(4), 306-312.
- Singh, S. P., Mohammadi, Y., and Kaushik, S. K. (2005). “Flexural fatigue analysis of steel fibrous concrete containing mixed fibers”. *ACI Materials Journal*, 102(6), 438-444.
- Skar, A., and Poulsen, P. N. (2015). “3-D cohesive finite element model for application in structural analysis of heavy duty composite pavements”. *Construction and Building Materials*, 101, 417-431.
- Speakman, J., and Scott III, H. (1996). “Ultra-thin, fiber-reinforced concrete overlays for urban intersections”. *Transportation Research Board*, 43.
- Suresha, S. N., and Satish, D. (2017). “Interface Bond Strength of Ultra-Thin Whitetopping (UTW) and Hot Mix Asphalt (HMA) Composites by Direct Shear”. *Testing and Evaluation*, 45(6).
- Taguchi, G. (1990) “Introduction to quality engineering”. Asian Productivity Organization (APO), Tokyo, Japan
- Talor, P., Yurdakul, E., Wang, X., and Wang, X. (2015). “Concrete Pavement Mixture Design and Analysis (MDA): An Innovative Approach to Proportioning Concrete Mixtures”. *In Trans Project Reports*. 106.
- Tashman, L., Nam, K., Papagiannakis, T., Willoughby, K., Pierce, L., and Baker, T. (2008). “Evaluation of construction practices that influence the bond strength at the interface between pavement layers”. *Performance of Constructed Facilities*, 22(3), 154-161.
- Tia, M., Wu, C. K., and Kumara, W. (2002). “Forensic investigation of the Ellaville weigh station UTW pavements”. *Technical Report, University of Florida*.

- Tia, M., Wu, C. K., Tapia, P., and Kumara, W. (2007). "Evaluation of feasibility of using composite pavements in Florida by means of HVS testing." *Technical Report, University of Florida*.
- Torres, N. H. Roesler, J., Ramussen, O. R., and Harrington, D. (2012). "Guide to design of concrete overlays using existing methodologies." *Rep. No. DTFH61-06-H-00011. National Concrete Pavement Technology Center*.
- Toutanji, H. A., and El-Korchi, T. (1995). "The influence of silica fume on the compressive strength of cement paste and mortar". *Cement and Concrete Research*, 25(7), 1591-1602.
- Tschegg, E. K., Macht, J., Jamek, M., and Steigenberger, J. (2007). "Mechanical and fracture-mechanical properties of asphalt-concrete interfaces". *ACI Materials Journal*, 104(5), 474-480.
- Tschegg, E. K., Kroyer, G., Tan, D. M., Tschegg, S. E.S., and Litzka, J. (1995). "Investigation of bonding between asphalt layers on road construction." *Transportation Engineering*, 121(04), 309-316.
- Vandenbossche, J. M., and Barman, M. (2010). "Bonded whitetopping overlay design considerations for prevention of reflection cracking, joint sealing, and the use of dowel bars." 2155, 3-11.
- Vandenbossche, J. M., and Rettner, D. L. (1998). "The construction of US-169 and I-94 experimental thin and ultrathin whitetopping sections in Minnesota." *Rep. No. MN/RC-2001-07, Minnesota Department of Transportation*.
- Vandenbossche, J., and Fagerness, A. (2002). Performance, analysis, and repair of ultrathin and thin whitetopping at Minnesota road research facility. *Transportation Research Board*, 1809, 191-198.
- Wainwright, P. J., and Rey, N. (2000). "The influence of ground granulated blast furnace slag additions and time delay on the bleeding of concrete". *Cement and Concrete Composites*, 22(4), 253-257.

- Wen, H. Li, X., and Martono, W. (2010). “Performance assessment of Wisconsin’s whitetopping and ultra-thin whitetopping projects.” *Rep. No. 10-03, Wisconsin Department of Transportation.*
- West, R. Zhang, J., and Moore, J. (2005). “Evaluation of bond strength between pavement layers.” *Rep. No. 05-08, National Center for Asphalt Technology.*
- Wu, C. L., and Sheehan, M. (2002). “Testing and performance evaluation of ultrathin whitetopping pavements at Spirit of St. Louis Airport”. *Transportation Research Board*, (1809), 218-227.
- Wu, L. C., Tia, M., and Choubane, B. (2007). “Forensic investigation of ultrathin whitetopping pavements in florida.” *Transportation Engineering*, 21(01), 78-88.
- Xie J, Elwi A.E., and MacGregor J.G, (1995). “Mechanical properties of three high-strength concretes containing silica fume,” *ACI Materials*, 92, 135.
- Yap, S. P., Alengaram, U. J., and Jumaat, M. Z. (2013). “Enhancement of mechanical properties in polypropylene–and nylon–fibre reinforced oil palm shell concrete”. *Materials and Design*, 49, 1034-1041.
- Yurdakul, E., Taylor, P. C., Ceylan, H., and Bektas, F. (2012). “Effect of paste-to-voids volume ratio on the performance of concrete mixtures”. *Materials in Civil Engineering*, 25(12), 1840-1851.
- Zhang, J., and Li, V. C. (2002). “Monotonic and fatigue performance in bending of fiber-reinforced engineered cementitious composite in overlay system”. *Cement and Concrete Research*, 32(3), 415-423.
- Zhang, P., and Li, Q. F. (2013). “Effect of polypropylene fiber on durability of concrete composite containing fly ash and silica fume”. *Composites Part B: Engineering*, 45(1), 1587-1594.
- Zhang. P., Li. Q., and Sun. Z (2011). “Influence of silica fume and polypropylene fiber on fracture properties of concrete composite containing fly ash”. *Reinforced Plastics and Composites*, 30(24), 1977–1988.

- Zhao, H., Cao, J., and Zheng, Y. (2017). “Investigation of the interface bonding between concrete slab and asphalt overlay”. *Road Materials and Pavement Design*, 18(3), 109-118.

LIST OF PUBLICATIONS

Publications based on Ph.D Research Work

International Journals

- 1) Jayakesh, K., and Suresha, S. N. (2018). “Experimental investigation of interface treatment technique on interface shear bond fatigue behavior of Ultra-Thin Whitetopping”. *Construction and Building Materials*, 161, 489-500.
- 2) Jayakesh, K., and Suresha, S. N. “Flexural Fatigue Analysis of Optimized Polyester Fiber Reinforced Concrete for Ultra-Thin Whitetopping Pavements”. *Journal of Transportation Engineering Part B- Pavements*, ASCE (under review).

International Conference

- 1) Jayakesh, K., and Suresha, S. N. (2017). “Experimental Analysis of Interface Shear Fatigue Performance of Ultra-Thin Whitetopping”. In *Airfield and Highway Pavements 2017*, ASCE, Philadelphia, US, 283-294.

BIO-DATA

NAME	JAYAKESH K	
ADDRESS	C/o VINEETH NILAYA, 1 ST CROSS, GANAPATHI LYT, VIDYANAGAR, SHIVAMOGGA-577203, KARANATAKA, INDIA.	
MOBILE NO.	+91 9964356894	
E-MAIL	jayakeshk22@gmail.com	
QUALIFICATION	(Ph.D in Civil Engineering) Registered : July-2013	National Institute of Technology Karnataka, Surathkal, Mangaluru.
	M.Tech. in Transportation Engineering (2013)	National Institute of Technology Karnataka, Surathkal, Mangaluru.
	B.E. in Civil Engineering (2011) Visvesvaraya Technological University	Sir M V I T, Bengaluru, Karnataka
	II P.U.C. (2006), Department of Pre-University Education, S.S.L.C. (2004), Karnataka	Sacred Heart PU College, Shivamogga. Karnataka
	Secondary Education Examination Board.	DVS High School, Shivamogga. Karnataka